AD A139 531 A MODEL OF RADAR PROPAGATION AND DETECTION(U) ROYAL AUSTRALIAN NAVY RESEARCH LAB EDGECLIFF M R BATTAGLIA ET AL. DEC 83 RANRL-TN-2/83 1/2

UNCLASSIFIED F/G 17/9 NL

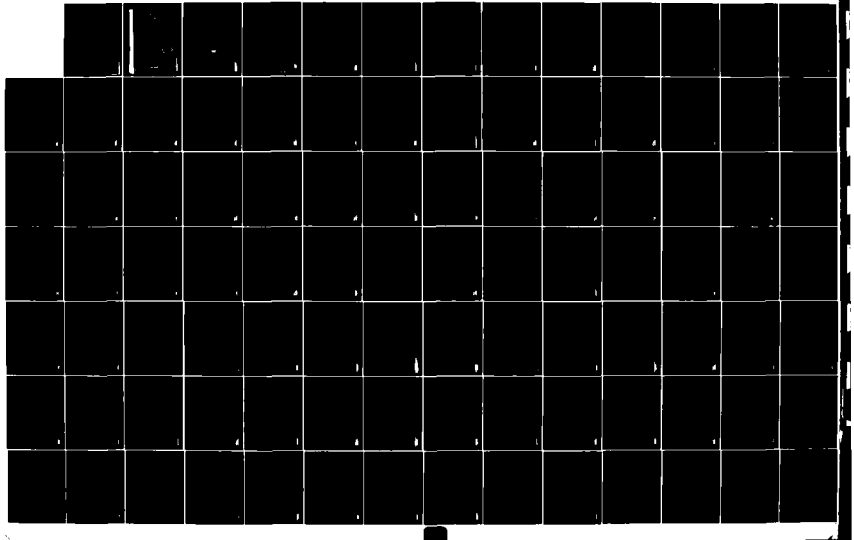

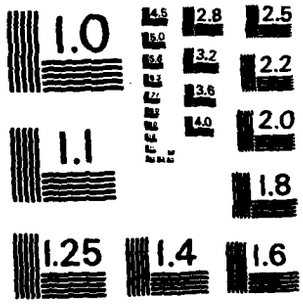

MICROCOPY RESOLUTION TEST CHART
NATIONAL BUREAU OF STANDARDS-1963-A

(12)

UNCLASSIFIED

RANRL T/N (EXT.) No. 2/83

AR Number: AR-002-706

DEPARTMENT OF DEFENCE
DEFENCE SCIENCE AND TECHNOLOGY ORGANISATION
R.A.N. RESEARCH LABORATORY
EDGECLIFF, N.S.W.

RANRL TECHNICAL NOTE (EXTERNAL) No. 2/83

A MODEL OF RADAR PROPAGATION AND DETECTION

M.R. BATTAGLIA
&
P. WILLIAMS

APPROVED FOR PUBLIC RELEASE

COPY No. 26

DECEMBER 1983

UNCLASSIFIED

UNCLASSIFIED

DEPARTMENT OF DEFENCE

R.A.N. RESEARCH LABORATORY

RANRL TECHNICAL NOTE (EXTERNAL) No 2/83

A MODEL OF RADAR PROPAGATION AND DETECTION

M.R.BATTAGLIA
and
P.WILLIAMS

ABSTRACT

A computer model of radar propagation and detection is described. The details of multipath, clutter, attenuation and probability of detection algorithms are contained in separate annexes.

POSTAL ADDRESS: The Director, RAN Research Laboratory
P.O. Box 706 Darlinghurst, N.S.W. 2010

CONTENTS

1. INTRODUCTION

The prediction of radar and ESM performance in a complex maritime environment has become a routine task for the naval operations analyst. With the emphasis on operational rather than environmental variables, resort is usually had to readily available computer programs for propagation and detection. If these are not available, several physical and mathematical approximations must be made to facilitate routine predictions.

Simple radar models employing 'standard' environment and detector have proved useful for ad hoc estimates of performance under globally averaged conditions. These models however often employ simple approximations for multipath effects, signal statistics, detection criteria, attenuation and backscatter and care is also needed to ensure that input variables are not outside the range of validity of the model.

The goal of the radar model described herein was threefold - (i) it should produce reliable data over a wide range of environmental and radar parameters, excluding ducting conditions, (ii) the programs should be written in a high-level scientific language and (iii) the model should be programmable on medium sized mini and microcomputers. In reference 1 a BASIC program was described which was specifically designed for the Tektronix 4051 system, and which was concerned with the performance of scanning search radars with fixed threshold detectors.

This model has since been enlarged and rewritten in PASCAL, and the detection subroutines have been extended and modified to improve numerical stability. Both fixed threshold and CFAR detection are treated for coherent and non-coherent detectors and various m-out-of-n detection criteria. This paper also presents a more detailed description of the physical principles and range of validity of the model. Each of the major subroutines is covered by a separate annex. To assist with program development, the results of each routine are also presented in graphical form.

With many aspects of radar performance prediction the literature presents several alternative techniques or relations used by

.../2

various authors with qualified reliability. The most important of such topics, which are considered to merit separate annexes, are

(i) refractivity and the effective earth radius
(ii) attenuation by the atmosphere
(iii) pattern propagation factor
(iv) antenna pattern function
(v) antenna noise temperature
(vi) surface and volume clutter
(vii) calculation of detection and acquisition probabilities

The annex on clutter is predominantly concerned with a description of the surface clutter routines, which have not been reported elsewhere. Probability of detection algorithms have been validated for accuracy and numerical stability over a wide range of probabilities and target scintillation parameters.

2. THEORETICAL BACKGROUND

The theory of radar detection is well documented in the literature (e.g. references 2 - 7), but will be briefly reviewed below to give a broad outline of the method used and to place in context the symbols and terms used in later sections.

2.1 The Radar Equation

In free space electromagnetic radiation spreads spherically, so that the power density at distance R in a tangential surface of area A is

$$\frac{P_r}{A} = \frac{P_t G_t}{4\pi R^2} \qquad (1)$$

where P_t is the transmitted power and G_t is the power gain of the transmit antenna in the direction of propagation. Equation 1 is the one-way transmission equation appropriate to communications or ESM/ECM. In the latter, A can be replaced by the effective antenna area A_e to calculate the received power in terms of the wavelength (λ) and the receive antenna gain (G_r)

.../3

$$A_e = \frac{G_r \lambda^2}{4\pi} \qquad (2)$$

The 'radar equation' in its simplest form assumes that the radiation incident on a scatterer is captured in an area σ and reradiated isotropically. This yields the bistatic radar equation

$$P_r = \frac{P_t G_r G_t \lambda^2 \sigma}{(4\pi)^3 R_1^2 R_2^2} \qquad (3)$$

where R_1 is the transmit antenna to target range, and R_2 is the target to receive antenna range. For monostatic radar $G_r=G_t=G$ and $R_1=R_2=R$. If more than one path is significant the received field is modified by a pattern propagation factor F. The usual definition of F (Annex C) includes the antenna pattern functions (Annex D) of the direct and indirect rays, so that G is replaced by the gain along boresight (G_o)

$$P_r = \frac{P_t G_o^2 \lambda^2 F^4 \sigma}{(4\pi)^3 R^4 L} \qquad (4)$$

The propagation path is calculated using the rules of geometric optics (ray theory) for a smoothly decaying pressure and moisture gradient, with the geometric variables transformed to the effective earth radius model to simplify calculations. The approach used in this model to calculate the pressure and humidity-dependence of the effective earth radius is described in Annex A.

Pattern propagation factors for targets over the horizon are evaluated using diffraction theory (ref 3), and an interpolation procedure is used for targets near the horizon.

Losses due to absorption by atmospheric gases and precipitation are accounted for by the loss factor L. This loss is computed using the calculated attenuation rate (Annex B) and the slant range. System losses are not included in equation 4 since the power is referred to the antenna. The incorporation of additional losses due to filter mismatch, pulse compression, etc are described in reference 1.

2.2 Clutter

The clutter return from the sea surface (P_c) is calculated from the radar equation (eqn 4) with the clutter cross-section given by

.../4

$$\sigma = \sigma^{o}A = \sigma^{o}\frac{R\theta^{H}c}{2B}.\sec\gamma \qquad (5)$$

where θ^{H} is the effective horizontal beamwidth, c is the speed of light, γ is the grazing angle and B is the bandwidth of the matched filter. Expressions for the clutter cross-section per unit area (σ^{o}) are described in annex F.

Volume backscatter from rain and snow is determined in an analogous manner, with

$$\sigma = \sigma_{v}^{o}V = \sigma_{v}^{o}\frac{\pi R^{2}\theta^{H}\theta^{V}c}{8B} \qquad (6)$$

2.3 Noise

Quasi-thermal noise is evaluated from the system noise temperature (T_s) referred to the antenna. The equivalent noise power (P_n) is then

$$P_n = E_n/\tau = kT_s/\tau \qquad (7)$$

where τ is the radiated pulse width and E_n is the spectral density of the noise power. (Care should be taken using bandwidth in the radar equation if τ is not of order $1/E_n$). The system noise temperature is

$$T_s = T_a + T_r(L_r-1) + L_rT_o(NF-1) \qquad (8)$$

in which T_a is the antenna temperature, L_r and T_r are the receiving line losses and temperature respectively, T_o=290 K and NF is the receiver noise figure. The method for evaluating T_a is outlined in annex E.

2.4 Probability of Detection

Gaussian statistics are assumed for clutter and noise, and the single pulse signal-to-noise ratio is defined as

$$S/N = P_r/(P_c + P_n) \qquad (9)$$

The probability of paint depends on S/N, the probability of

.../5

false alarm, the degree of pre-detection (coherent) and post-detection (non-coherent) integration, and the target fluctuation statistics. A generalized Chi-square distribution is used to synthesize the amplitude statistics of the target return, with a single distribution parameter which is determined by the relative timescale of target scintillation. Non-fluctuating targets, Swerling cases I-IV and Weinstock targets are included. Programs for evaluating paint probability from S/N are described in annex G. A general method for determining acquisition ranges for m-out-of-n detection criteria is also described together with results for 1/1, 2/2, and 2/3 detectors.

REFERENCES

1. Battaglia, M.R. (1983). RAN Research Laboratory. A Computer Program for the Prediction of Search Radar Performance. (U) RANRL Tech Note (Ext) 1/83. UNCLASSIFIED

2. Blake, L.V. (1980). Radar Range-Performance Analysis. D.C. Heath and Co., Lexington.

3. Kerr, D.E. (Ed) (1951). Propagation of Short Radio Waves. M.I.T. Radiation Lab Series, Vol 13, McGraw-Hill, New York.

4. Skolnik, M.I. (1962). Introduction to Radar Systems, McGraw-Hill, New York.

5. Barton, D.K. (1964). Radar System Analysis, Prentice-Hall, New Jersey

6. Nathanson, F.E. (1969). Radar Design Principles, McGraw-Hill New York.

7. Skolnik, M.I. (Ed) (1970). The Radar Handbook, McGraw-Hill New York.

8. Battaglia, M.R. (1979). in Non-linear Behaviour of Atoms, Molecules and Ions in Electric, Magnetic and Electromagnetic Fields, Elsevier, Amsterdam.

9. Herzberg, G. (1950). Spectra of Diatomic Molecules, Van Nostrand, New York.

10. Weast, R.C. (Ed) (1975). Handbook of Chemistry and Physics, CRC Press, 55th ed.

11. Liebe, H.J. (1969). 'Calculated Tropospheric Dispersion and Absorption due to the 22 GHz Water Vapour Line', I.E.E.E. Trans AP-17 No 5, P621.

.../8

12. Van Vleck, J.H. (1951). 'Theory of Absorption of Uncondc sed Gases' in ref 3.

13. Rivers, W. (1980) 'Attenuation by Rain, Snow, Ice and Fog', unpublished expressions cited in ref 2.

14. Goldstein, H. (1951) 'Attenuation by Condensed Water' in ref 3.

15. Abramowitz, M. and Stegun, I.A. (1972). Handbook of Mathematical Functions, Dover, New York.

16. Marcum, J.I, (1963). 'A Statistical Theory of Target Detection by Pulsed Radar', I.R.E. Trans IT-6 p59.

17. Swerling, P. (1960). 'Probability of Detection for Fluctuating Targets'. I.R.E. Trans IT-6 p269.

18. Di Franco, J.V. and Rubin, W.L. (1968). Radar Detection, Prentice Hall, Englewood Cliffs, New Jersey.

19. Mitchell, R.L. and Walker J.F. (1971). 'Recursive Methods for Computing Detection Probabilities', I.E.E.E. Trans on Aerospace and Electronic Systems, AES-7, p671.

20. Johnson, M.A. (1979). 'Radar Detection Calculations with the HP-65 and HP-67', R79EMH5, General Electric Co., Syracuse, New York.

21. Castella, F.R. (1976). 'Sliding Window Detection Probabilities', I.E.E.E. Trans on Aerospace and Electronic Systems, AES-12, p815.

22. Postema, G.B. (1982). 'Radar Track Aquisition Range', I.E.E.E. Trans on Aerospace and Electronic Systems AES-18, p147.

23. Youle, E. (1969). 'The Detection Performance of the Radar Operator' (U) WRE Tech Note SAD-235. UNCLASSIFIED.

.../9

24. Porter, R.A. and Wentz, F.J. (1971). 'Microwave Radiometric Study of Ocean Surface Characteristics', Contract I-35140, Radiometric Technology Inc., Wakefield, Mass.

25. Wu, S.T. and Fung, A.K. (1973). 'A Theory of Microwave Apparent Temperature over the Ocean', NASA CR-2329.

26. Beckmann, P. and Spizzichino, A (1963). The Scattering of Electromagnetic Waves from Rough Surfaces, Permagon, New York.

27. Domb, C and Pryce, M.H.L. (1947). 'The Calculation of Field Strengths over a Spherical Earth', Journal I.E.E., 94(3), p325.

28. Colegrove, S.B. (1974) Radar Sea Echo : A Critical Review (U) WRE Tech Memo 1219(AP). UNCLASSIFIED.

ANNEX A

REFRACTIVITY AND EFFECTIVE EARTH RADIUS

Variation in the refractive index (n) of air with altitude causes electromagnetic rays to follow curved paths through the atmosphere. The classical method for dealing with this phenomenon, when calculating ray geometry, is to replace the earth's radius (a) with an effective earth's radius (a_e)

$$a_e = Ka \tag{A-1}$$

and to assume an equivalent homogeneous atmosphere. From Snell's Law

$$K = [1 + a\frac{dn}{dh}]^{-1} \tag{A-2}$$

where $\frac{dn}{dh}$ is the change in refractive index with height. Replacing refractive index with refractivity N ($= 10^6(n-1)$) gives

$$K = [1 + \frac{a}{10^6}(\frac{dN}{dh})]^{-1} \tag{A-3}$$

The model makes the further assumption that N varies exponentially from its sea level value N_s to its value at the tropopause N_t

$$N = N_s e^{\frac{h}{h_t}\log_e \frac{N_t}{N_s}} \tag{A-4}$$

and $$\frac{dN}{dh} = \frac{N_s}{h_t}\log_e\left[\frac{N_t}{N_s}\right] e^{\frac{h}{h_t}\log_e \frac{N_t}{N_s}} \tag{A-5}$$

where h_t is the height of the tropopause. Since most of the ray bending occurs in the first few kilometres of the atmosphere, where $\frac{dN}{dh}$ is relatively constant, a linear approximation is made using the value of $\frac{dN}{dh}$ at sea level.

$$K = \left[1 + \frac{a}{10^6}\frac{N_s}{h_t}\log_e \frac{N_t}{N_s}\right]^{-1} \tag{A-6}$$

and the tropopause is assumed to have a constant height of 13 kilometers with the refractivity constant at 61 units at that height. Substituting for N_t and h_t

.../A-2

$$K = \left[1 + 0.00049\ N_s\ \log_e \frac{61}{N_s}\right]^{-1} \qquad \text{(A-7)}$$

The refractive index of a pure gas is given by the Debye relation (ref 8) and, assuming ideal gas behaviour, this becomes

$$n-1 = \frac{P}{2\varepsilon_0 RT}\left[\alpha + \frac{\mu^2}{3KT}\right] \qquad \text{(A-8)}$$

where P is the pressure, R is the gas constant, α is the electronic polarizability, μ is the electric dipole moment, T is the temperature and ε_0 is the permittivity of free space. For a mixture of gases P is replaced by the partial pressures and the term on the right is summed over all species which contribute to the polarization - mainly oxygen, nitrogen and water for air near sea level. This equation is valid only if the electric dipole μ can rotate in phase with the applied electric field. At RF and low microwave frequencies and for a normal atmosphere this reduces to

$$N = 10^6(n-1) = \frac{77.6}{T}\left[P + \frac{4810P_w}{T}\right] \qquad \text{(A-9)}$$

where P and P_w are total pressure and partial pressure due to water vapour in mbar and T is the temperature in Kelvin

The lowest frequency rotational resonance for water is at 22 GHz (f_o). Using the Kramers - Konig relationship and Lorentzian line shape assumption (i.e. collisional broadening), the variation in the real part of the dielectric constant across an absorption band is given by

$$\delta\varepsilon_1 = \frac{\gamma^{max}\ c\ 10^6}{4\pi\omega\ \log_e 10} \qquad \text{(A-10)}$$

where γ^{max} is the peak absorption (dB/km), ω is the frequency and c is the speed of light. Taking a worst case (100% humidity and 300 K) $\delta\varepsilon_1 = 0.4 \times 10^{-6}$ (or $\delta N = 0.2$ for $N = 400$) across the 22 GHz absorption band - an insignificant error. The general variation in N due to dispersion in the molecular polarizability from the IR to RF region (ref 8) could account for 10 - 40% in N. However, since the range of validity of the overall model is restricted to RF and microwave bands, only a mean value for refractivity dispersion is used in the model.

The model uses environmental inputs of temperature, total

.../A-3

pressure and relative humidity (H) to calculate N_s (using equation (A-9)). To calculate partial pressure due to water vapour (from the input parameters) an empirical form of the Clausius - Clapeyron relation is used

$$P_w = k_1 H e^{\frac{-k_2}{T}} \qquad \text{(A-11)}$$

where $k_1 = 1.8178 \times 10^7$ mbar

$k_2 = 5329$ K

and H is the relative humidity in percent

If the relative humidity is not known explicitly, equation (A-11) can be rewritten in terms of wet and dry bulb temperatures. The saturated vapour pressure at the wet bulb temperature is obtained from equation (A-11) with $T = T_w$ and $H = 100$. To obtain the vapour pressure at ambient temperaure, the wet bulb depression ΔP_w is subtracted. For total pressure P in mbar, T in degrees Celsius, this is

$$\Delta P_w = [0.646 \times 10^{-3} P (1 + 0.00094T_w)](T - T_w) \qquad \text{(A-12)}$$

The considerable variability of N_s and hence K is illustrated in figures A-1 and A-2. In figure A-1, N_s is plotted against H for several temperatures at a constant pressure of 1013.25 mbars. In figure A-2, K is plotted against H for a similar range of values.

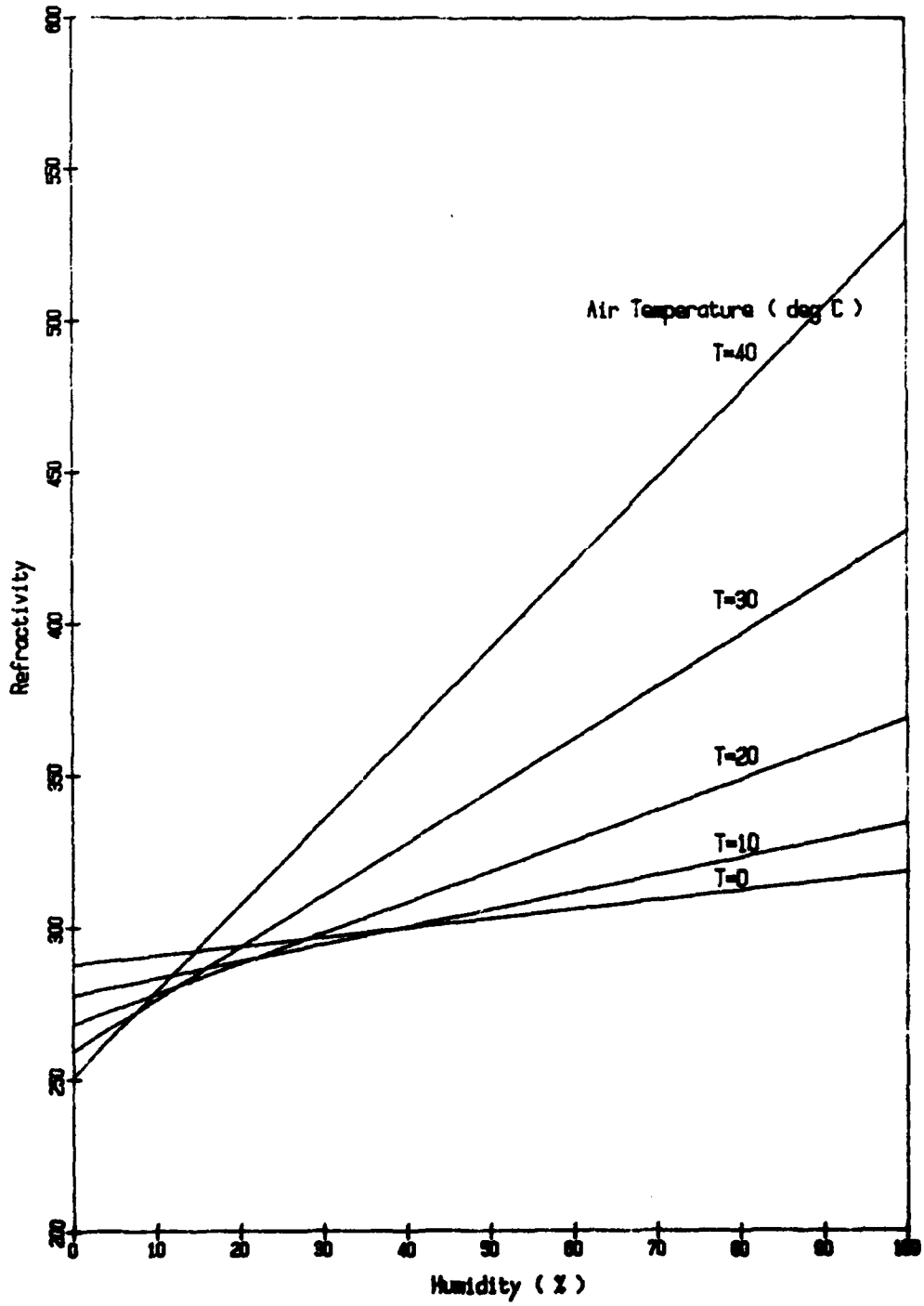

Figure A-1. Atmospheric Refractivity
Barometric Pressure is 1013.25 mbar

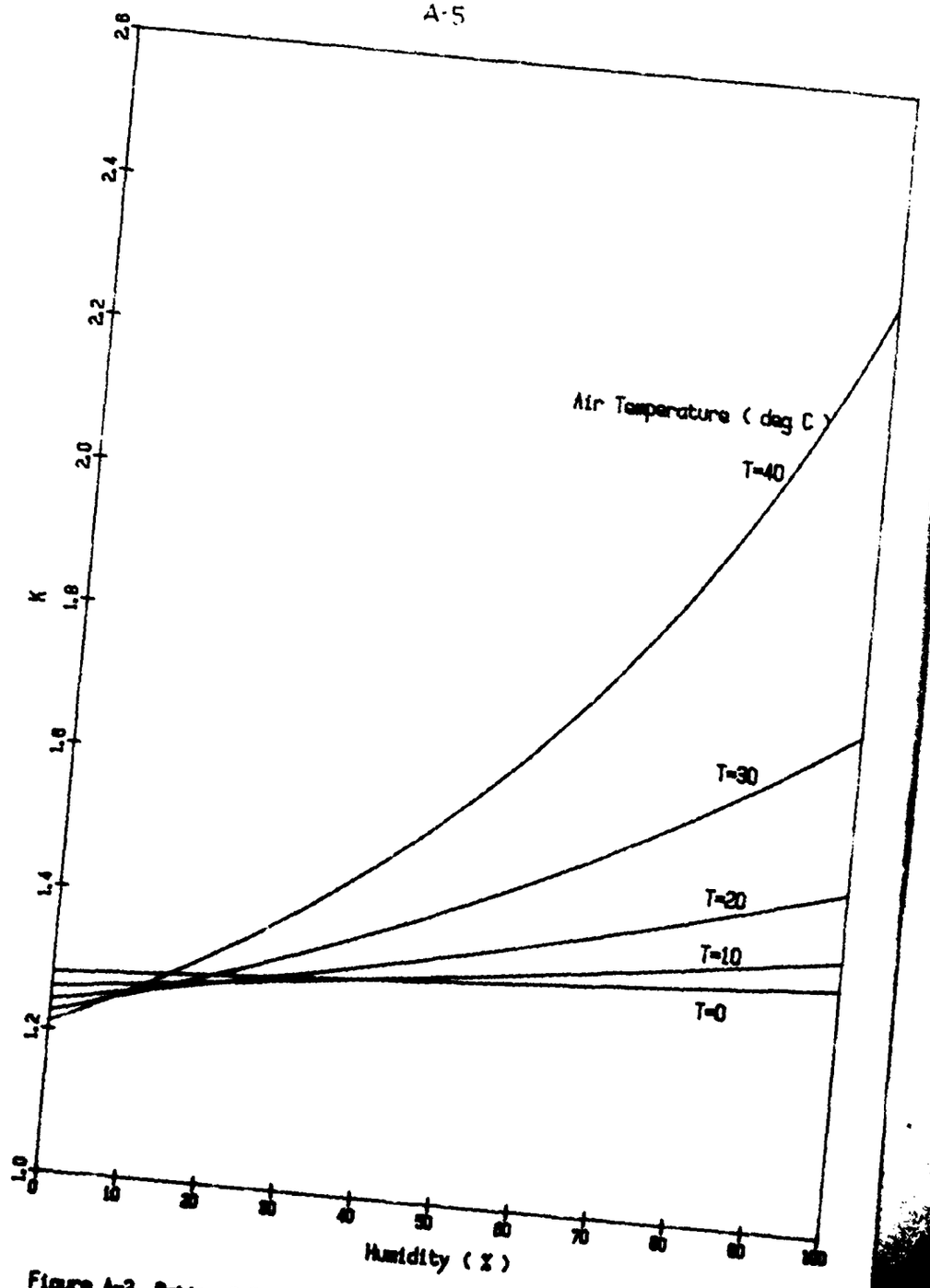

Figure A-2. Ratio of Earth's Effective Radius (K)
Barometric Pressure is 1013.25 mbar

ANNEX B

ATTENUATION BY THE ATMOSPHERE

Atmospheric Absorption Due to Uncondensed Gases

General

The one way absorption (A_j), due to constituent gas j, for a beam traversing a path in the atmosphere is obtained by integrating the absorption coefficient (γ_j) over the ray path

$$A_j = \int_0^R \gamma_j(s)\, ds \qquad \text{(B-1)}$$

where s = the distance along the ray path
R = the total length of the raypath (ie the slant range)

Assuming absorption is proportional to partial pressure with an exponential model for each atmospheric constituent, the absorption coefficient, as a function of height, is

$$\gamma_j(h) = \gamma_{jo}\, e^{-h/H_j} \qquad \text{(B-2)}$$

where γ_{jo} is the coefficient of absorption at sea level for constituent j and H_j is a constant for constituent j. The height of the direct ray at a distance (s) along the ray path is given by

$$h = \sqrt{s^2+2s(a_e+h_1)\sin\phi_e+(a_e+h_1)^2} - a_e \qquad \text{(B-3)}$$

where a_e = effective earth's radius
h_1 = antenna height above sea level
ϕ_e = elevation angle of the ray at the antenna

Substituting equation B-2 into equation B-3 gives

$$\gamma_j(s) = \gamma_{jo}\, e^{-\frac{\sqrt{s^2+2s(a_e+h_1)\sin\phi_e+(a_e+h_1)^2} - a_e}{H_j}} \qquad \text{(B-4)}$$

and therefore

.../B-2

$$A_j(s) = \gamma_{jo}\int_0^R e^{-\frac{\sqrt{s^2+2s(a_e+h_1)\sin\theta_e+(a_e+h_1)^2}-a_e}{H_j}} ds \qquad (B\text{-}5)$$

This integral is solved numerically in the model using n-point Gaussian quadrature techniques in which

$$A_j = \gamma_{jo} R \sum_{i=1}^{n} w_i \, f(x_i.R) \qquad (B\text{-}6)$$

where $$f(s) = e^{-\frac{\sqrt{s^2+2s(a_e+h_1)\sin\theta_e+(a_e+h_1)^2}-a_e}{H_j}} \qquad (B\text{-}7)$$

and x_i and w_i are tabulated in column k=0 of table 25.8 of reference 15 for various n. In this model n=8 is used.

Total Absorption

The total one way absorption (A) is calculated by summing A_j for all constituent gases where A and A_j are in decibels:

$$A = \sum_j A_j \qquad (B\text{-}8)$$

At microwave frequencies, absorption of electromagnetic radiation by uncondensed gases is due to the interaction with molecular dipoles rotating on a 10^9 Hz timescale (ref 9). The strongest molecular absorber is water which has a permanent electric moment and gives rise to a strong line at 22.235 GHz and other lines in the millimetre region. Oxygen lacks a permanent electric moment but displays a magnetic fine structure at 120 GHz and some fifty observable lines between 40 and 80 GHz. Although this magnetic interaction is much weaker than the electric dipole interaction, oxygen (by virtue of its much greater density) is responsible for an absorption comparable with water at sea level and greater at higher altitudes. No other polar or paramagnetic tropospheric gases give rise to significant absorption at the frequencies of interest and, therefore, in this model total one way absorption for uncondensed gases is assumed to be

$$A = A_o + A_w \qquad (B\text{-}9)$$

A_o and A_w are calculated from equation 6 above using

.../B-3

H_o = 6.1986 kilometres
H_w = 2.4261 kilometres

and values for γ_{oo} and γ_{wo} calculated from the models described below using sea level environmental parameters as input.

Absorption Coefficients - General

Microwave spectral 'lines' have vanishingly small width only in the limit of zero pressure. The width of the spectral lines varies inversly with the excited state lifetimes or dephasing times, which are of the same order as the rate of 'effective' molecular collisions. At sea level these occur on a 10^9 Hz time-scale for both water and oxygen (ref 10). Low altitude radars usually do not operate near the peak of an absorption line, however the calculated residual intensity in the 'tail' of the absorption is critically dependent on a model of the relaxation process. An exponential decay is assumed, resulting in a Lorentzian power spectrum.

Absorption Coefficient - Water

The main water band of interest in the microwave region is the 22.235 GHz line although there is some background absorption from the 180 GHz and 320 GHz bands. From ref 11, the expression for the line width (Δf) is

$$\Delta f = 1.349 \times 10^{-3} \left[\left[\frac{300}{T} \right] P_w + 0.20846 (P - P_w) \left[\frac{300}{T} \right]^{0.63} \right] \text{GHz} \qquad \text{(B-10)}$$

where P and P_w are the total pressure and partial pressure due to water vapour in millibars, T is in degrees Kelvin. Although water collisions are more 'effective' than those of other molecules, the line-width is approximately proportional to the total pressure. The expression for water vapour absorption is then given by

$$\gamma_w = 1.9014 \times 10^{-3} \left[f P_w \left[\frac{300}{T} \right]^{7/2} e^{2.144 \left[1 - \frac{300}{T} \right]} F + \gamma_{res} \right] \text{dB/km} \qquad \text{(B-11)}$$

where f is the frequency in gigahertz and F is a shape factor given by

$$F = \frac{f}{f_o} \left[\frac{\Delta f}{(f - f_o)^2 + (\Delta f)^2} + \frac{\Delta f}{(f + f_o)^2 + (\Delta f)^2} \right] \qquad \text{(B-12)}$$

.../B-4

where f_o = 22.235 GHz and γ_{res} is the residual water vapour absorption due to the tails of lines above 100 GHz given by the empirical expression

$$\gamma_{res} = 1.591\ T^{-7/2} P.P_w f^2 \quad dB/km \qquad (B-13)$$

Absorption Coefficient - Oxygen

Although O_2 does not have a permanent electric moment, it is paramagnetic and its microwave absorption is due to the fine-structure transitions in which the magnetic moment assumes various directions with respect to the rotational angular momentum of the molecule. The coupling of the rotational angular momentum (quantum number N) with spin (quantum number S=1) results in total angular momentum with quantum number J = (N-1), N or N+1. The selection rules for the microwave transitions are

$$J = N \longrightarrow J = N \pm 1 \qquad (B-14)$$

The relative intensities of these lines are related to the Boltzmann population factors for the J-states.

$$N_J \simeq (2J+1)\frac{hB}{kT} e^{-J(J+1)hB/kT} \qquad (B-15)$$

Spectroscopic data for O_2 (ref 9) gives (kT/hB)=145 at 300K. To account for contributions from overlapping lines summation up to frequencies corresponding to J=45 have been carried out to determine the O_2 absorption. The positions of the O_2 lines (ref 2) are listed in table B-1. To compute the total oxygen absorption the Van Vleck-Weisskopf theory (ref 12) is used which, after some substitution, reduces to

$$\gamma_o = 2.0058\ PT^{-3} f^2 \sum_N A_N \quad dB/km \qquad (B-16)$$

where $$A_N = \left[F_{N+}\mu_{N+} + F_{N-}\mu_{N-} + F_o\mu_{No}\right] e^{-2.068N(N+1)/T} \qquad (B-17)$$

$$F_o = \frac{\Delta f}{f^2+(\Delta f)^2} \qquad (B-18)$$

$$F_{N\pm} = \frac{\Delta f}{(f_{N\pm}-f)^2+(\Delta f)^2} + \frac{\Delta f}{(f_{N\pm}+f)^2+(\Delta f)^2} \qquad (B-19)$$

$$\mu_{N+} = \frac{N(2N+3)}{N+1} \qquad (B-20)$$

.../B-5

$$\mu_{N-} = \frac{(N+1)(2N-1)}{N} \qquad \text{(B-21)}$$

$$\mu_{No} = \frac{2(N^2+N+1)(2N+1)}{N(N+1)} \qquad \text{(B-22)}$$

are line shape factors, P is barometric pressure in millibars, T is in Kelvin, f is the frequency in GHz and Δf is the line width.

To account for the breakdown of the Van Vleck - Weisskopf theory for overlapping lines, semi-empirical line widths have been used to give good agreement at sea level. At moderate altitudes the linewidth narrows according to the expression

$$\Delta f = 0.18949 \frac{P}{T} \quad GHz \qquad \text{(B-23)}$$

Above 50 km doppler broadening and Zeeman splitting must also be included since these begin to dominate the apparent linewidth.

Condensed Water

The attenuation beyond the Rayleigh region cannot be treated as absorption but rather as a resonant multiple scattering, which depends on the distribution of drop sizes. At very high water densities such as fog or rain, the absorption of water can be calculated from simple empirical expressions. Rain attenuation is usually expressed in the form

$$\gamma_{rain} = \alpha r^{\beta} \qquad \text{(B-24)}$$

where r is the rainfall rate in mm/hr and α,β are functions of frequency. Rivers (ref 13) has suggested the following semi-empirical expressions based on Mie scattering theory and raindrop size distributions.

$$\alpha = \frac{3.1\times10^{-5}f^2(1+f^2/9)^{1/2}}{(1+f^2/1225)^{1/2}(1+f^2/2500)^{1/2}(1+f^2/12100)^{1/2}} \qquad \text{(B-25)}$$

and

$$\beta = 1.30 + 0.0372\left[1-\left[1+\left[\frac{\log(f/10)}{0.06}\right]^2\right]^{1/2}\right] \qquad \text{(B-26)}$$

i.e. there is a maximum in the power law at I-band.

Goldstein (ref 14) has deduced a formula for attenuation by fog:

.../B-6

$$\gamma_{fog} = 4.89 \times 10^{-4} M f^2 \qquad \text{(B-27)}$$

where M is water content in g/m³. Comparing (B-24) and (B-27) it is clear that at UHF frequencies (say 1 GHz) a 1mm/hr rainfall rate gives an attenuation comparable with a fog of density 0.67 g/m³. (100 m visibility). Also, from eqn (B-11), uncondensed water of the same average density results in about one tenth of the attenuation. Fog attenuation is often recorded as optical visibility (d). An empirical relation between M and d can be deduced from Goldstein's data

$$M \simeq k\, d^{-1.43} \qquad \text{(B-28)}$$

where k = 1670 when d is in feet and 305.4 when d is in metres.

Table B-1

Oxygen Resonance Frequencies

N	f_{N+} (GHz)	f_{N-} (GHz)
1	56.2648	118.7505
3	58.4466	62.4863
5	59.5910	60.3061
7	60.4348	59.1642
9	61.1506	58.3239
11	61.8002	57.6125
13	62.4112	56.9682
15	62.9980	56.3634
17	63.5685	55.7839
19	64.1272	55.2214
21	64.6779	54.6728
23	65.2240	54.1294
25	65.7626	53.5960
27	66.2978	53.0695
29	66.8313	52.5458
31	67.3627	52.0259
33	67.8923	51.5091
35	68.4205	50.9949
37	68.9478	50.4830
39	69.4741	49.9730
41	70.0000	49.4648
43	70.5294	48.9582
45	71.0497	48.4530

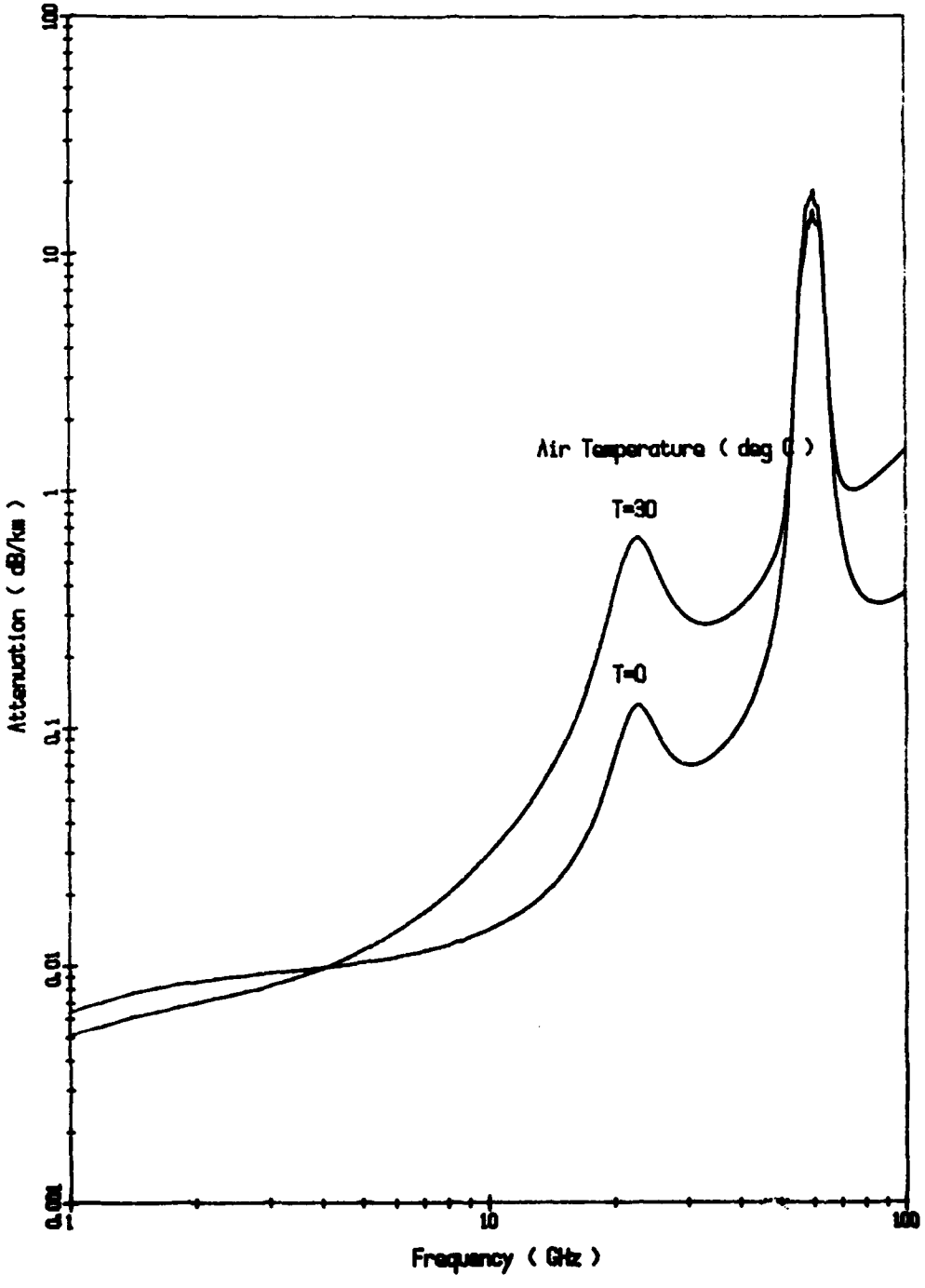

Figure B-1. Atmospheric Attenuation Due To Uncondensed Gases
Barometric Pressure is 1013.25 mbar
Humidity is 100 %

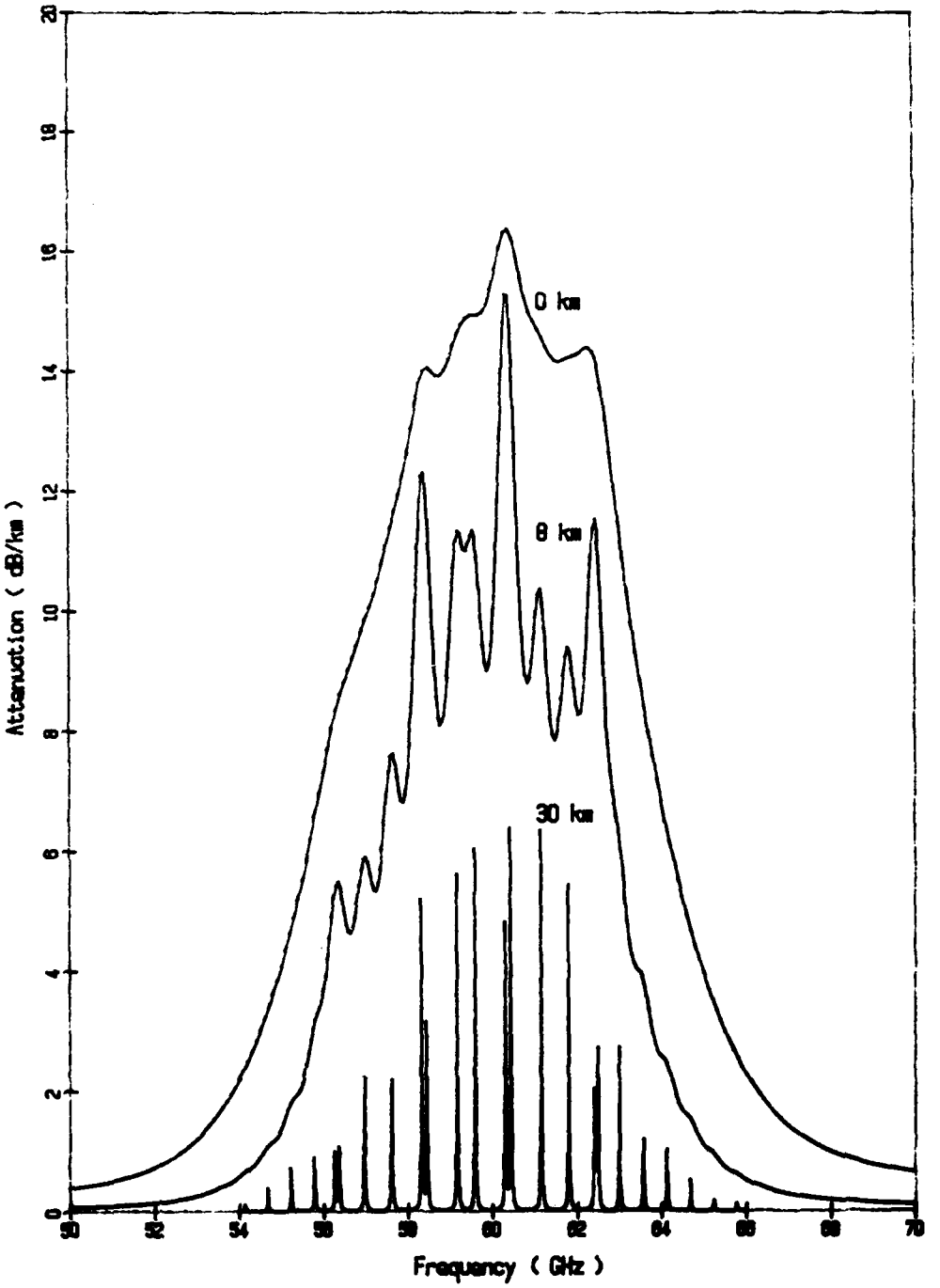

Figure B-2. Atmospheric Attenuation by Uncondensed Gases
Altitude is 0 , 8 , and 30 km
Humidity is 58.5 %

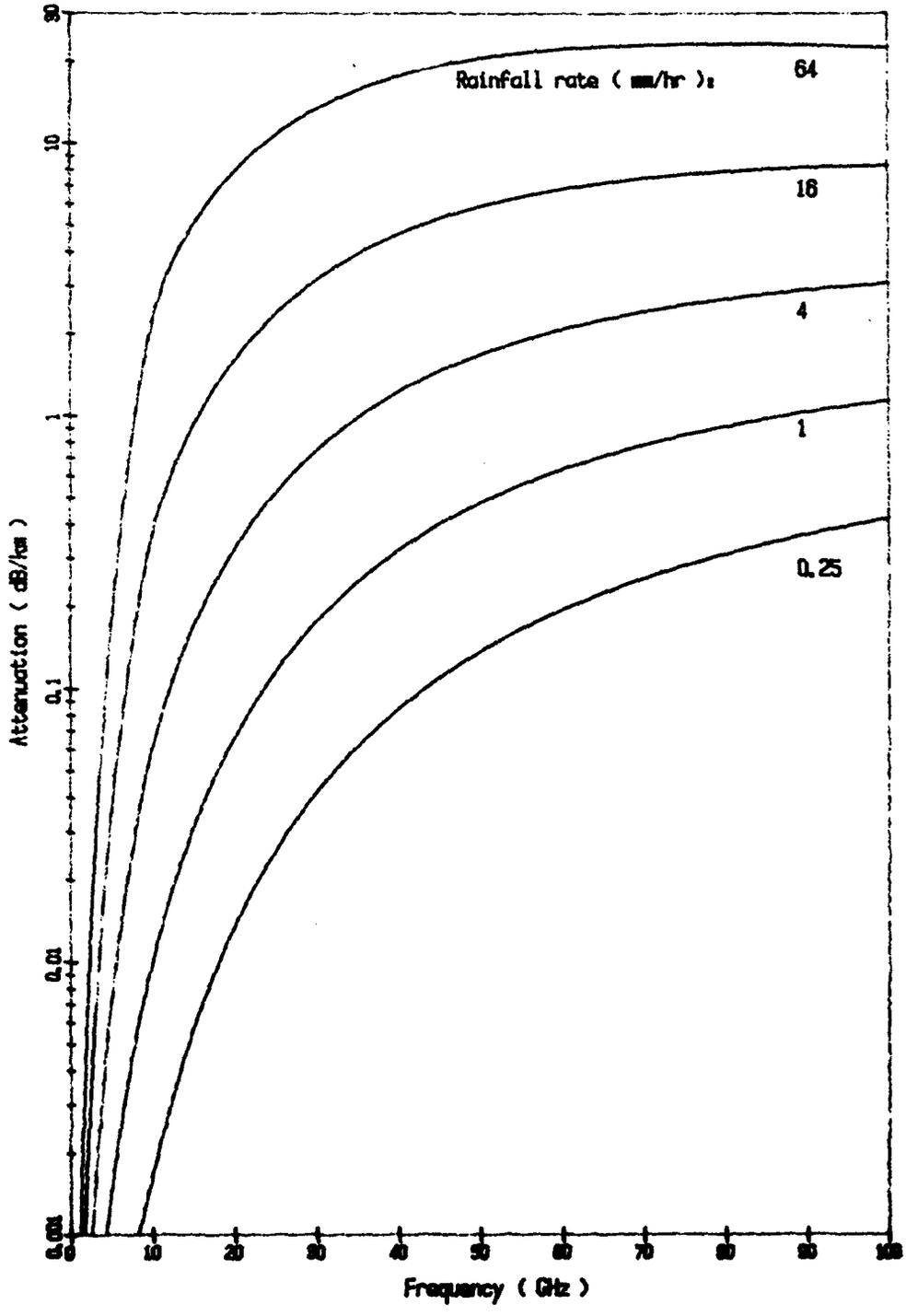

Figure B-3. Attenuation by Rain

ANNEX C

PATTERN PROPAGATION FACTOR (F)

General

The form of the radar equation used to define the pattern propagation factor (F) is

$$P_r = \frac{P_t G^2 \sigma \lambda^2 F^4}{(4\pi)^3 R^4} \qquad \text{(C-1)}$$

so that F includes terms in the antenna pattern function and the received field due to multipath, diffraction and scattering effects.

The Interference Region

In the interference region (between the radar and a critical ground range (G_c)), F is calculated using ray theory for one direct ray and one ray reflected from the sea surface. G_c is near the optical horizon for millimetre to centimetre wavelengths but is typically only 60% of the horizon range for UHF radars. Expressions for the calculation of G_c are at equations C-32 and C-33.

Within the interference region ($0<G<G_c$) F is obtained simply as

$$F = f(\theta_1)\sqrt{1+x^2+2x.\cos(\textstyle\sum \phi_i)} \qquad \text{(C-2)}$$

where $$x = \frac{\rho r D f(\theta_2)}{f(\theta_1)} \qquad \text{(C-3)}$$

and $f(\theta)$ is the antenna pattern function (see Annex D)
θ_1 is the elevation angle of the direct ray
θ_2 is the elevation angle of the indirect ray
$\sum \phi_i$ is the phase difference between the direct and indirect ray
r is the roughness coefficient
D is the divergence factor
ρ is the magnitude of the sea surface reflectivity

The phase difference ($\sum \phi_i$) between the direct and indirect ray is the sum of the geometric phase difference due to different path

.../C-2

lengths, and the phase shift at reflection for the indirect ray due to dielectric effects. Direct subtraction of the direct and indirect path lengths may lead to numerical instability and the preferred method of calculating the path difference (δ) is

$$\delta = \lambda(\phi/2\pi) = \frac{4R_1R_2\sin^2\gamma}{R_1+R_2+R} \qquad (C-4)$$

where the symbols are as shown in figure C-1. The slant ranges (R_1,R_2,R) are first evaluated as the corresponding ground ranges (G_1,G_2,G) which are the solutions of the approximate relation (ref.3)

$$2G_1^3+2a_eh_1G-3GG_1^2+[G^2-2a_e(h_1+h_2)]G_1 = 0 \qquad (C-5)$$

viz $$G_1 = G/2 - p.\sin(\xi/3) \qquad (C-6)$$

where $$p = 2\sqrt{\frac{a_e(h_1+h_2)+(G/2)^2}{3}} \qquad (C-7)$$

$$\xi = \sin^{-1}\frac{2a_eG(h_2-h_1)}{p^3} \qquad (C-8)$$

and where h_1 and h_2 are the antenna and target height respectively from which the slant range is calculated

$$R = \sqrt{(h_2-h_1)^2+4(a_e+h_1)(a_e+h_2).\sin^2[(G_1+G_2)/2a_e]} \qquad (C-9)$$

R_1 (R_2) is obtained by substituting h_2=0 (h_1=0) and G_2=0 (G_1=0).The solutions for the angles θ_1, θ_2 and γ are

$$\theta_1 = \sin^{-1}\frac{2a_e(h_2-h_1)+h_2^2-h_1^2-R^2}{2(a_e+h_1)R} \qquad (C-10)$$

$$\theta_2 = \sin^{-1}\frac{2a_eh_1+h_1^2+R_1^2}{2(a_e+h_1)R_1} \qquad (C-11)$$

$$\gamma = \sin^{-1}\frac{2a_eh_1+h_1^2-R_1^2}{2a_eR_1} \qquad (C-12)$$

The divergence factor (D) accounts for the fact that the ray reflected from the curved earth's surface diverges more rapidly than if the earth was flat. For moderate grazing angles ($0<G<G_c$)

$$D \approx \sqrt{\frac{a_eG.\sin\gamma.\cos\gamma}{(2G_1G_2/\cos\gamma+a_eG.\sin\gamma)(1+h_1/a_e)(1+h_2/a_e)}} \qquad (C-13)$$

.../C-3

The electromagnetic contribution to the phase difference ($\sum\phi_i$) and reflectivity (ρ) is obtained from the complex reflection coefficient

$$\Gamma = \rho e^{-j\phi} \tag{C-14}$$

These parameters are determined by the grazing angle (γ) and the complex dielectric constant of sea water.

$$\varepsilon_c = \varepsilon_1 - j\varepsilon_2 \tag{C-15}$$

$$= \varepsilon_1 - j60\lambda\sigma \tag{C-16}$$

where ε_1 and ε_2 are the real and imaginary parts of ε_c, λ is the wavelength and σ is the total sea water conductivity. The complex reflectivity for horizontal and vertical polarizations are

$$\Gamma_h = \frac{\sin\gamma - \sqrt{\varepsilon_c - \cos^2\gamma}}{\sin\gamma + \sqrt{\varepsilon_c - \cos^2\gamma}} \tag{C-17}$$

$$\Gamma_v = \frac{\varepsilon_c \sin\gamma - \sqrt{\varepsilon_c - \cos^2\gamma}}{\varepsilon_c \sin\gamma + \sqrt{\varepsilon_c - \cos^2\gamma}} \tag{C-18}$$

The real and imaginary parts of ε_c are evaluated from the expressions

$$\varepsilon_1 = 4.8 + \frac{(\varepsilon_s - 4.8)\left[1 + (\lambda_s/\lambda)^{1-\alpha}(\pi x 10^{-2})\right]}{1 + 2(\lambda_s/\lambda)^{1-\alpha}(\pi x 10^{-2}) + (\lambda_s/\lambda)^{2(1-\alpha)}} \tag{C-19}$$

$$\varepsilon_2 = \frac{(\varepsilon_s - 4.8)(\lambda_s/\lambda)^{1-\alpha}}{1 + 2(\lambda_s/\lambda)^{1-\alpha}(\pi x 10^{-2}) + (\lambda_s/\lambda)^{2(1-\alpha)}} + \frac{18\sigma_i}{f} \tag{C-20}$$

where $\alpha \simeq 0.02$, f is in GHz, λ_s is the wavelength corresponding to the dielectric relaxation frequency, ε_s is the static dielectric constant and σ_i is the ionic conductivity in mho/metre. Variations in salinity and surface temperature are taken into account through the empirical expressions (reference 24, 25)

$$\varepsilon_s = 87.8 - 15.3N - 0.363T \tag{C-21}$$

$$100\lambda_s = 3.38 - 0.11T + 0.00147T^2 + 0.0173TN - 0.52N \text{ metres} \tag{C-22}$$

$$\sigma_i = 5N + 0.12TN + 0.04T \tag{C-23}$$

in which T is the temperature in degrees Celsius and N is the electrolyte

.../C-4

normality (equivalents/litre). The relevant temperature is the water 'skin' temperature, and the default value in the model is the sea level air temperature. The default value for salinity is N=0.6 (3.4%).

Equations C-19 and C-20 include a parameter α which accounts for the non-Lorentzian spectral distribution due to the spread in relaxation frequencies in the region of 15 GHz. Contributions to ε_1 from water can be ignored at UHF frequencies where it is dominated by the $18\sigma_i/f = 60\lambda\sigma_i$ term as shown in figure C-2 in which ε_1 and ε_2 are plotted up to 100 GHz for T=0, 15 and 30°C. At higher temperatures the dielectric relaxation processes are faster ($1/\tau \approx 20$GHz) resulting in strong temperature dependence of ε_1 and ε_2 in the frequency range of interest shown in the expanded scale of figure C-3.

Dielectric subroutines, employing the relations described above, were used to plot the phase and magnitude of the reflectivity in figures C-4 and C-5 (the apparent 2π phase difference at normal incidence is due to the sign convention for ϕ). Results for 1 and 35 GHz display significant temperature dependence of ρ and ϕ for vertical polarization.

The dielectric reflectivity (ρ) is multiplied by the roughness factor (r) to obtain the overall reflectivity in equation C-3. Reference 1, using data for vertical coverage diagrams for several sea states, stresses the importance of a realistic model for the roughness factor. Although the literature provides <u>a priori</u> models for r (refs. 2, 26) these are in general not in good agreement with experimental data. The model uses a semi-empirical relation

$$r = e^{-2s^2} \qquad s < 0.6366$$
$$= e^{-1.2732s} \qquad \text{otherwise} \qquad \text{(C-24)}$$

where $s = \pi \bar{H}_{1/3} \sin\gamma / 2\lambda$ (C-25)

in which $\bar{H}_{1/3}$ is the significant wave height, which is approximately related to the Douglas sea state S_D by

$$\bar{H}_{1/3} \simeq 0.5\ S_D^2 \qquad \text{(C-26)}$$

for $\bar{H}_{1/3}$ in feet.

.../C-5

The Diffraction Region

Mechanisms for propagation over the horizon include diffraction, ducting, troposcatter and ionospheric reflection. In the absence of anomolous propagation and at the frequencies and ranges of interest for radar predictions, diffraction is the most important. The model assumes that for distances greater than 1.05 times the horizon range the single mode approximation to the diffraction field is adequate (ref.3). Using standard nomenclature

$$F = f(\theta_1)\sqrt{U(Z_1).U(Z_2).V(X)} \qquad \text{(C-27)}$$

where Z_1, Z_2 and X are the antenna and target heights and target range (in natural units) respectively, and θ_1 is the elevation angle to the horizon. The natural unit of range is (ref 27)

$$L = (a_e^2\lambda/\pi)^{1/3} \qquad \text{(C-28)}$$

and the natural unit of height is

$$H = \tfrac{1}{2}(a_e\lambda^2/\pi^2)^{1/3} \qquad \text{(C-29)}$$

The attenuation factor in dB is then

$$V(X) = 10.99+10\log_{10}X-17.55X \qquad \text{(C-30)}$$

For the height gain factors the model uses the approximate expressions given by Blake (ref.2)

$$\begin{aligned} U(Z) &= 20\log_{10}Z && Z<0.6 \\ &= -4.3+51.04[\log_{10}(Z/0.6)]^{1.4} && 0.6\leq Z\leq 1 \\ &= 19.85(Z^{0.47}-0.9) && \text{otherwise} \end{aligned} \qquad \text{(C-31)}$$

The Intermediate Region

Near the horizon (γ=0) the calculated divergence factor approaches zero and the ray theory expressions would predict F~1, whereas F~0 near the horizon. In the model ray theory is only used up to the critical ground range

.../C-6

$$G_c = a_e[\pi - 2\gamma_c - \sin^{-1}(a_e\cos\gamma_c/(h_2+a_e)) - \sin^{-1}(a_e\cos\gamma_c/(h_2+a_e))] \quad \text{(C-32)}$$

where γ_c is the critical grazing angle

$$\gamma_c = \tan^{-1}(\lambda/2\pi a_e)^{1/3} \quad \text{(C-33)}$$

Between this range and 1.05 times the horizon range it is assumed that F decays exponentially (i.e. linearly in decibels). This simple interpolation is used since the predicted detection range in the intermediate region is likely to be much more sensitive to a realistic model for target scintillation than the interpolation technique.

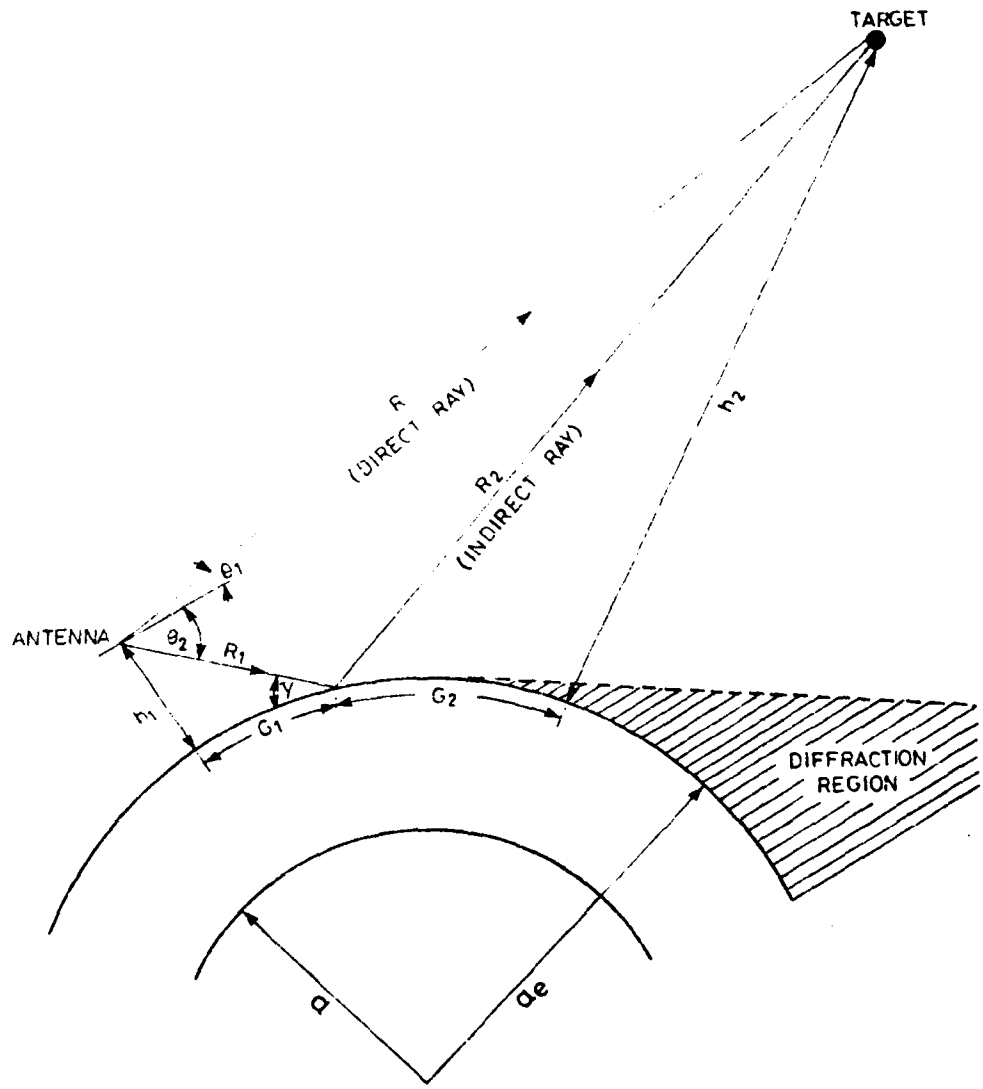

Figure C-1. Illustration of Multipath Geometry.

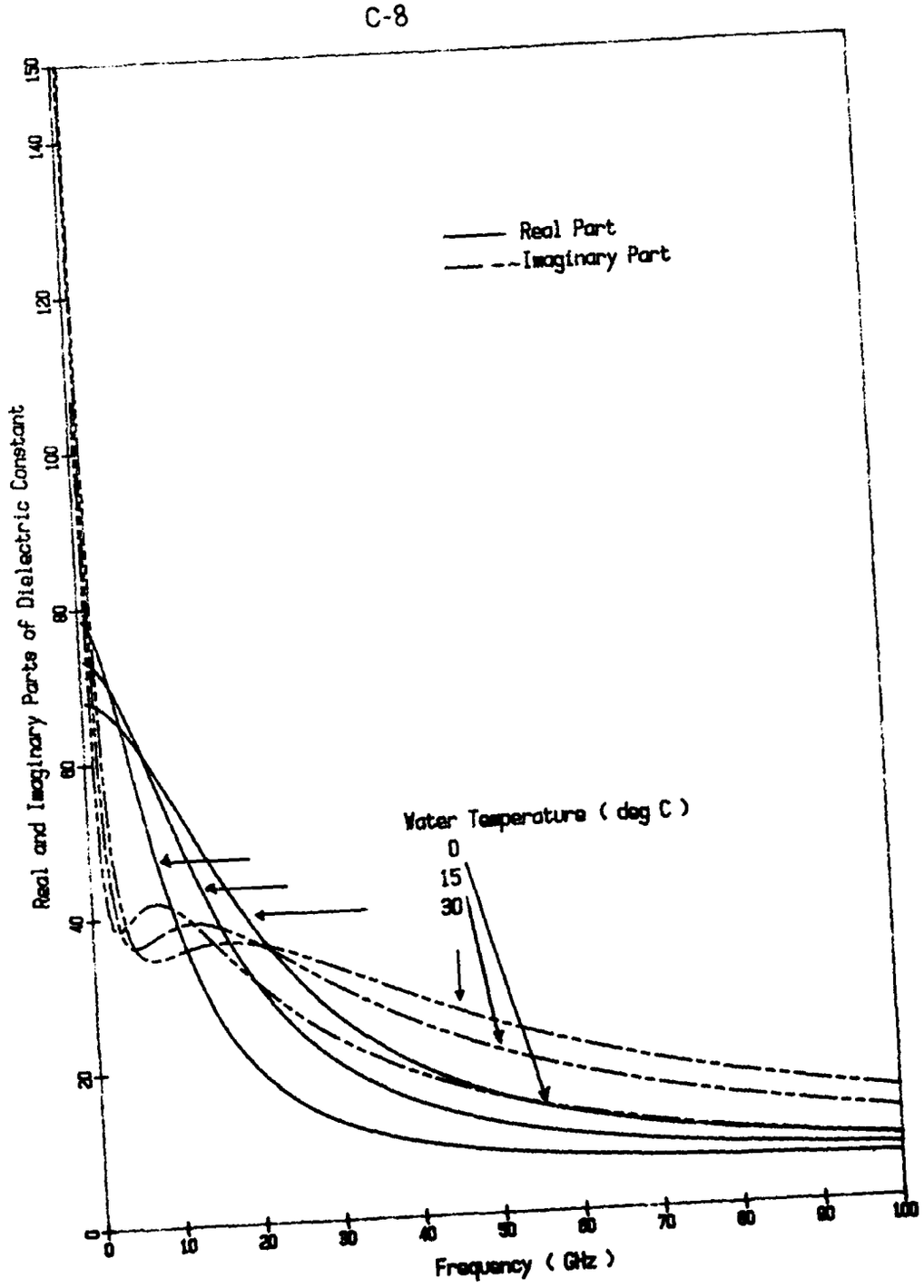

Figure C-2. Complex Dielectric Constant of Sea Water
Salinity is 3.4 %

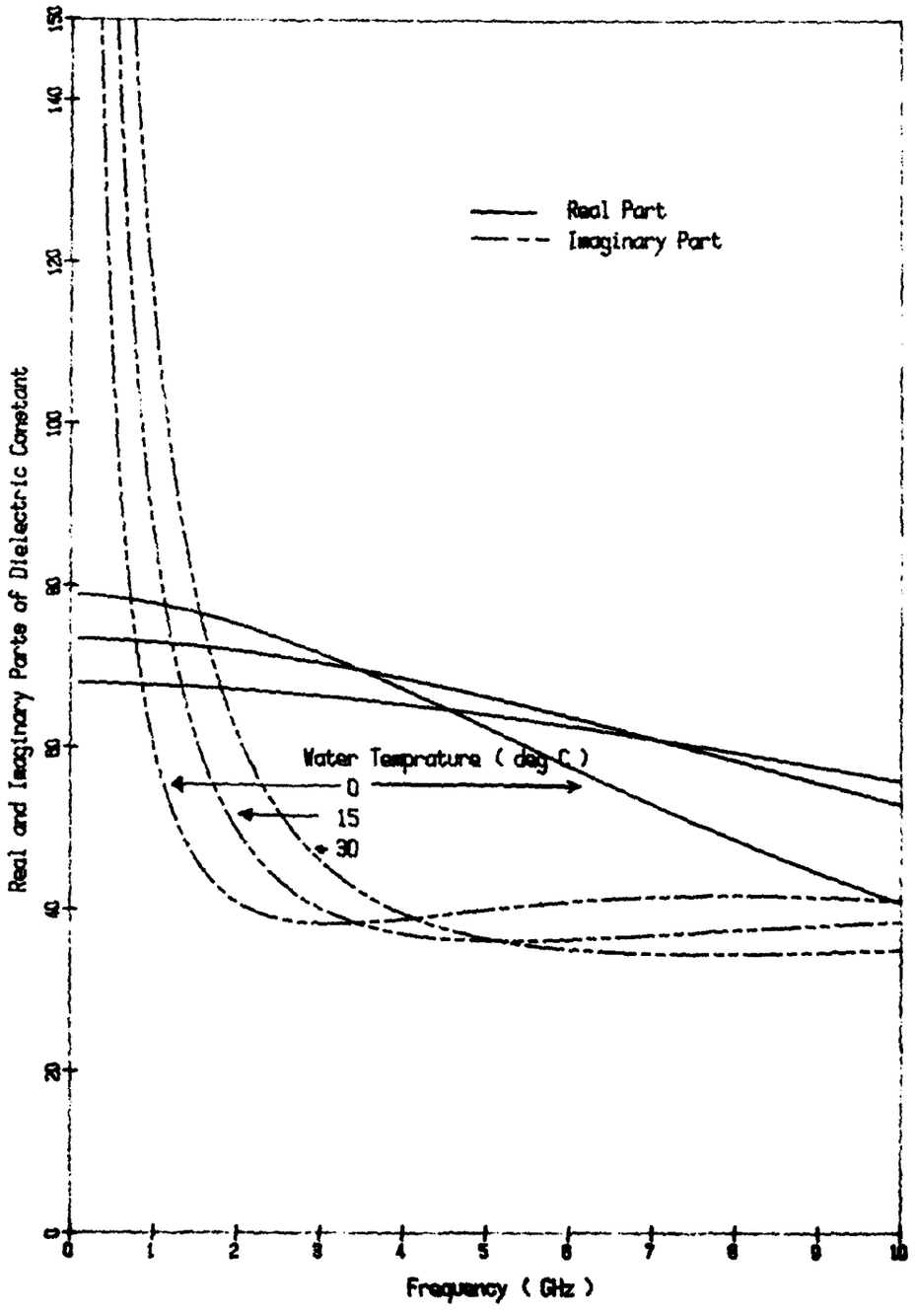

Figure C-3. Complex Dielectric Constant of Sea Water
Salinity is 3.4 %

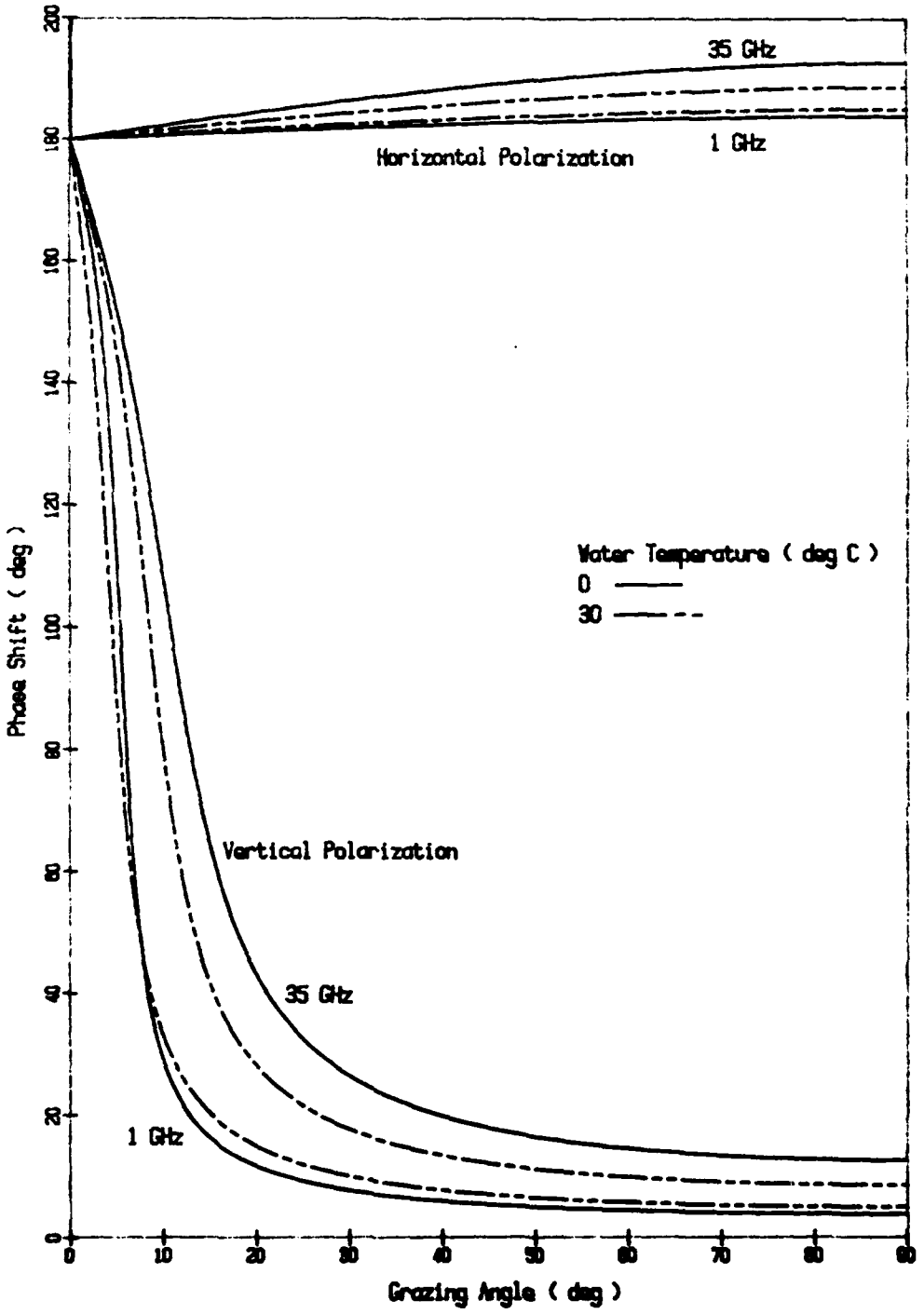

Figure C-4. Phase of Complex Reflectivity
Salinity is 3.4 %

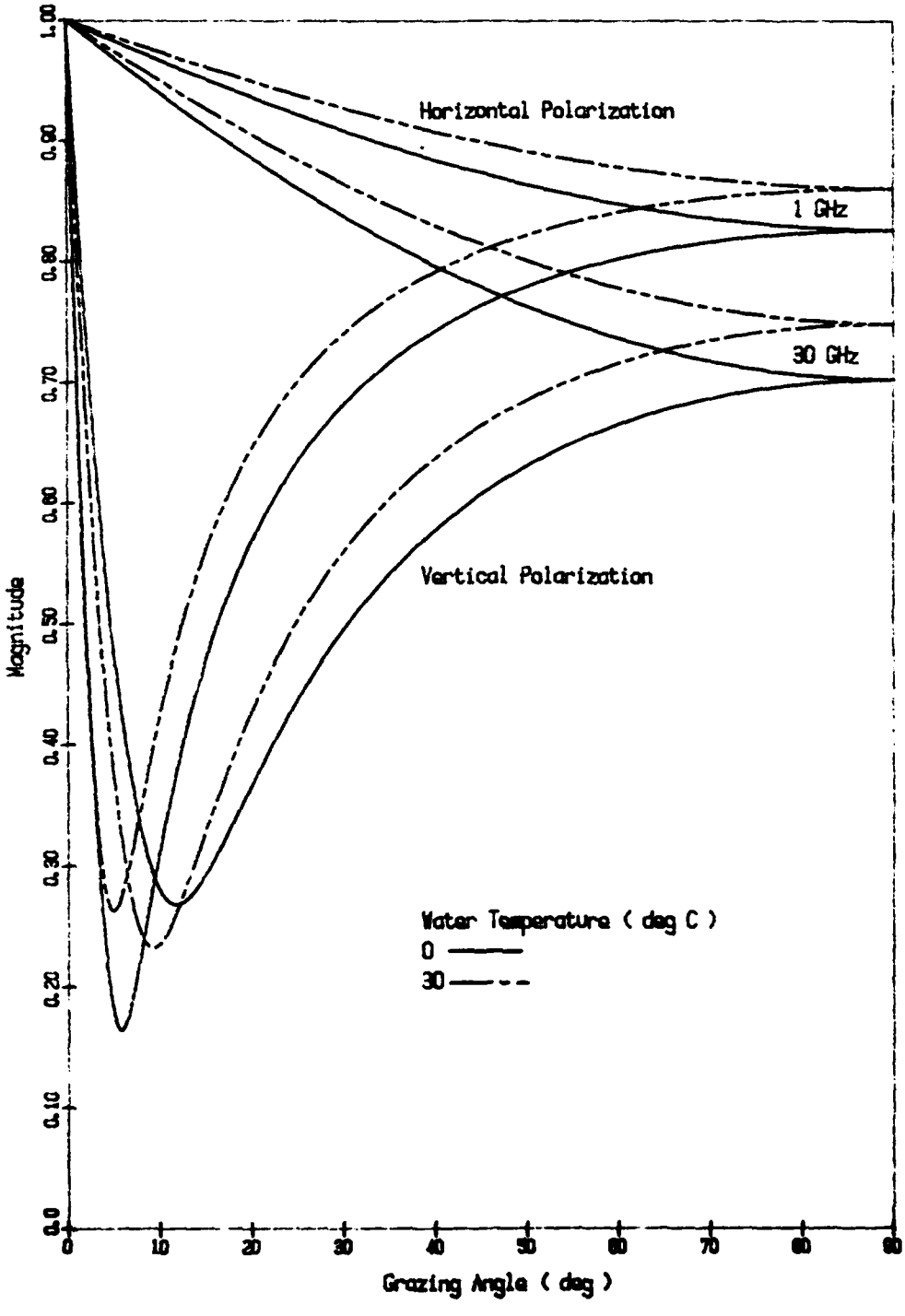

Figure C-5. Magnitude of Complex Reflectivity
Salinity ie 3.4 %

ANNEX D

ANTENNA PATTERN FUNCTION

The power gain (G) describes the distribution in elevation and azimuth of the power available at the antenna. In the model this appears as the product of the power along boresight (G_o) and the normalized antenna pattern function

$$G(\theta,\phi) = G_o E^2(\theta,\phi)$$
$$= G_o E_1(\theta).E_2(\phi) \qquad \text{(D-1)}$$

where $$G_o = \frac{4\pi\eta E^2_{max}}{\int_0^{2\pi}\int_0^{\pi} E^2(\theta,\phi)\sin\theta \; d\theta \; d\phi} \qquad \text{(D-2)}$$

for an antenna of effiency factor η. The required inputs to the antenna subroutines are (i) general type of antenna (pencil, etc.), (ii) horizontal and vertical 3-dB beamwidths (θ^H,θ^V), (iii) maximum power gain and (iv) the level of the first vertical sidelobe. If θ^H and θ^V are known, but not G_o, the default value is

$$G_o = 0.8\ (4\pi/\theta^H\theta^V) \qquad \text{(D-3)}$$

$E(\theta)$ can be calculated from the current distribution across the aperture, however usually only a few far field parameters are available from radar manuals. These parameters are used in the model to synthesize two general classes of antenna (i) modified (sin u)/u and (ii) cosecant squared. These patterns form the basis functions for other patterns. If the effects of aperture blockage are important, the pattern may be synthesized from a linear combination as described in reference 1.

Modified (sin u)/u

This pattern results from a one parameter aperture distribution of the form

$$A(z) = \frac{1}{2\pi} J_o(i\pi B\sqrt{1-4z^2/d^2}\,) \qquad \text{(D-4)}$$

where J_o is the Bessel function of the first kind and z is in the range $\pm d/2$. The resulting pattern is

.../D-2

$$E(\theta) = \frac{\sin \pi\sqrt{u^2-B^2}}{\pi\sqrt{u^2-B^2}} \qquad \text{(D-5)}$$

Equation D-5 is valid for real or imaginary arguments and is equivalent to

$$E(\theta) = \frac{\sinh \pi\sqrt{B^2-u^2}}{\pi\sqrt{B^2-u^2}} \qquad \text{(D-6)}$$

B is calculated from the sidelobe level by iteratively solving the relation

$$SL = (SL)_o \frac{\sinh \pi B}{\pi B} \qquad \text{(D-7)}$$

where $(SL)_o$ is the sidelobe voltage of the (sin u)/u pattern (~4.603). To normalize D-5 and D-6 the RHS is divided by the normalized sidelobe ratio (SL/4.603). This ratio also determines the aperture efficiency through the relation

$$\frac{SL}{(SL)_o} = \frac{\sqrt{2}\sinh \pi\sqrt{B^2-(\beta_o/2)^2}}{\pi\sqrt{B^2-(\beta_o/2)^2}} \qquad \text{(D-8)}$$

with

$$\beta_o = (d/\lambda)\ \theta^{3dB} \qquad \text{(D-9)}$$

Equations D-7 and D-8 are solved iteratively with the initial estimates given by the polynomial relations

$$B^2 = -0.6604597+0.03086396x+0.001323133x^2 +9.498675X10^{-6}x^3-1.040798X10^{-7}x^4 \qquad \text{(D-10)}$$

and

$$\beta_o = 0.58114+0.023468x+3.6432X10^{-5}x^2 -6.7425X10^{-6}x^3+7.9701X10^{-8}x^4 \qquad \text{(D-11)}$$

where x is the level of the first sidelobe in dB. The solutions for B^2 and β_o are plotted in figure D-1. Representative plots of $E(\theta)$ using equations D-5 to D-8 are shown in figures D-2 to D-4.

Cosecant Squared

These antennae are designed to detect, with constant return,

.../D-3

targets at constant altitude or displacement off the boresight (if the tilt is non-zero). The corresponding pattern is

$$E(\theta) = \frac{\sin(\theta^{3dB}/2)}{\sqrt{2}\sin\theta} \qquad 0.5\theta^{3dB} < \theta < \theta_{max}$$

$$= E_e(\theta) \qquad \text{elsewhere} \qquad \text{(D-12)}$$

where $E_e(\theta)$ is the pencil pattern described above. The gain of the cosecant squared antenna is less than the value determined by equation D-3 by a factor

$$\frac{G_a}{G} \simeq 2 - \frac{\theta^{3dB}}{2\tan(\theta_{max})} \qquad \text{(D-13)}$$

The default value of G for cosecant squared antennae is 3dB less than equation D-3 (i.e. $2\theta_{max} >> \theta^{3db}$ is assumed.) Plots of seaborne and airborne cosecant-squared patterns are shown in figures D-5 and D-6.

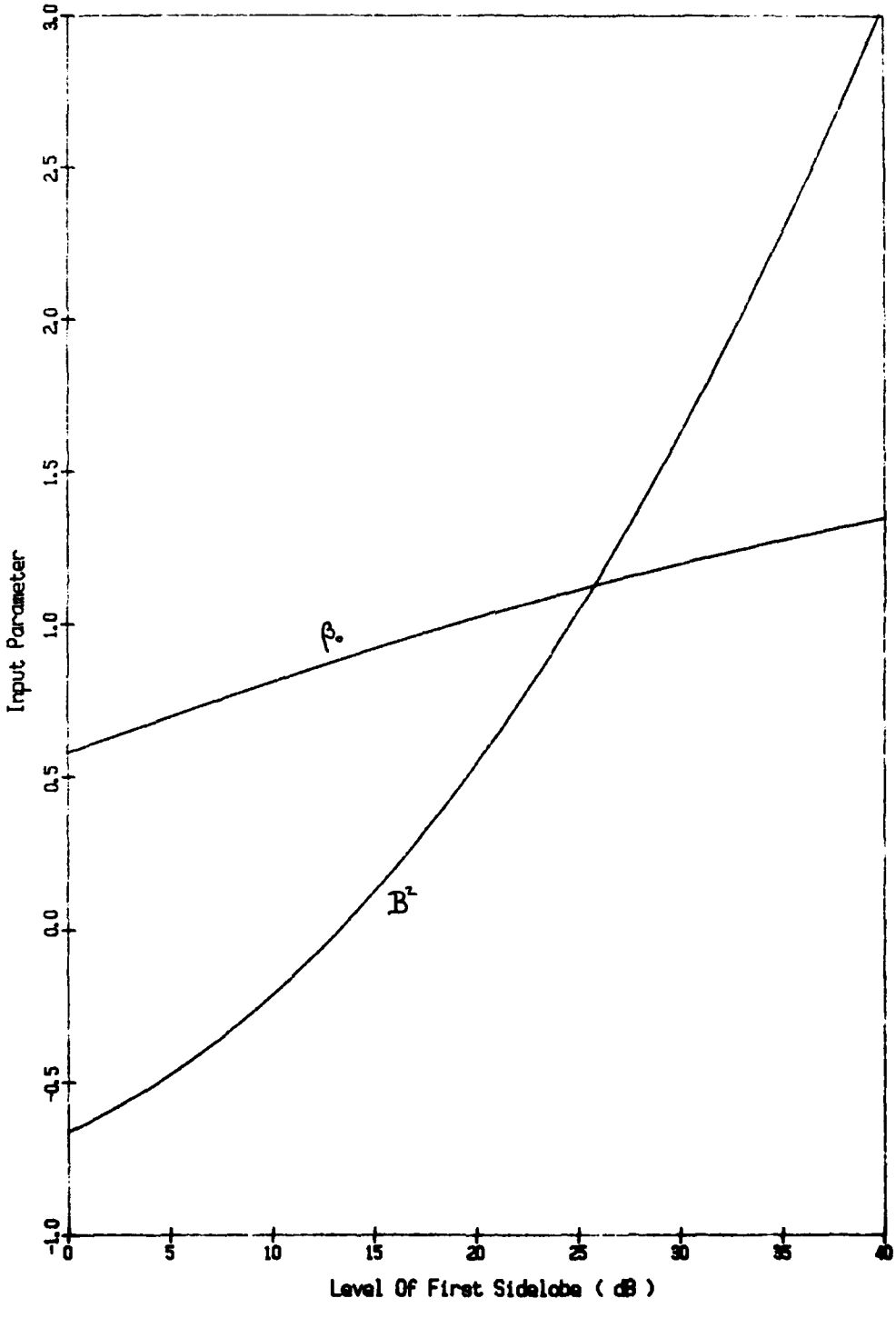

Figure D-1. Input Parameters For Modified (sin u)/u Pattern

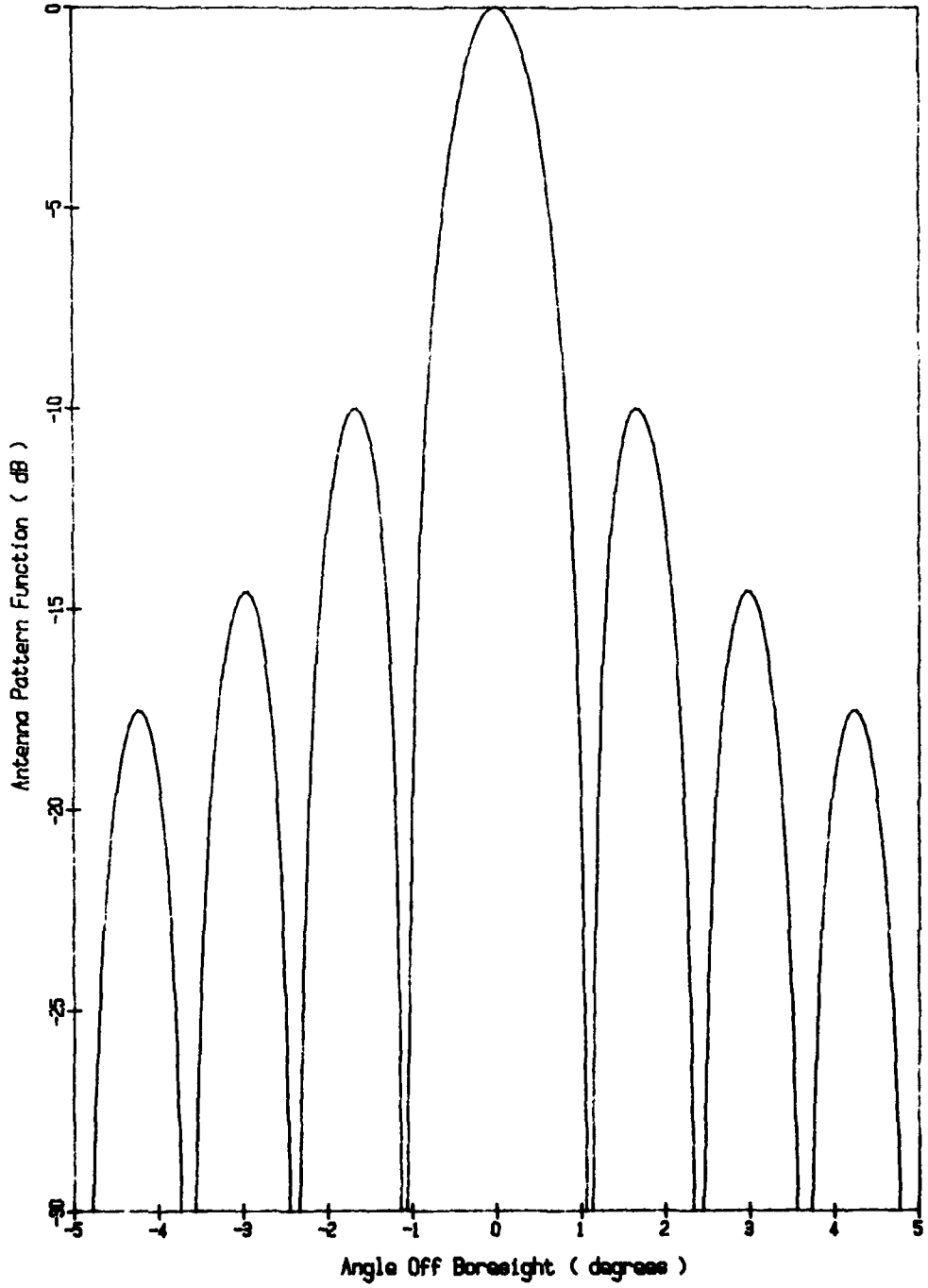

Figure D-2. Modified (sin u)/u Antenna Pattern Function
Level of First Sidelobe is 10 dB down
Half-power Beamwidth is 1 degree

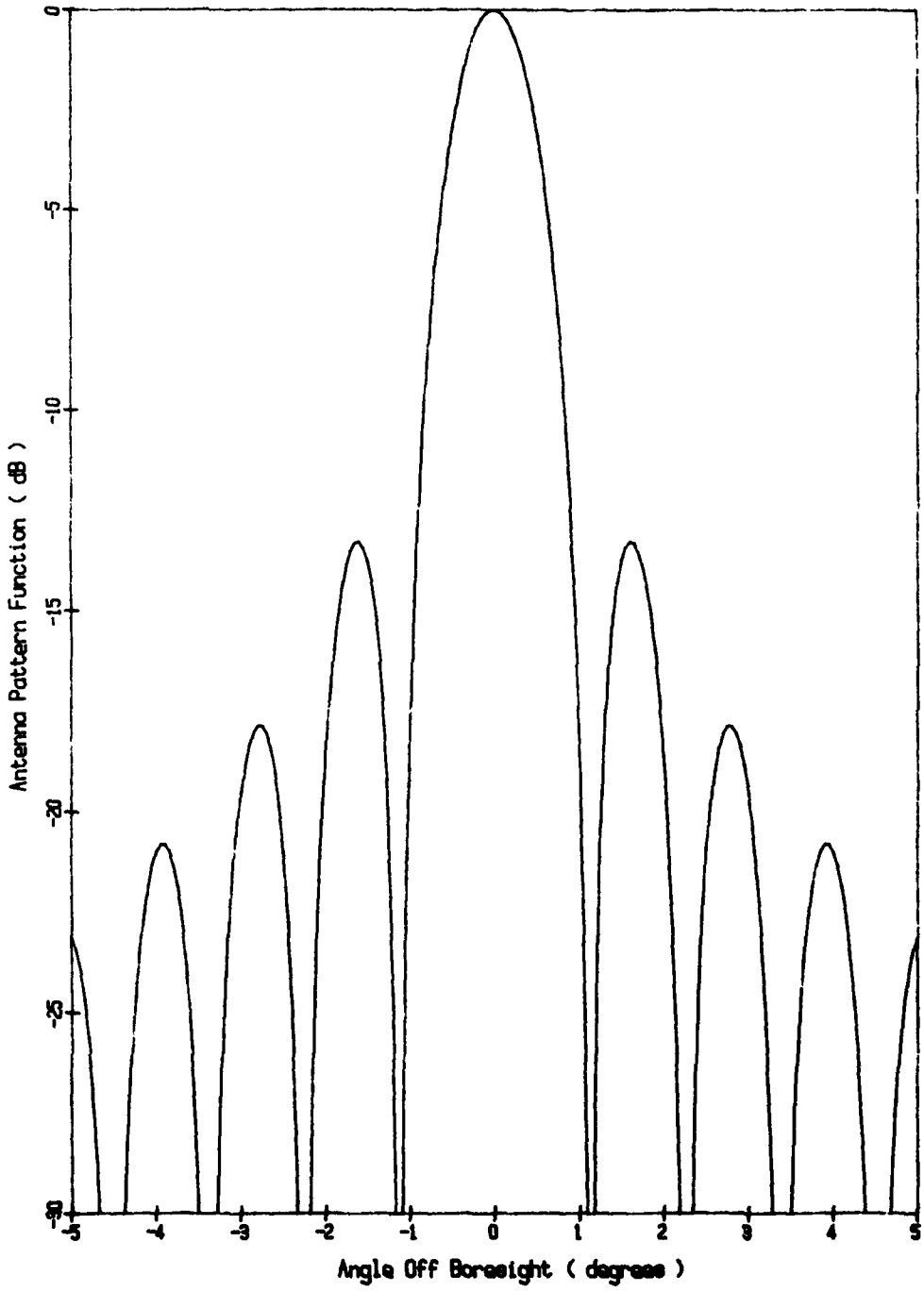

Figure D-3. Modified (sin u)/u Antenna Pattern Function
Level of First Sidelobe is 13.26 dB down
Half-power Beamwidth is 1 degree

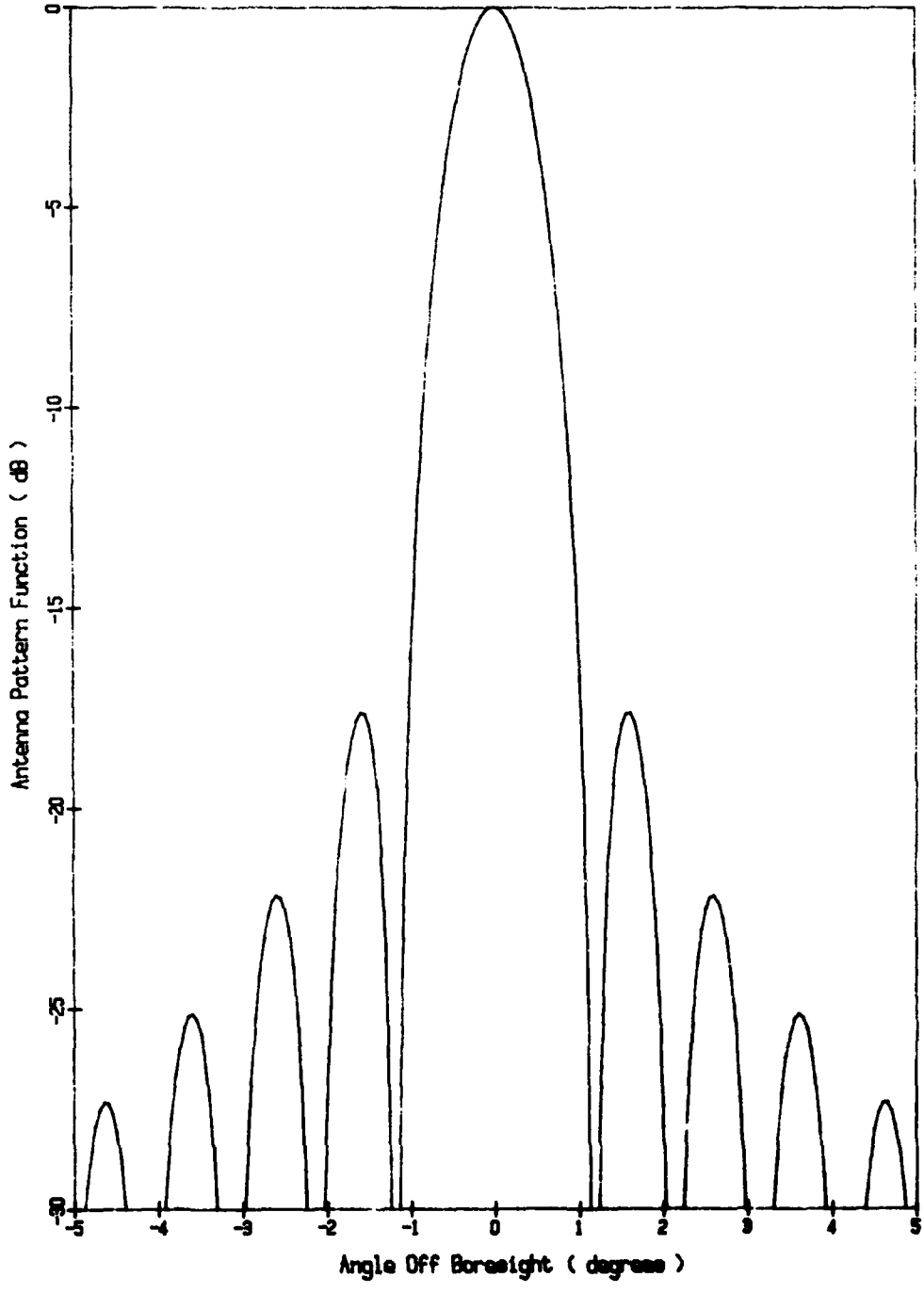

Figure D-4. Modified (sin u)/u Antenna Pattern Function
Level of First Sidelobe is 17.6 dB down
Half-power Beamwidth is 1 degree

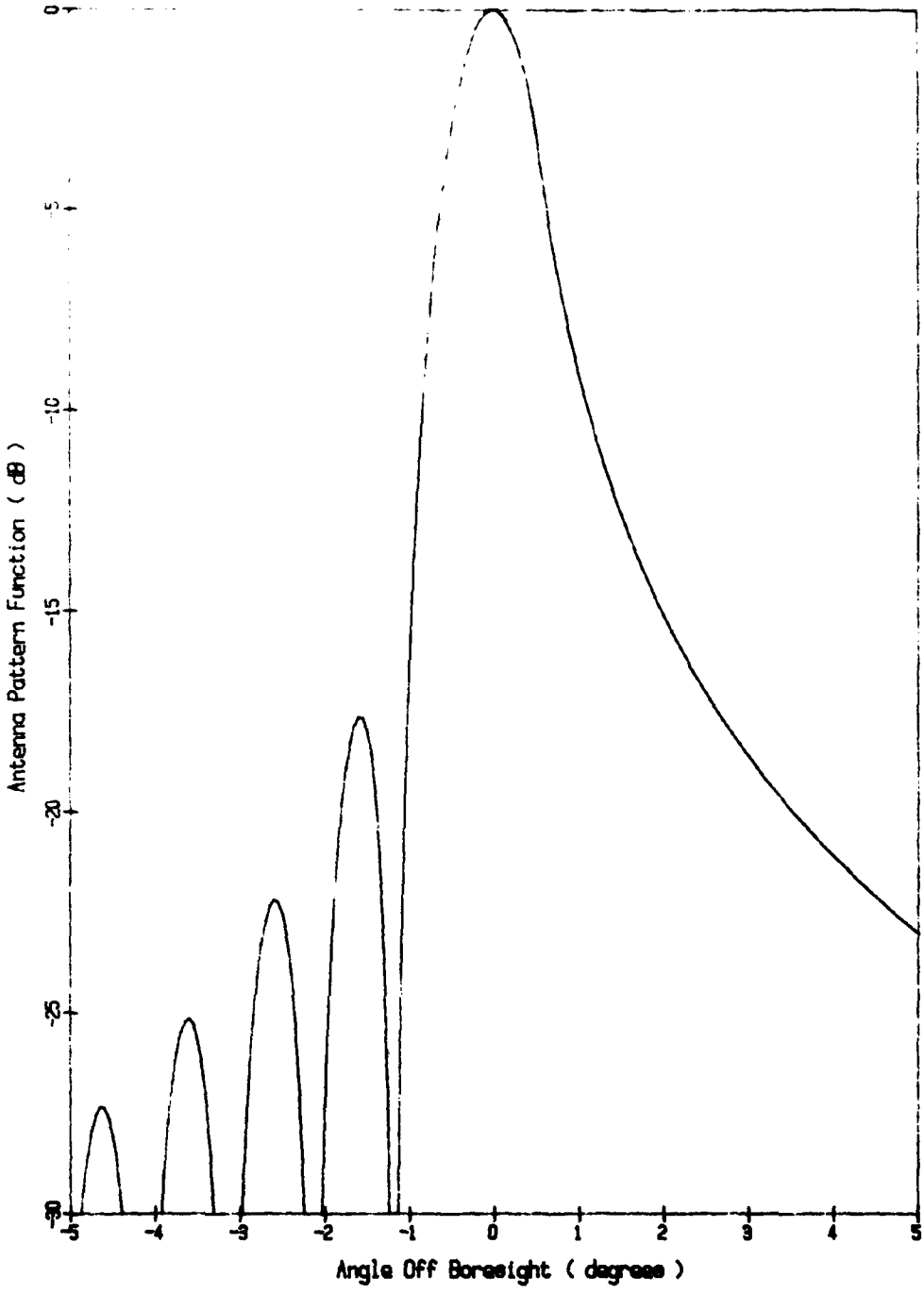

Figure D-5. Cosecant Squared Antenna Pattern Function (Seaborne)
Level of First Sidelobe is 17.6 dB
Half-power Beamwidth is 1 degree

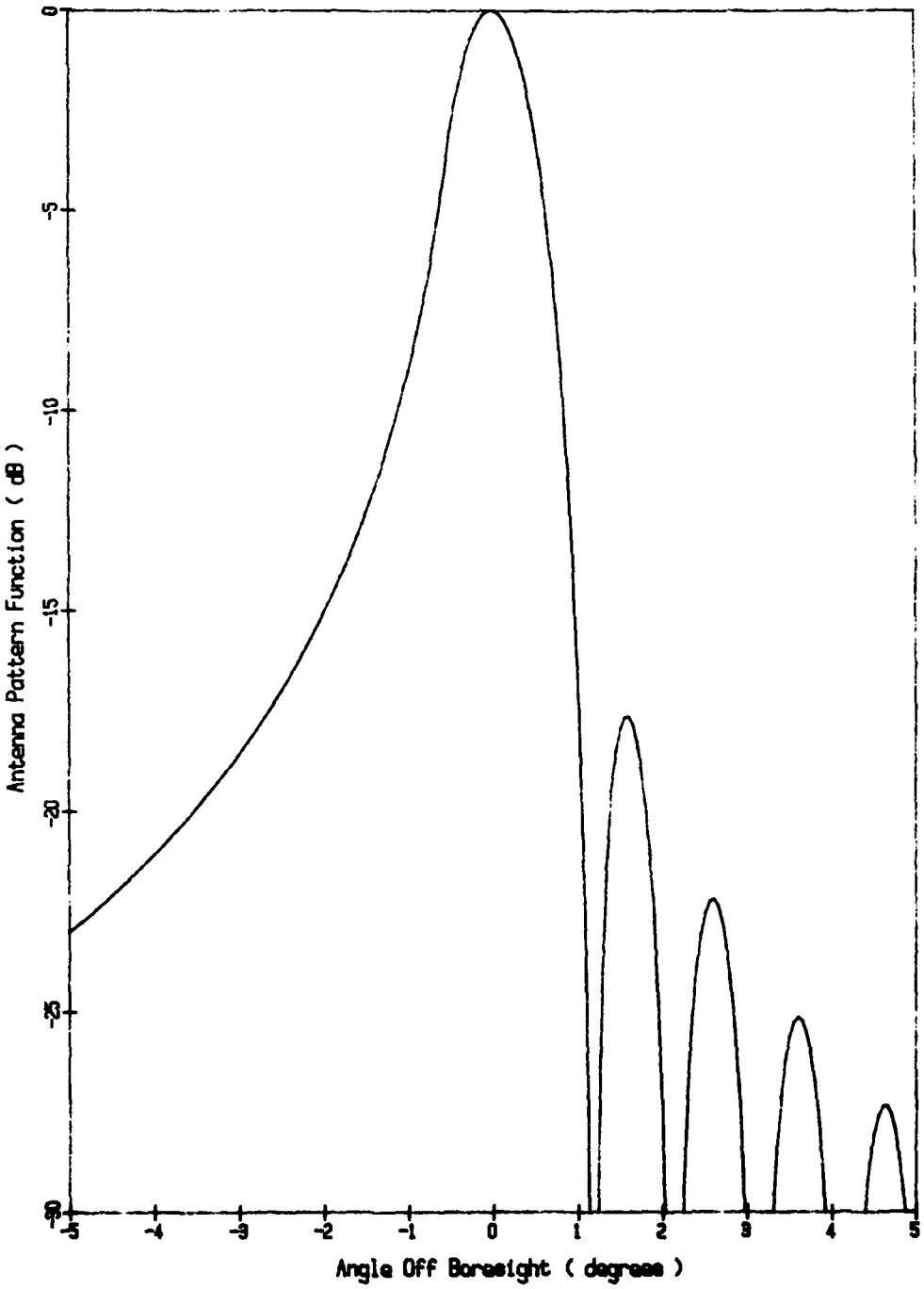

Figure D-6. Cosecant Squared Antenna Pattern Function (Airborne)
Level of First Sidelobe is 17.6 dB
Half-power Beamwidth is 1 degree

ANNEX E

ANTENNA NOISE TEMPERATURE

The antenna noise temperature accounts for the noise from the black body, cosmic and man made sources. If the antenna senses n noise sources of brightness temperature T_{bi} then

$$T_a = \frac{1}{4\pi}\sum_{i=1}^{n}\int_0^{2\pi}\int_0^{\pi} T_{bi}(\theta,\phi)G(\theta,\phi)\sin\theta \, d\theta \, d\phi \qquad \text{(E-1)}$$

where $G(\theta,\phi)$ is the antenna gain as a function of elevation and azimuth

$T_{bi}(\theta,\phi)$ is the noise temperature as a function of elevation and azimuth.

If the angle dependence $T_{bi}(\theta,\phi)$ of each noise temperature source is known then equation E-1 can be solved numerically. However, in this model a simplified approach is adopted, where the source is considered to be contained in a solid angle of average gain G and average brightness temperature T_{bi} and

$$T_a = \sum_i k_i \bar{T}_{bi} \qquad \text{(E-2)}$$

where k_i is the gain weighted solid angle divided by 4π. For reasons discussed later contributions from the sea are ignored, and for atmospheric and cosmic sources $k_i \simeq 0.9$ the following values are assumed.

$$k_{cos}T_{cos} = \frac{5.8X10^{23}.f^{-5/2} + 5}{L_A} \qquad \text{(E-3)}$$

$$k_{sun}T_{sun} = \frac{10^{5}.f^{-1}}{L_A} \qquad \text{(E-4)}$$

$$k_{atm}T_{atm} = 290\ (1-1/L_A) \qquad \text{(E-5)}$$

where f is the frequency in hertz, the resultant temperatures are in Kelvin and L_A is the total one-way atmospheric loss along the antenna boresight.

The total one-way atmospheric loss along the boresight is calculated in a manner similar to that discussed in Annex B for antenna to target absorption.

.../E-2

$$L_A = \sum_j L_{Aj} \qquad \text{(E-6)}$$

where L_{Aj} is the total one-way atmospheric loss due to constituent j. However, in this case it is necessary to integrate along the raypath from the antenna to infinity. There are two cases to be considered (i) where the tilt angle of the antenna is greater than the elevation angle of the horizon (and, therefore, the ray points directly at the sky) and (ii) where the tilt angle is less than the elevation angle of the horizon (and the ray is reflected from the sea surface).

$$L_{Aj} = \gamma_{jo}\int_o^\infty f(s)ds \qquad \text{when } \phi_t > \theta_h \qquad \text{(E-7)}$$

$$= \gamma_{jo}\int_o^R f(s)ds + \int_o^\infty g(s)ds \qquad \text{otherwise} \qquad \text{(E-8)}$$

where $f(s) = e^{-\frac{\sqrt{s^2+2s(a_e+h_1)\sin\phi_t+(a_e+h_1)^2}-a_e}{H_j}}$ (E-9)

$$g(s) = e^{-\frac{\sqrt{s^2+2sa_e\sin\gamma_o+a_e^2}-a_e}{H_j}} \qquad \text{(E-10)}$$

$$\gamma_o = \cos^{-1}[(1+h_1/a_e)\cos\phi_t] \qquad \text{(E-11)}$$

= grazing angle of boresight ray

$$R = \sqrt{a_e^2+4a_e(a_e+h_1)\sin^2[(\phi_t+\gamma_o)/2]} \qquad \text{(E-12)}$$

ϕ_t is the antenna tilt angle

h_1 is the antenna height

a_e is the earth's effective radius (see Annex A)

$$\theta_h = \sin^{-1}\left[\frac{a_e}{h_1+a_e}\right] - \frac{\pi}{2} \qquad \text{(E-13)}$$

= the elevation angle of the horizon

H_j is a constant for constituent j

γ_{oj} is the sea level absorption for constituent j (see Annex B)

The integrals in equations E-7 and E-8 do not lend themselves to analytical solution and numerical methods described at annex B are used. The integrals from zero to infinity are approximated by integrals from zero to an effective atmospheric limit R_e, which is the range that coincides with an assumed atmospheric thickness h_a (150 km in the model).

.../E-3

$$R_e = \sqrt{(h_a+a_e)^2-(h_1+a_e)^2\cos^2\theta_t} - (a_e+h_1)\sin\theta_t \qquad \text{(E-14)}$$

This enables equations E-7 and E-8 to be approximated by

$$L_{Aj} = \gamma_{jo} R_e \sum_{i=1}^{n} w_i f(x_i.R_e) \qquad \text{when } \theta_t > \theta_h \qquad \text{(E-15)}$$

$$= \gamma_{jo} R \sum_{i=1}^{n} w_i f(x_i.R) + R_e \sum_{i=1}^{n} w_i g(x_i.R_e) \qquad \text{otherwise} \qquad \text{(E-16)}$$

where x_i and w_i are tabulated in column k=0 of table 25.8 of reference 15 for various n. In this model n=8 is used, enabling the same subroutine to be used as is used to solve equation B-6.

Equations E-3 to E-5 are based on the assumption that all cosmic and black body radiation enters the antenna directly or by reflection from a perfectly reflecting sea. With airborne radar the boresight may be pointing into the sea at near the quasi-Brewster angle. The brightness temperature of the sea is

$$T_{b(sea)} = T_{t(sea)}(1-R(\theta))^2 \qquad \text{(E-17)}$$

where $T_{t(sea)}$ is the thermodynamic temperature and
$R(\theta)$ is the Fresnel reflection coefficient.

Using the subroutine described in annex C for $R(\theta)$, T_b has been plotted in figure E-1. At the maximum for T_b (5-10°) the error in T_a using only equations E-3 to E-5 is in the order of a few degrees and is therefore neglected.

In the cases where T_a does not contribute significantly to the total noise temperature, such as receivers with NF >> 5dB, approximate formulae may be used. Reference 1 gives approximate expressions for ground based radars. Equations E-3 to E-5 are used with

$$L_A \simeq \gamma_o[3.5+107(1-\tfrac{2|\theta|}{\pi})^{3.4}] \qquad \text{(E-18)}$$

where θ is the elevation angle and γ_o is the sea level attenuation in dB/n.mile.

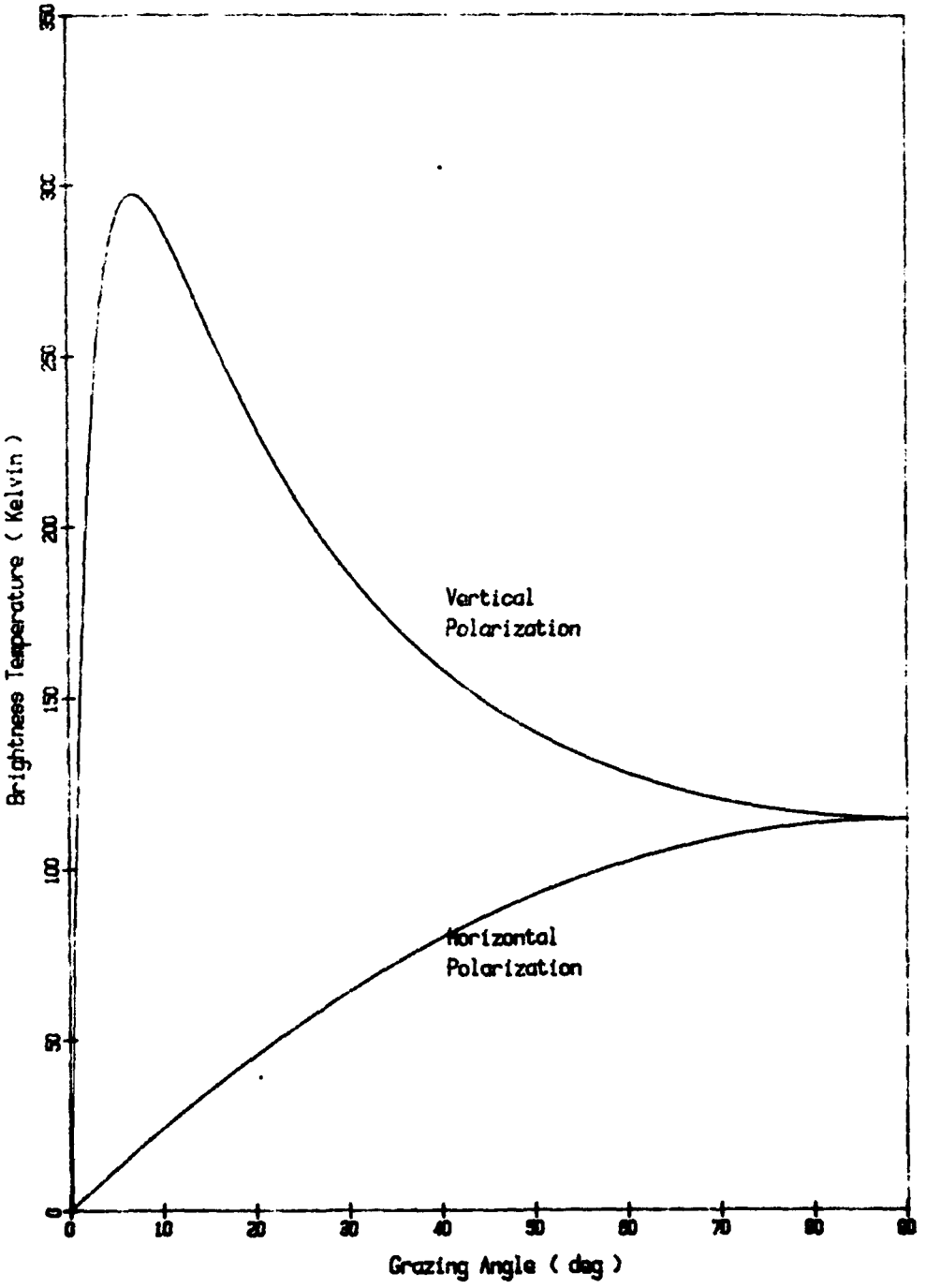

Figure E-1. Brightness Temperature of the Sea
Frequency is 10 GHz
Salinity is 3.4 %

ANNEX F

CLUTTER

Sea Clutter

The radar equation for sea clutter may be written as

$$P_c = \frac{P_t G^2 \lambda^2 f^4(\theta)}{(4\pi)^3 R^4} . \sigma(R,\gamma) \qquad (F-1)$$

where $f(\theta)$ is the antenna pattern function for the ray to the clutter cell which makes grazing angle γ at slant range R. For an irregular sea surface more than one ray is possible so that equation F-1 differs from the normal radar equation due to the implicit inclusion of multipath effects in the clutter cross section $\sigma(R,\gamma)$.

Clutter return depends on the area of sea illuminated in the minimum time resolution possible. For a matched-filter receiver with rectangular spectral envelope the corresponding range resolution (ΔR) is

$$\Delta R = c/2B \qquad (F-2)$$

for receiver bandwidth B. For simple uncoded pulses

$$\Delta R \simeq c\tau/2 \qquad (F-3)$$

where c is the speed of light and τ is the pulse width. For pulse compression radar the time-bandwidth product of the transmitted pulse equals the pulse compression ratio so that τ in equation F-3 can also be interpreted as the compressed pulse width.

Unlike point scatterers the clutter normally 'fills' the beam in azimuth. It is customary to assume an effective beamwidth ($\theta^H = \theta_{3dB}$) outside which the clutter return is negligible. This introduces an overestimate of ≈1.5 dB in the calculated clutter return for the types of antenna patterns discussed in Annex D. To compensate for this a smaller effective horizontal beamwidth is used in the calculations.

$$\theta^H = 0.75\ \theta_{3dB} \qquad (F-4)$$

.../F-2

The clutter cross section is then

$$\sigma(R,\gamma) = \sigma^{\circ} A \qquad \text{(F-5)}$$

where $A = 0.375\, R\theta^{H}_{3dB} c\tau_{comp} . \sec\gamma$

is the 'illuminated area' and σ° is the clutter cross-section per unit area.

There are numerous models for σ° in the literature (refs 2-6,28) however these do not in general give good agreement over the wide range of frequencies, grazing angle and pulse widths required for this model. It was considered more appropriate to develop a general semi-empirical model with frequency (f), grazing angle (γ) and sea state (S) as the only input parameters. The desired range of validity was 0.4 GHz$<$f$<$35 GHz, t$>$0.25μs and 0.1°$<\gamma<$10° and 0$<$S$<$6. Nathanson and others (refs 6, 28) have reported σ° over this range and these data were chosen to fit the semi-empirical parameters.

The grazing angle dependence of scatter from the sea surface can be divided into three regions. At near normal incidence (γ = 90°) the scatter is specular and is greater for smooth seas than for rough. At intermediate grazing angles the backscatter is only weakly dependent on surface roughness ('the plateau region'). Below some critical grazing angle (γ_c), which depends on the frequency and the surface roughness, the scatter is greater for rough seas than for smooth. The model is concerned with the region around γ_c.

At sea state 3, microwave backscatter is strongly correlated with the appearance of whitecaps. This enables γ_c to be estimated by analogy with backscatter from a target at a constant height and consideration of multipath effects (discussed at Annex C). Plots of the pattern propagation factor (F) for an array of scatterers at a height of 1.5 metres above sea level display typical interference lobing, with the lowest angle lobe at a grazing angle near the limit of ray theory applicability (Annex C). The lowest lobe maxima for 1 GHz and 10 GHz are observed at γ_c = 3° and 0.3° respectively. A linear interpolation is assumed for all frequencies at sea state 3

$$\gamma_c = \frac{3.0}{f(\text{GHz})} \text{ degrees} \qquad \text{(F-6)}$$

.../F-3

The sea state dependence of γ_c is complex, since the relative importance of physical scatterers (swell, sea, capillery waves and foam) changes with both frequency and sea state. In the absence of detailed experimental data near γ_c it is assumed that γ_c is inversely proportional to sea state. Fitting Nathanson's horizontal polarization data for $\tau>0.5$ μs, $0.1<\gamma<10°$, and an average of upwind/downwind data and sea state 3 :

$$\sigma°(dB/m^2/m^2) = -159 + 31.6\log(f) + 19.9\log(\gamma_c) + 170\log(\gamma/\gamma_c)/f^{0.4} \quad \text{for } \gamma<\gamma_c$$
$$= -159 + 19.9\log(\gamma) + 31.6\log(f) \quad \text{otherwise} \qquad (F-7)$$

for f in MHz and γ in degrees.

Data for vertical polarization does not exhibit a low angle plateau region and $\sigma°$ ($dB/m^2/m^2$) vs log γ is fairly linear over the region of interest. For sea state 3 and vertical polarization, the fit of Nathanson's data yields :

$$\sigma°(dB/m^2/m^2) = -30 + 410f^{-0.4}\log(\gamma/10) + 2.5\log(f/50000)\log(\gamma/\gamma_c^V) \quad \text{for } \gamma>\gamma_c^V$$
$$= -30 + 410f^{-0.4}\log(\gamma/10) \quad \text{otherwise} \qquad (F-8)$$

The critical angle for vertical polarization (γ_c^V) appears to be insensitive to wavelength and wave height and an arbitary value of 1° has been chosen.

Variations in the wave height affect not only the critical angle γ_c, but also fluctuations in numbers and positions of scatterers. This contribution appears to vary as the fourth power of sea state for horizontal polarization

$$\sigma°(S) = \sigma°(S=3) + 40\log(S/3) \qquad (F-9)$$

This simple behaviour is not seen for vertical polarization, where $\sigma°$ appears to vary by about 4.3 dB per sea state below sea state 3. Above sea state 3, where clutter is strongly correlated with the appearance of white caps, and shadowing occurs for low γ, $\sigma°$ seems to vary by only 3.5 dB per sea state.

Figures F-1 to F-6 show computed $\sigma°$ for typical radar and

.../F-4

environmental parameters. The overall level of agreement is ± 5 dB which is comparable with the accuracy of the data. Wind aspect dependence of σ° is not included in the model since the only data, which is for larger grazing angles (10 - 60 degrees), does not display a well behaved relation between σ° and aspect angle (ref 28). Most models assume some circular function, such as a cosine, to predict the wind aspect dependence of σ°. From the available data it is not clear that this is valid for the wide range of grazing angles and frequencies of interest. This model therefore accounts for wind aspect only as an additional uncertainty of ±5 dB in σ° for simulation purposes.

Non-integer sea states are allowed in the model in order to facilitate small variations in wave height for simulation purposes. Data for nominal sea state 0 in reference 6 was used to fit S=2/3 in the plots for horizontal polarization, consistent with Nathanson's comments about minimum wave height.

Amplitude and Temporal Statistics

The previous sub-section describes the calculation of median clutter return for UHF to microwave frequencies and low grazing angles. To calculate probability of detection from signal-to-clutter ratios a model is also required for the amplitude and temporal statistics of the clutter.

This model assumes that the clutter resolution cell is sufficiently large for a large number of independent scatterers of random phase to be detected. Under these conditions the clutter is Rayleigh distributed. A minimum area of 10^4 m^2 seems reasonable at I-band and corresponds to $\tau > 0.2$ μs ($B < 5$ MHz) and $\theta^R > 1^\circ$ for typical ranges. This range is confirmed by Nathanson's short-pulse I-band distribution (ref 6) which shows that the ratio of σ° to its standard deviation is near unity for horizontal polarization only for $\tau > 0.1$μs. Vertical clutter seems less spikey even at very small pulse widths, and the Rayleigh distribution is probably adequate for all pulse widths of interest.

A model of temporal statistics is required for estimation of some clutter reduction techniques. Within the range of validity of the Rayleigh

.../F-5

amplitude distribution, the clutter appears tc decorrelate on a millisecond timescale. This is not true for very short pulses where the decorrelation time may be of the order of several seconds. Under these conditions clutter returns at different frequencies may not be decorrelated, so that the criterion $\Delta f \gg 1/\tau$ for frequency agility decorrelation may not be valid. This subject requires deeper investigation before short-pulse decorrelation techniques can be modelled adequately.

In summary the sea clutter model used in the programs is expected to produce realistic probabilities of detection for $\tau > 0.2$ µs, $0.4 < f < 35$GHz, sea states 0 tc 6, $0.1° < \gamma < 10°$, horizontal or vertical polarization for standard pulse radars.

Volume Clutter

The volume clutter cross section (σ) is

$$\sigma = \sigma_v V = \sigma_v \cdot \frac{\pi}{4} R^2 \theta^H \theta^V \Delta R \qquad \text{(F-10)}$$

where R is the slant range, θ^H and θ^V are the effective beamwidths ($\sim\pi/4$ times the 3dB beamwidth) and the range resolution ΔR is

$$\Delta R = c/2B \qquad \text{(F-11)}$$

for matched filter of bandwidth B.

Rain

The specific clutter cross section (σ_v) is strongly frequency dependent. At UHF and low microwave frequencies (<10GHz) Rayleigh scattering behaviour applies and, ignoring multiple scattering effects

$$\sigma_v = \frac{\pi^5}{\lambda^4} \left| \frac{\varepsilon_c - 1}{\varepsilon_c + 2} \right|^2 \sum_i d_i^6 = \frac{\pi^5}{\lambda^4} |K|^2 Z \qquad \text{(F-12)}$$

where ε_c is the complex dielectric constant of water, d_i is the diameter of the ith scatterer and the summation is over all particles in the clutter cell. Using the formulae for ε_c (for pure water) described in annex C.

$$|K|^2 = 0.93 \pm 0.01 \qquad \text{(F-13)}$$

.../F-6

over the range of frequencies and temperatures of interest. An empirical expression for the reflectivity (Z) is (ref 4)

$$Z = 2X10^{-16}\ r^{1.6} \qquad \text{(F-14)}$$

where r is the rainfall rate in mm/hour. Combining equations F-12 to F-14

$$\sigma_v = \frac{5.7X10^{-14}}{\lambda^4}\ r^{1.6} \qquad \text{(F-15)}$$

Snow

Snow can be treated in a similar manner due to a fortuitous cancellation of small $|K|^2$ and large Z-r coefficient:

$$|K|^2 \simeq 0.20 \qquad \text{(F-16)}$$

$$Z \simeq 10^{-15}\ r^{1.6} \qquad \text{(F-17)}$$

where r is interpreted as the snowfall rate after the snow has melted (ref 4).

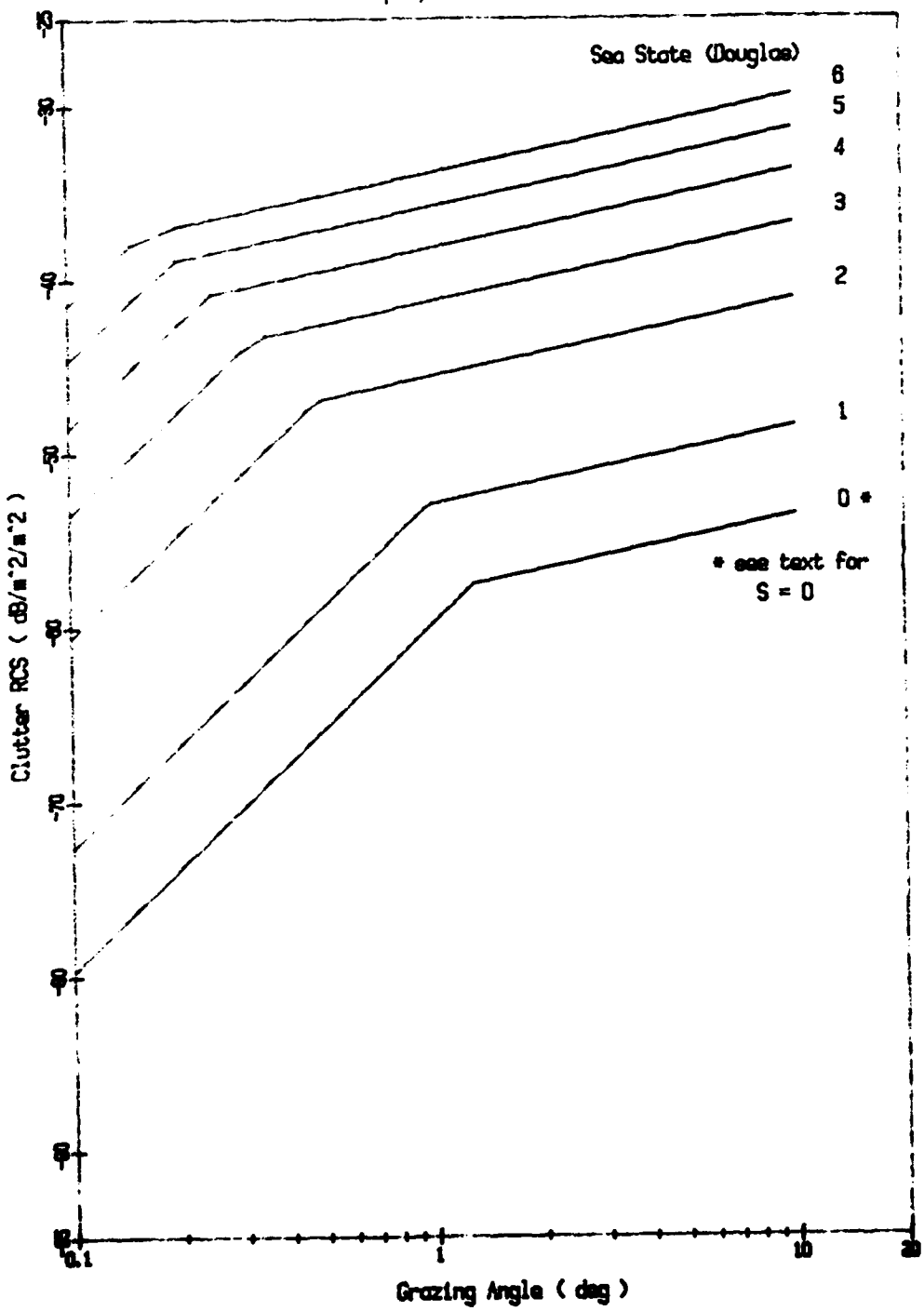

Figure F-1. Sea Clutter Cross-section at 9.3 GHz
Polarization is Horizontal

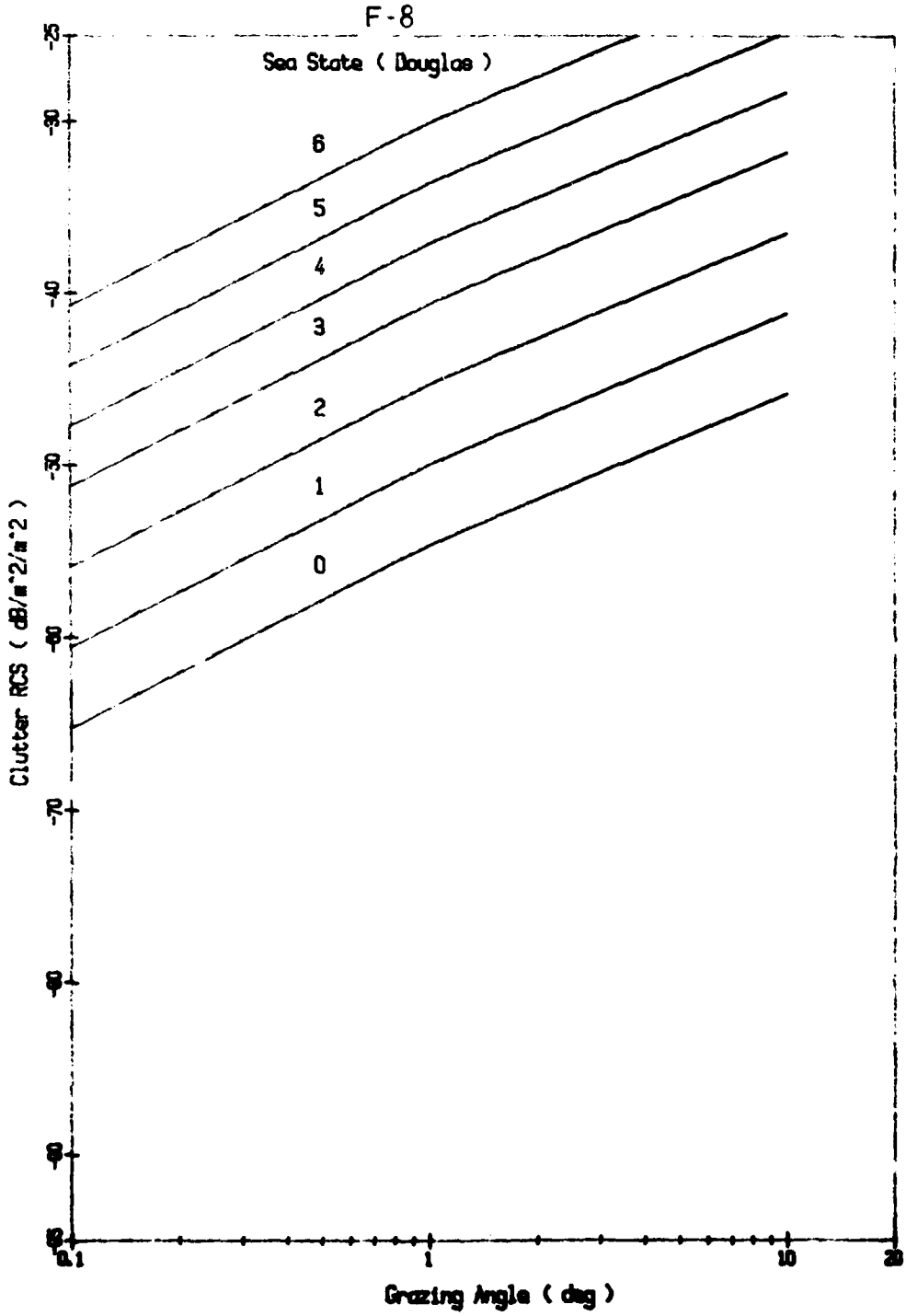

Figure F-2. Sea Clutter Cross-section at 9.3 GHz
Polarization is Vertical

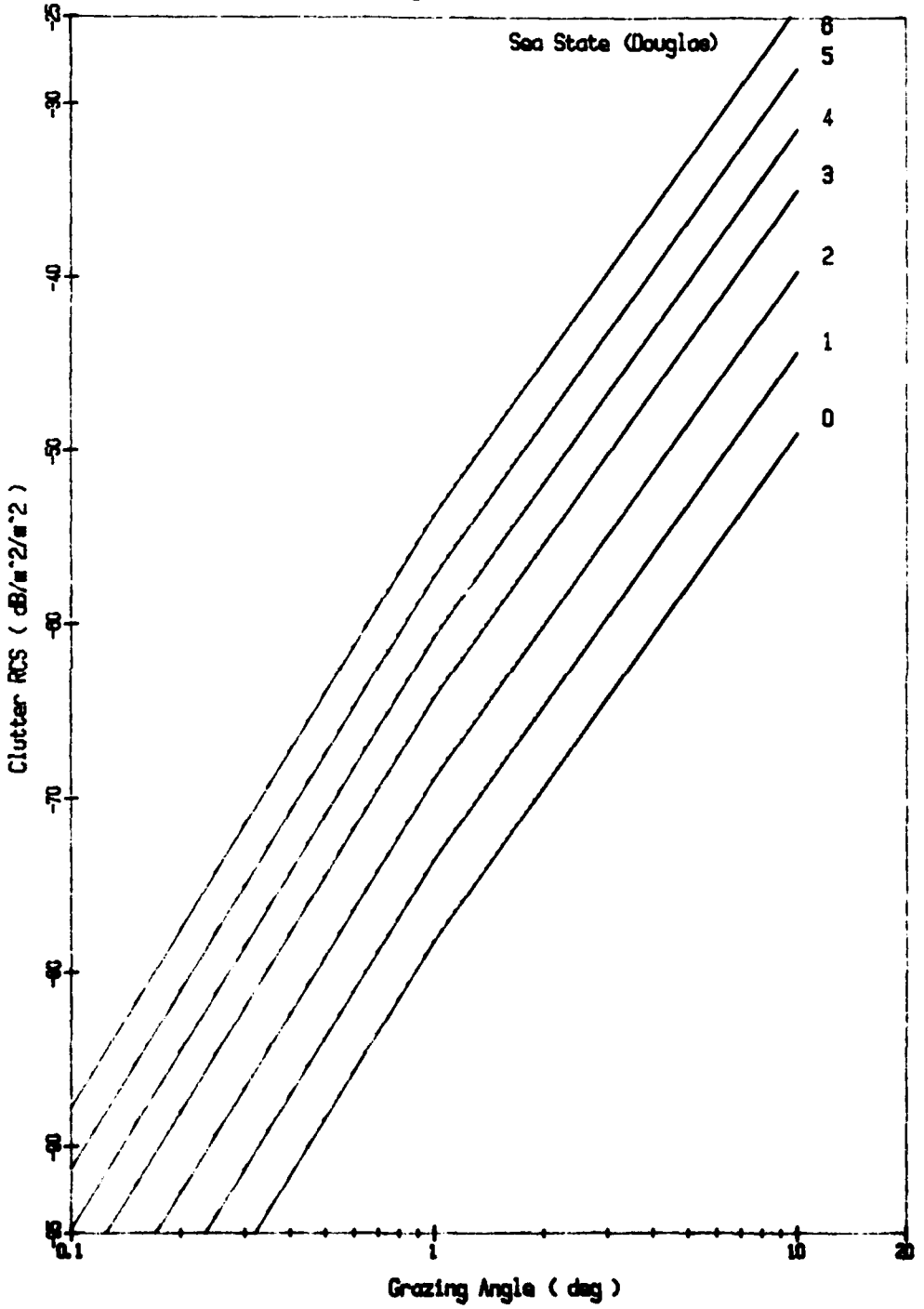

Figure F-3. Sea Clutter Cross-section at 500 MHz
Polarization is Vertical

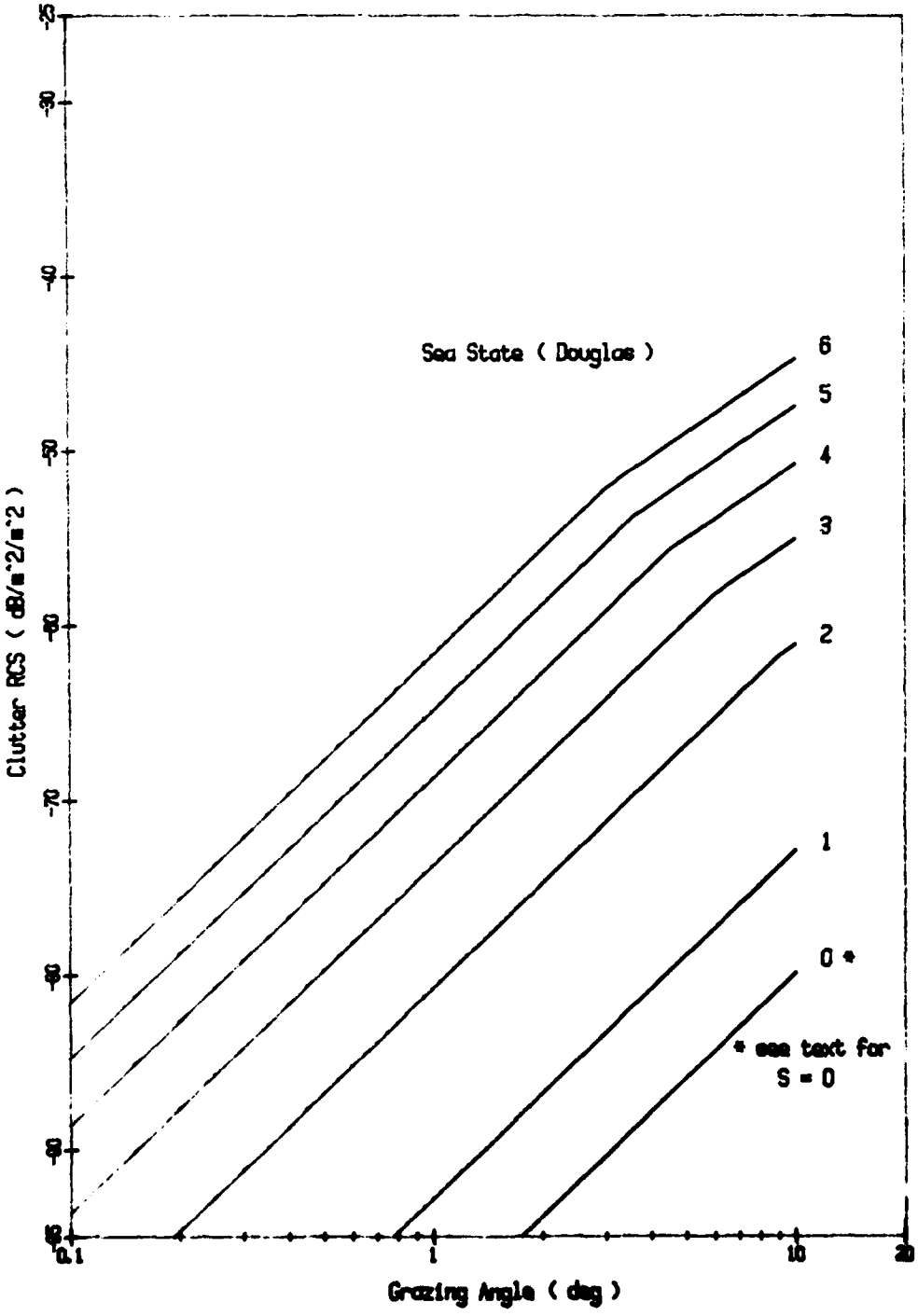

Figure F-4. Sea Clutter Cross-section at 500 MHz
Polarization is Horizontal

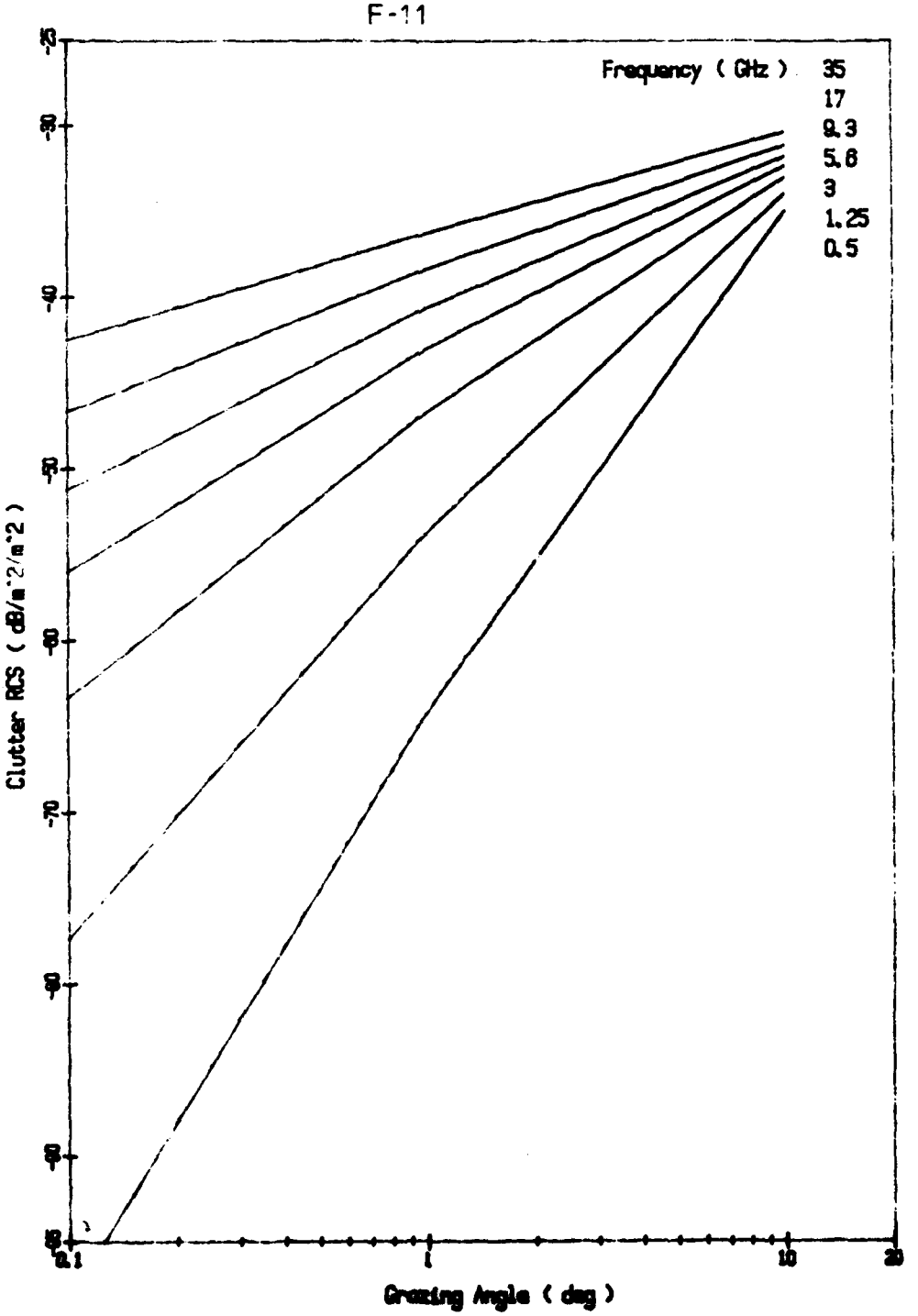

Figure F-5. Sea Clutter Cross-section for Sea State 3
Polarization is Vertical

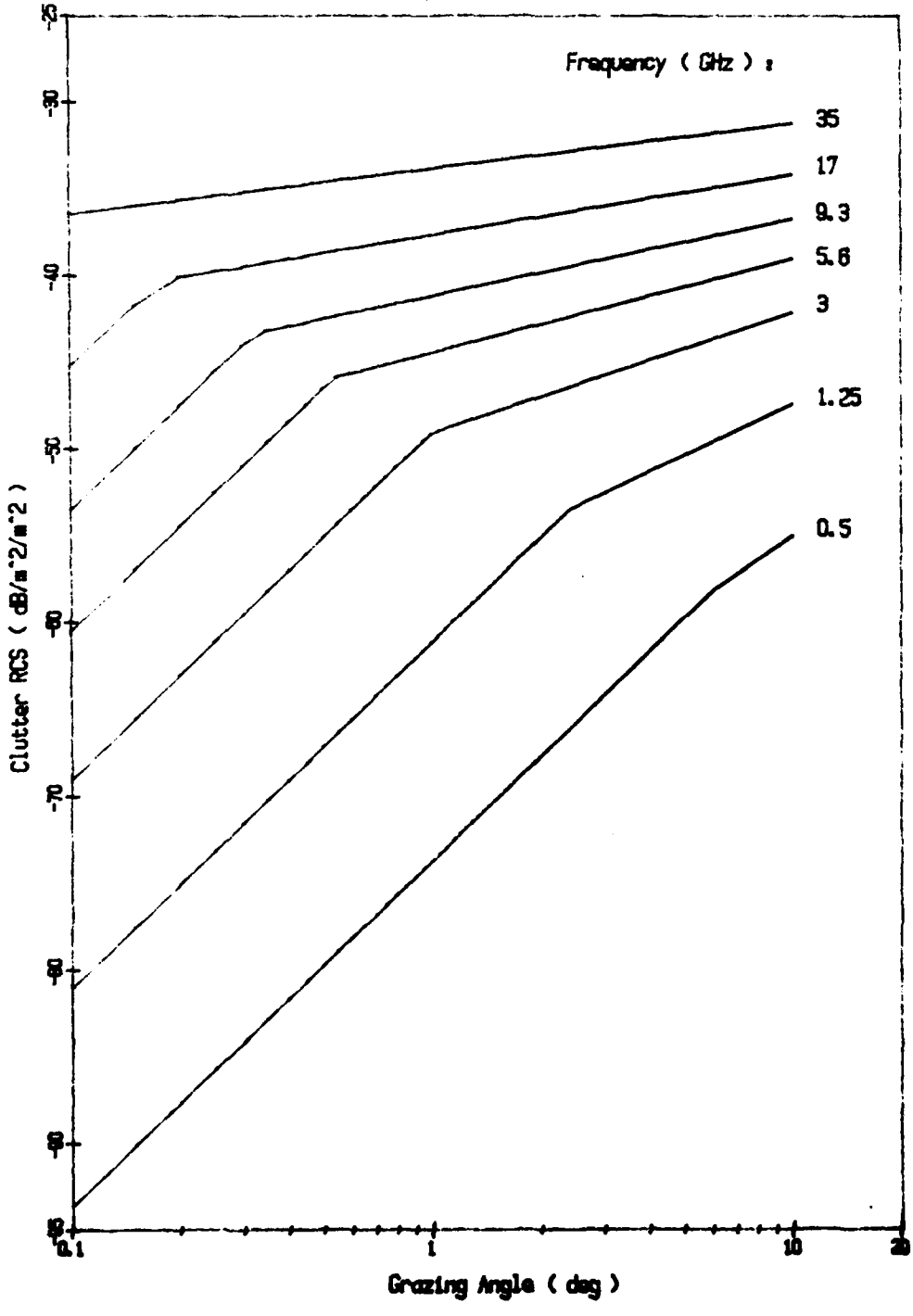

Figure F-6. Sea Clutter Cross-section for Sea State 3
Polarization is Horizontal

ANNEX G

PROBABILITY OF DETECTION

Probability of detection is calculated in the model for fixed and adaptive threshold (CFAR) detectors. Rayleigh amplitude statistics are assumed for the reciever noise and clutter, while the target can be non-fluctuating or of a generalized Chi-square distribution.

The general method for calculating paint probability has been described by Marcum (ref 16), Swerling (ref 17) and Rubin and Di Franco (ref 18). Recursive algorithms are similar to those described elswhere in the literature (refs 19, 20) with additional scaling algorithms to reduce the dependence of the results on the numerical precision and/or dynamic range of the computer in use.

Non-coherent Detection

Assuming Rayleigh noise/clutter statistics, the distribution of the integrated signal-plus-noise-plus-clutter variate (v) for a given integrated signal-to-noise-plus-clutter ratio (z), where v is normalized with respect to the average noise level is given by

$$f_N(v|z) = \sum_{n=0}^{\infty} z^n v^{N+n-1} e^{-(v+z)} \qquad \text{(G-1)}$$

where N = the number of pulses incoherently integrated

$z = Nx$

x = the single pulse signal-to-noise-plus-clutter ratio

Fixed Threshold

The probability that v will exceed a fixed threshold (Y) is given by

$$P(v>Y|z) = \int_Y f_N(v|z)\, dv$$

$$= \sum_{n=0}^{\infty} \frac{z^n e^{-z}}{n!} \sum_{m=0}^{N+n-1} \frac{Y^m e^{-Y}}{m!} \qquad \text{(G-2)}$$

For a non-fluctuating target it is sufficient to replace z with the mean

.../G-2

integrated signal-to-noise-plus-clutter ratio (Z) and evaluate this equation.

To determine this probability for a fluctuating target it is necessary to integrate over the target distribution w(z, Z) and

$$P_d = \int_0^\infty w(z,Z)\ P(v>Y|z)\ dz \qquad (G\text{-}3)$$

In this paper w(z, Z) is assumed to be in the form of the Chi-square distribution and

$$w(z,Z) = \left(\frac{K}{Z}\right)^K \frac{z^{K-1} e^{-\frac{Kz}{Z}}}{\Gamma(K)} \qquad (G\text{-}4)$$

where K is a distribution parameter selected as required to synthesize actual target fluctuations. K may only take positive values and is of the order of the number of independently fading scatterers. The four Swerling cases may be evaluated by substituting K = 1, N, 2, and 2N respectively. Substituting equation G-4 into equation G-3 and performing the necessary integration gives

$$P_d = \sum_{n=0}^{\infty} \frac{\Gamma(K+n)}{n!\,\Gamma(K)} \left(\frac{K}{K+Z}\right)^K \left(\frac{Z}{K+Z}\right)^n \sum_{m=0}^{N+n-1} \frac{Y^m e^{-Y}}{m!} \qquad (G\text{-}5)$$

The probability of false alarm (P_{fa}) is the probability that v will exceed Y in the absence of signal and may be found by substituting Z = 0

$$P_{fa} = \sum_{m=0}^{N-1} \frac{Y^m e^{-Y}}{m!} \qquad (G\text{-}6)$$

Constant False Alarm Rate (CFAR)

In the case of CFAR detection the fixed threshold Y is replaced by a variable threshold (y) which is derived from the sum (u) of R independent Rayleigh noise-plus-clutter samples of unit average power. Therefore u has the distribution

$$p(u) = \frac{u^{R-1} e^{-u}}{(R-1)!} \qquad (G\text{-}7)$$

Substituting y = u/T, where T is a calibrating factor, and performing the necessary integration gives the overall probability of v exceeding Y as

.../G-3

$$P_d = \sum_{n=0}^{\infty} \frac{\Gamma(K+n)}{n!\,\Gamma(K)} \left(\frac{K}{K+Z}\right)^K \left(\frac{Z}{K+Z}\right)^n \sum_{m=0}^{N+n-1} \frac{(R+m-1)!}{m!\,(R-1)!} \left(\frac{T}{T+1}\right)^R \left(\frac{1}{T+1}\right)^m \qquad (G-8)$$

As before the probability of false alarm may be found by substituting Z = 0 and

$$P_{fa} = \sum_{m=0}^{N-1} \frac{(R+m-1)!}{m!\,(R-1)!} \left(\frac{T}{T+1}\right)^R \left(\frac{1}{T+1}\right)^m \qquad (G-9)$$

Algorithms for P_d

Let

$$F(n) = \frac{Z^{n_e} - Z}{n!} \quad \text{for non-fluctuating targets}$$

$$= \frac{\Gamma(K+n)}{n!\,\Gamma(K)} \left(\frac{K}{K+Z}\right)^K \left(\frac{Z}{K+Z}\right)^n \quad \text{for fluctuating targets} \qquad (G-10)$$

$$G(m) = \frac{Y^{n_e} - Y}{n!} \quad \text{for fixed threshold detectors}$$

$$= \frac{(R+m-1)!}{m!\,(R-1)!} \left(\frac{T}{T+1}\right)^R \left(\frac{1}{T+1}\right)^m \quad \text{for CFAR detectors} \qquad (G-11)$$

so that

$$P_{fa} = \sum_{m=0}^{N-1} G(m) \qquad \text{for all cases} \qquad (G-12)$$

Now, $$\sum_{n=0}^{\infty} F(n) = \sum_{m=0}^{\infty} G(m) = 1 \qquad (G-13)$$

and $$P_d = \sum_{n=0}^{\infty} F(n) \sum_{m=0}^{N+n-1} G(m) \qquad (G-14)$$

Expanding this and regrouping the summations gives

$$P_d = \sum_{m=0}^{N-1} G(m) + \sum_{m=N}^{\infty} G(m) \left[1 - \sum_{n=0}^{m-N} F(n)\right]$$

$$= \sum_{m=0}^{N-1} G(m) + \sum_{m=N}^{B} G(m) \left[1 - \sum_{n=0}^{m-N} F(n)\right] + \sum_{m=B+1}^{\infty} G(m) \left[1 - \sum_{n=0}^{m-N} F(n)\right]$$

where B>N (G-15)

Therefore

$$P_d = \sum_{m=0}^{N-1} G(m) + \sum_{m=N}^{B} G(m) \left[1 - \sum_{n=0}^{m-N} F(n)\right] + \varepsilon \qquad (G-16)$$

where the error term

.../G-4

$$\varepsilon = \sum_{m=B+1}^{\infty} G(m)\left[1 - \sum_{n=0}^{m-N} F(n)\right] \qquad \text{where } B>N \qquad \text{(G-17)}$$

$$< \left(1 - \sum_{m=0}^{B} G(m)\right)\left(1 - \sum_{n=0}^{B-N} F(n)\right) \qquad \text{(G-18)}$$

This error term may be used to truncate the infinite summation when a specified error limit is reached. Alternatively, the expressions

$$H = \sum_{m=0}^{N-1} G(m) + \sum_{m=N}^{B} G(m)\left[1 - \sum_{n=0}^{m-N} F(n)\right] \qquad \text{(G-19)}$$

and

$$I = \sum_{m=0}^{N-1} G(m) + \sum_{m=N}^{B} G(m)\left[1 - \sum_{n=0}^{m-N} F(n)\right] + \left(1 - \sum_{m=0}^{B} G(m)\right)\left(1 - \sum_{n=0}^{B-N} F(n)\right) \qquad \text{(G-20)}$$

both converge on

$$P_d = \sum_{m=0}^{N-1} G(m) + \sum_{m=N}^{\infty} G(m)\left[1 - \sum_{n=0}^{m-N} F(n)\right] \qquad \text{as } B\to\infty \qquad \text{(G-21)}$$

The value of I converges more rapidly on P_d than does that of H and is therefore used in the model. Summation is terminated when successive estimates of P_d differ by less than a specified amount and the 'error term' is less than 0.1/N. (This latter condition is necessary to prevent premature truncation of the series for high signal-to-noise-plus-clutter ratios).

Recursive Relations

The terms in the infinite series are evaluated recursively using the following relations :

a. $F(n+1) = \frac{Z}{n+1} F(n)$

with $F(0) = e^{-Z}$ for non-fluctuating targets (G-22)

b. $F(n+1) = \frac{K+n}{n+1} \frac{Z}{K+Z} . F(n)$

with $F(0) = \left(\frac{K}{K+Z}\right)^K$ for fluctuating targets (G-23)

c. $G(m+1) = \frac{B+n}{n+1} \frac{1}{1+I} . G(m)$

.../G-5

with $G(0) = \left(\frac{T}{T+1}\right)^R$ for CFAR detection (G-24)

d. $G(m+1) = \frac{Y}{m+1} . G(m)$

with $G(0) = e^{-Y}$ for fixed threshold detection (G-25)

Evaluation of Threshold

In most applications of the model, the user wishes to calculate the performance of the radar for a given false alarm rate or probability of false alarm and it is therefore necessary to calculate a value for the threshold as a function of the probability of false alarm.

When the number of pulses integrated (N) is 1, the solutions are given by

$Y = - \log_e (P_{fa})$ for fixed threshold detection (G-26)

and

$T = Z / (1 - Z)$ for CFAR detection (G-27)

where $Z = exp [\log_e(P_{fa}) / R]$

When $N > 1$, there is no analytical solution and the value of Y is determined by Newton's method. The relationship between Y and P_{fa} described at equation G-6 does not satisfy all of the prerequisites for Newton's method and therefore the following well-behaved, normalised function is used

$g(X) = \log_e[f(X) / P_{fa}]$ (G-28)

and succesive iterations for the solution of $g(X) = 0$ are

$Y_{k+1} = Y_k - \frac{f(Y_k)}{f'(Y_k)} . g(Y_k)$ (G-29)

For the fixed threshold detector Y replaces X and

$f(Y) = \sum_{m=0}^{N-1} \frac{e^{-Y} Y^m}{m!}$ (G-30)

.../G-6

and

$$f'(Y) = -\frac{e^{-Y}Y^{N-1}}{(N-1)!} \tag{G-31}$$

which yields

$$Y_{K+1} = Y_K + \frac{\sum_{m=0}^{N-1} G(m)}{G(N-1)} \cdot \log \frac{\sum_{m=0}^{N-1} G(m)}{P_{fa}} \tag{G-32}$$

For CFAR detectors T replaces X and

$$f(T) = \sum_{m=0}^{N-1} \frac{(R+m-1)!}{m!(R-1)!} \left(\frac{T}{T+1}\right)^R \left(\frac{1}{T+1}\right)^m \tag{G-33}$$

and

$$f'(T) = \frac{R}{T} \sum_{m=0}^{N-1} \frac{(R+m-1)!}{m!(R-1)!} \left(\frac{T}{T+1}\right)^R \left(\frac{1}{T+1}\right)^m - \sum_{m=1}^{N} \frac{m(R+m-1)!}{m!(R-1)!} \left(\frac{T}{T+1}\right)^R \left(\frac{1}{T+1}\right)^m$$

$$= \frac{R}{T} \sum_{m=0}^{N-1} G(m) - \sum_{m=1}^{N} mG(m) \tag{G-34}$$

Number of Pulses Integrated: 2-D Radar

The number of pulses incoherently intgerated (N) for a scanning radar is assumed to be

$$N = \frac{\theta^H prf}{\dot{\theta}} \tag{G-35}$$

where θ^H is the horizontal beamwidth,
prf is the pulse repitition frequency in Hz, and
$\dot{\theta}$ is the target/boresight azimuth rate

$$\dot{\theta} = 6rpm + \frac{180V \cdot \sin\theta_r}{\pi R} \tag{G-36}$$

in which R is the target range, V is the target velocity in range units per sec and θ_r is the angle between the radar-target axis and the target velocity vector. The effect of the target term is neglected for routine calculations, since it is significant only for very short range crossing targets with small N. In the preceding sections N is rounded down to an integer value.

3-D Radar

Simultaneous azimuth and elevation scanning is normally performed

.../G-7

by phased array antennae. The number of hits per scan, ignoring target motion, is

$$N = \frac{\theta^H \theta^V p r f}{\delta \omega_v t_v r p m} \tag{G-37}$$

where ω_v is the vertical scan rate, t_v is the vertical scan period. Typical values for 3-D target indication radar are $(\theta^H.\theta^V) \simeq 4$ deg^2, 10rpm, prf = 500Hz, $\omega_v = 10^3$deg/sec, t_v = 30msec yielding $N \simeq 1$.

Elevation scanning is often performed by frequency jumping in discrete increments to provide one pulse per beam which are typically about $\frac{1}{2}\theta^V$ apart to ensure continuous vertical coverage. This means that there is a significant contribution up to the 2nd or 3rd beam off the line of sight and increases the effective number of pulses per scan by a factor of 2 or 3. If these pulses are integrated on a PPI an additional collapsing loss (L_c) must be included.

$$L_c = \Delta\theta/\theta^V \tag{G-38}$$

where $\Delta\theta$ is the total coverage.

Coherent Detection

The radar equation for coherent processing can be generalized in terms of signal-to-noise-plus-clutter energy ratios

$$\frac{E}{N_o} = \frac{(N_c P_t \tau) G_e^2 \lambda^2 \sigma F^4}{k T_s (4\pi)^3 R^4 L} \tag{G-39}$$

where τ is the radiated pulse width. The equivalent number of pulses N_c is considered for three detectors i) simple coherent processing, (ii) pulse doppler and (iii) pulse compression.

With simple coherent detection N_c is the number of pulses integrated. Assuming no post detection integration (N_i=1) the threshold level is given as

$$Y = -\log_e(P_{fa}) \tag{G-40}$$

Figures G-12 and G-13 show comparisons between pure coherent and

.../G-8

incoherent integrators with a non-fluctuating target. For a constant N, the incoherent processing loss is only weakly dependent on the signal-to-noise-plus-clutter ratio. Also near unity signal-to-noise-plus-clutter ratio the 'integration loss' varies only by a few dB between 1 and 100 pulses and can be represented by the simple empirical expressions described in the literature (ref 5).

Pulse doppler radar is also described by equation G-39 with

$$P_t \tau N_c \simeq P_t \tau prf / B_n = P_{av} / B_n \qquad \text{(G-41)}$$

where B_n is the doppler filter bandwidth, assuming that the range gate is of the order of one pulse width.

The analysis of pulse compression radar is essentially the same as for a radar which radiates at the compressed pulse width τ_c with increased power $P_t N_c$ where N_c is the time-bandwidth product (or pulse compression ratio)

$$P_t \tau_c N_c = P_t \tau = P_t N_c / B_n \qquad \text{(G-42)}$$

The effect of additional non-coherent integration has already been described. Frequency weighting is usually employed to reduce the time/range sidelobes below the 13 dB for unweighted linear FM. The family of Taylor weightings is commonly used, and are specified by a single parameter n. As n becomes large the sidelobe reduction, for a given pulse broadening, approaches that of the Dolph-Chebyshev weighting at the expense of total sidelobe energy. Typical performance figures are 50% pulse broadening for 25 to 45 dB sidelobe level resulting in a processing loss of 0.5 to 1.5 dB. The default value in the model is 1.5 dB.

Acquisition Probabilities

The probability of detection $P_N(\frac{m}{n})$ is the probability of achieving m points out of n successive trials (scans) for the first time on the Nth trial. Cumulative probability of detection $P_N^c(\frac{m}{n})$ is the probability that the target has been initially detected by the Nth trial, and the complement $Q_N^c(\frac{m}{n})$ is the probability that no initial detection has

.../G-9

occured by the Nth trial.

The previous section describes the calculation of probability of a paint p_i for a given scan i. Recursive algorithms for computing $P_N(\frac{m}{n})$, $P^c_N(\frac{m}{n})$ and $Q^c_N(\frac{m}{n})$ are described below

$$P^c_N(\tfrac{m}{n}) = 0 \qquad \text{for } N < m$$

$$= 1 - Q^c_N(\tfrac{m}{n}) \qquad \text{otherwise} \qquad \text{(G-43)}$$

$$P_N(\tfrac{m}{n}) = P^c_N(\tfrac{m}{n}) - P^c_{N-1}(\tfrac{m}{n})$$

$$= Q^c_{N-1}(\tfrac{m}{n}) - Q^c_N(\tfrac{m}{n}) \qquad \text{(G-44)}$$

The expansion of these expressions becomes more unweildy as more complex detection criteria are evaluated and no generalized m/n probability algorithms in terms of p_i are possible. In the current model three specific detection criteria are addressed, i) one-out-of-one, (ii) two-out-of-two and (iii) two-out-of-three, and algorithms are

1/1 Detection Criterion

$$Q^c_1(\tfrac{1}{1}) = (1 - p_1)$$
$$Q^c_N(\tfrac{1}{1}) = (1 - p_N)Q^c_{N-1}(\tfrac{1}{1}) \qquad \text{for } N>1 \qquad \text{(G-45)}$$

2/2 Detection Criterion

$$Q^c_1(\tfrac{2}{2}) = 1$$
$$Q^c_N(\tfrac{2}{2}) = (1 - p_N p_{N-1})Q^c_{N-1}(\tfrac{2}{2}) \quad \text{for } N>1 \qquad \text{(G-46)}$$

2/3 Detection Criterion

$$Q^c_1(\tfrac{2}{3}) = 1$$
$$Q^c_2(\tfrac{2}{3}) = 1 - p_1p_2$$
$$Q^c_3(\tfrac{2}{3}) = (1 - p_1p_2)(1 - p_3) + p_3(1-p_2)(1 - p_1)$$
$$Q^c_N(\tfrac{2}{3}) = (1 - p_N)Q^c_{N-1}(\tfrac{2}{3}) + p_N(1 - p_{N-1})(1 - p_{N-2})Q^c_{N-3}(\tfrac{2}{3})$$
$$\text{for } N>3 \qquad \text{(G-47)}$$

The development of similar recursive expressions for other m/n criteria

.../G-10

using Markov state diagrams has been described by Castella (ref 21) and Postema (ref 22).

Operator Efficiency

The probabilities p_i are probabilities of paint and do not take into account degradation in operator performance due to fatigue, etc. This results in an unrealistically narrow distribution in the detection range. In the model p_i is scaled by an operator efficiency factor p_{op} which represents the probability that the operator will see a paint given that a paint occurs.

Acquisition Range

Two quantities of interest are i) what is the probability that a detection occurs on a given target run and (ii) given that detection occured, what is the expected range? The former is simply the cumulative probability of detection $P_N^c(\frac{m}{n})$.

The expectation values of the detection delays N and N^2 are also calculated in the programs

$$\bar{N} = \sum N P'_N$$
$$\bar{N^2} = \sum N^2 P'_N \qquad \text{(G-48)}$$

where $P'_N = P_N / \Sigma P_N$

from which the mean and standard deviation of the acquisition time can be calculated

$$\bar{T} = \bar{N}\,\delta t \qquad \text{(G-49)}$$

$$\sigma_T = \delta t \sqrt{\bar{N^2} - \bar{N}^2} \qquad \text{(G-50)}$$

where δt is the time per scan. Also calculated are the median delay ($P_N^c(\frac{m}{n})$=0.5) and quartile ($P_N^c(\frac{m}{n})$=0.25,0.75) delays. These are especially relevant with multi-modal distributions produced in the multipath environment.

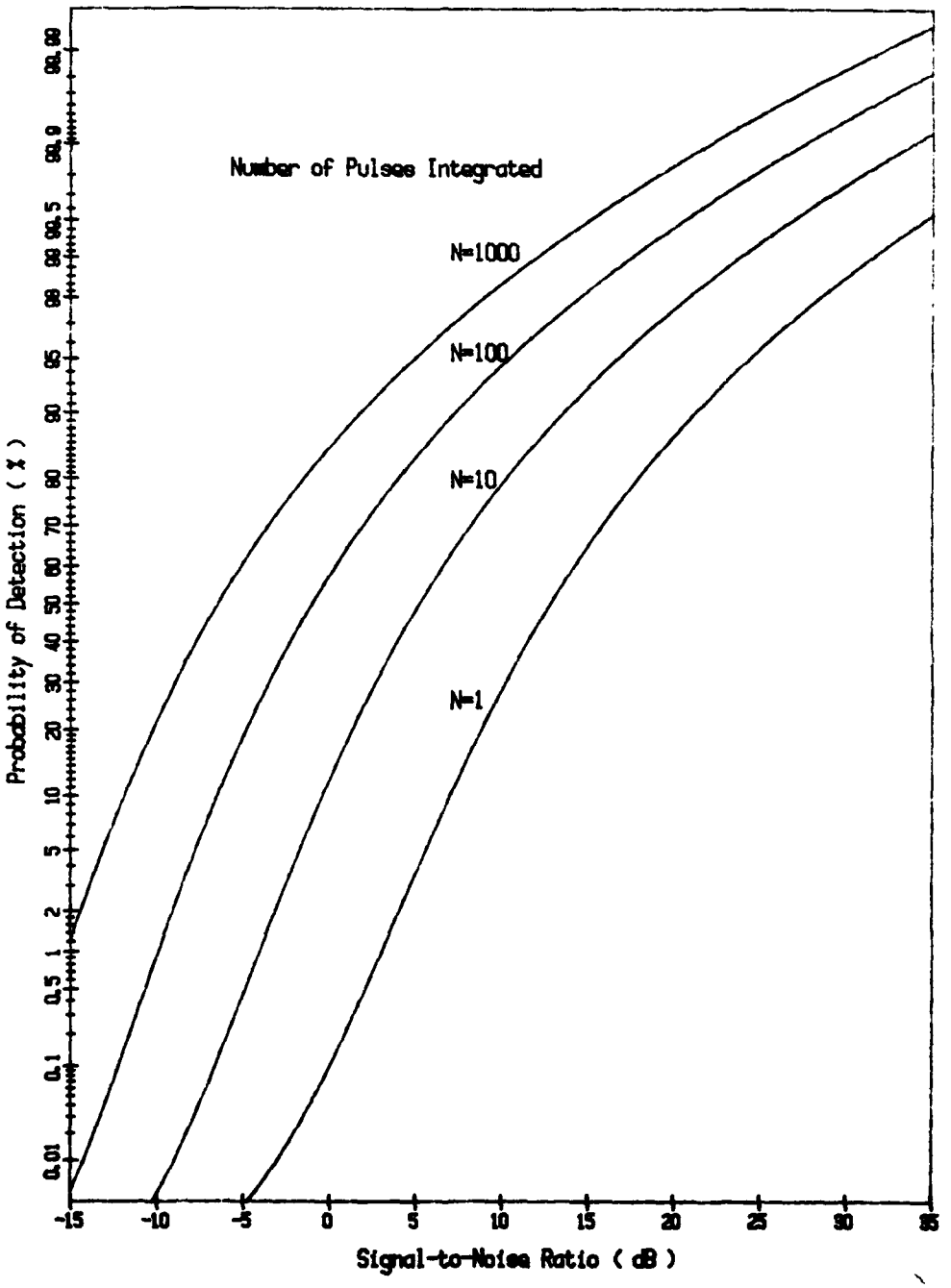

Figure G-1. Probability of Detection (Blip/Scan Ratio)
Threshold - Fixed
Probability of False Alarm is 0.000001
Target Statistics - Swerling Case I

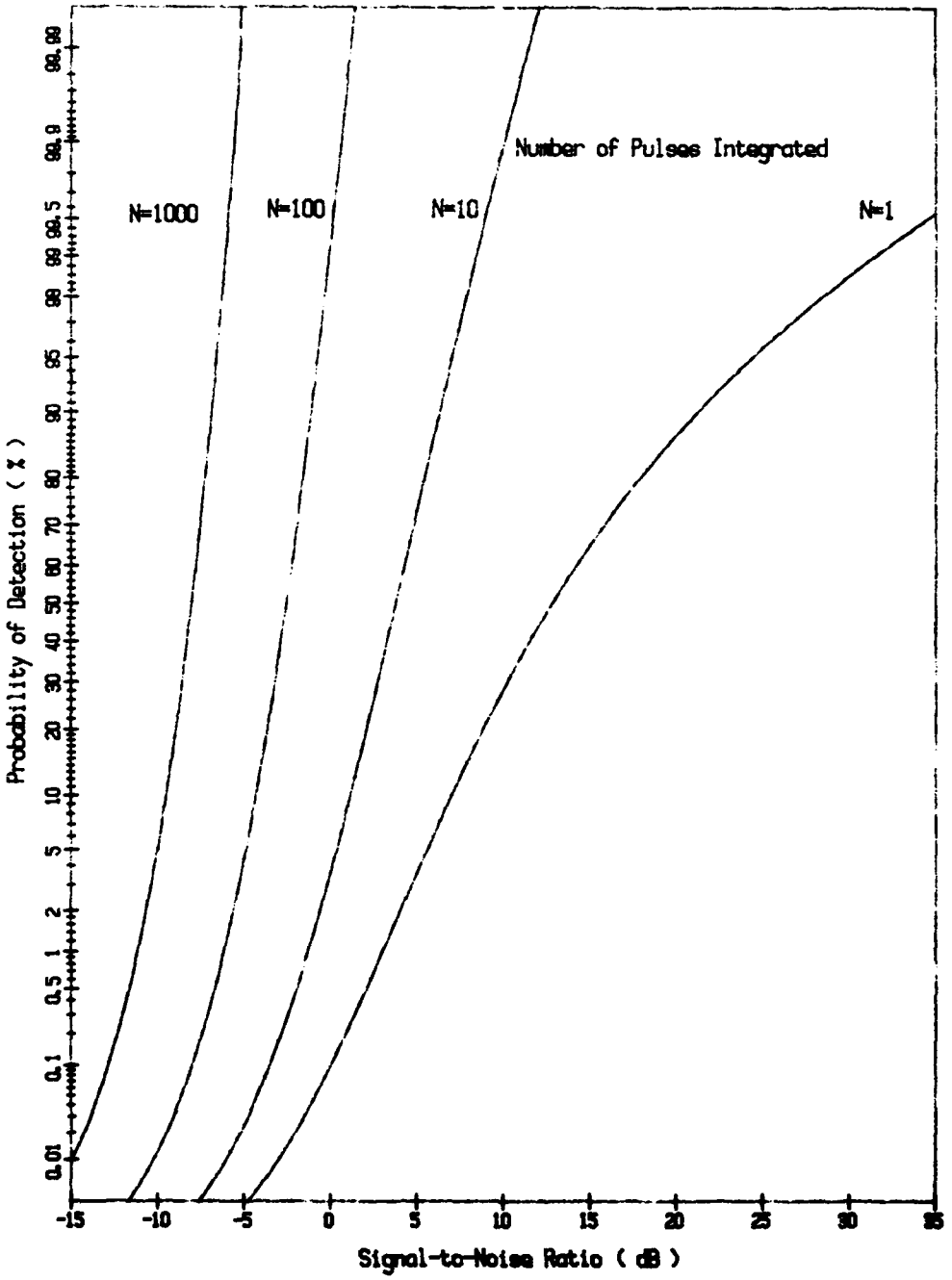

Figure G-2. Probability of Detection (Blip/Scan Ratio)
Threshold - Fixed
Probability of False Alarm is 0.000001
Target Statistics - Swerling Case II

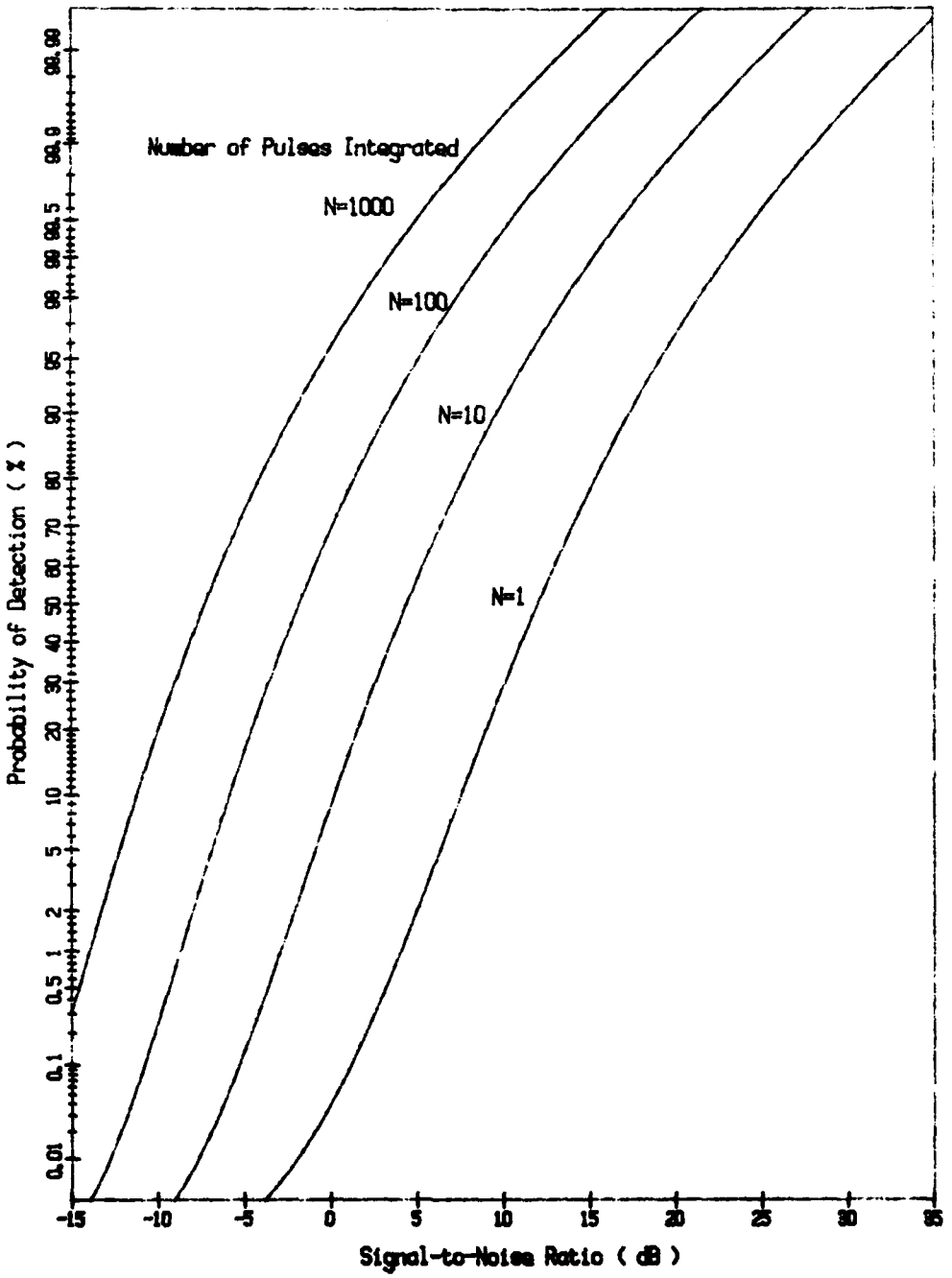

Figure G-3. Probability of Detection (Blip/Scan Ratio)
Threshold - Fixed
Probability of False Alarm is 0.000001
Target Statistics - Swerling Case III

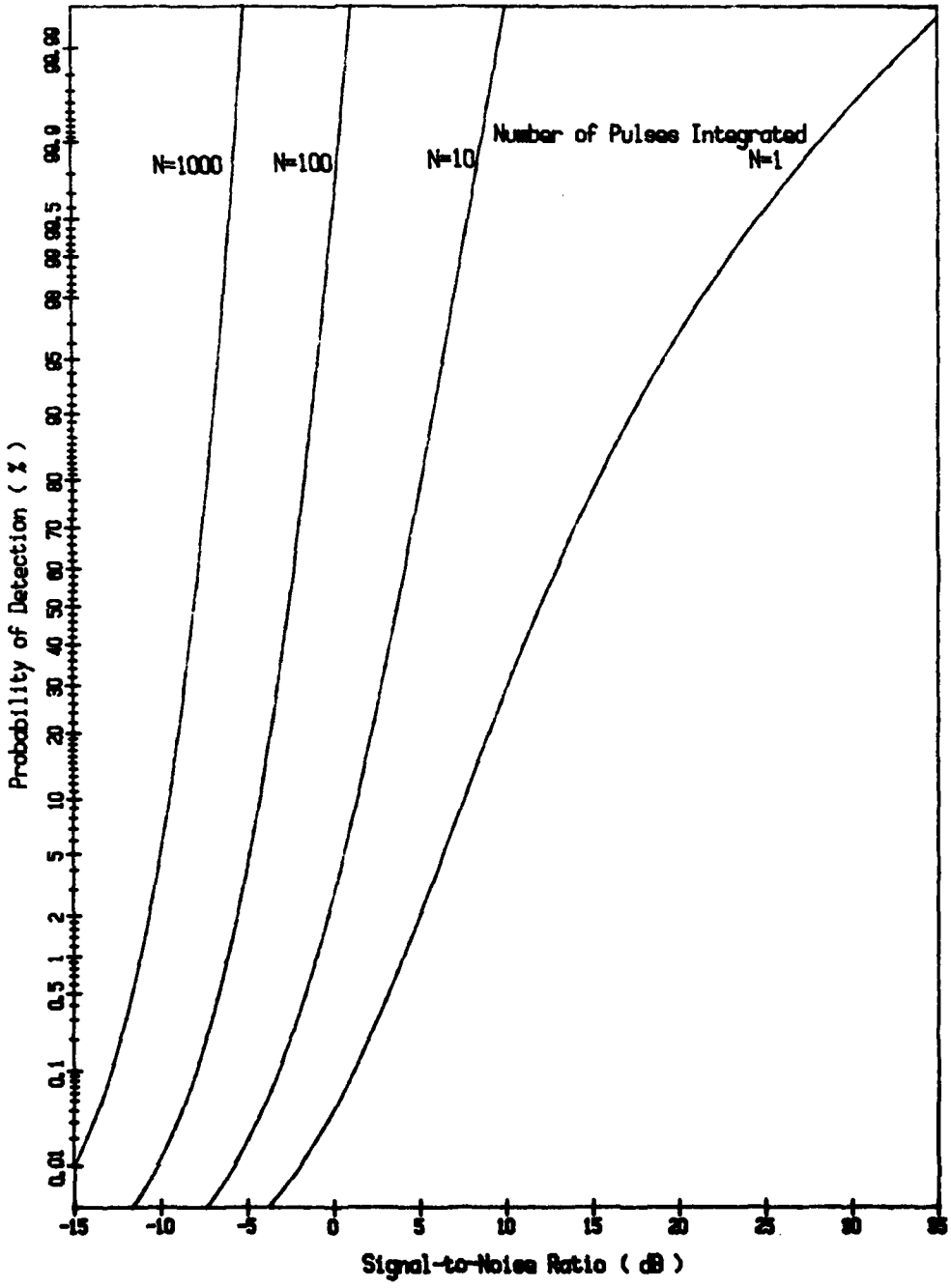

Figure G-4. Probability of Detection (Blip/Scan Ratio)
Threshold - Fixed
Probability of False Alarm is 0.000001
Target Statistics - Swerling Case IV

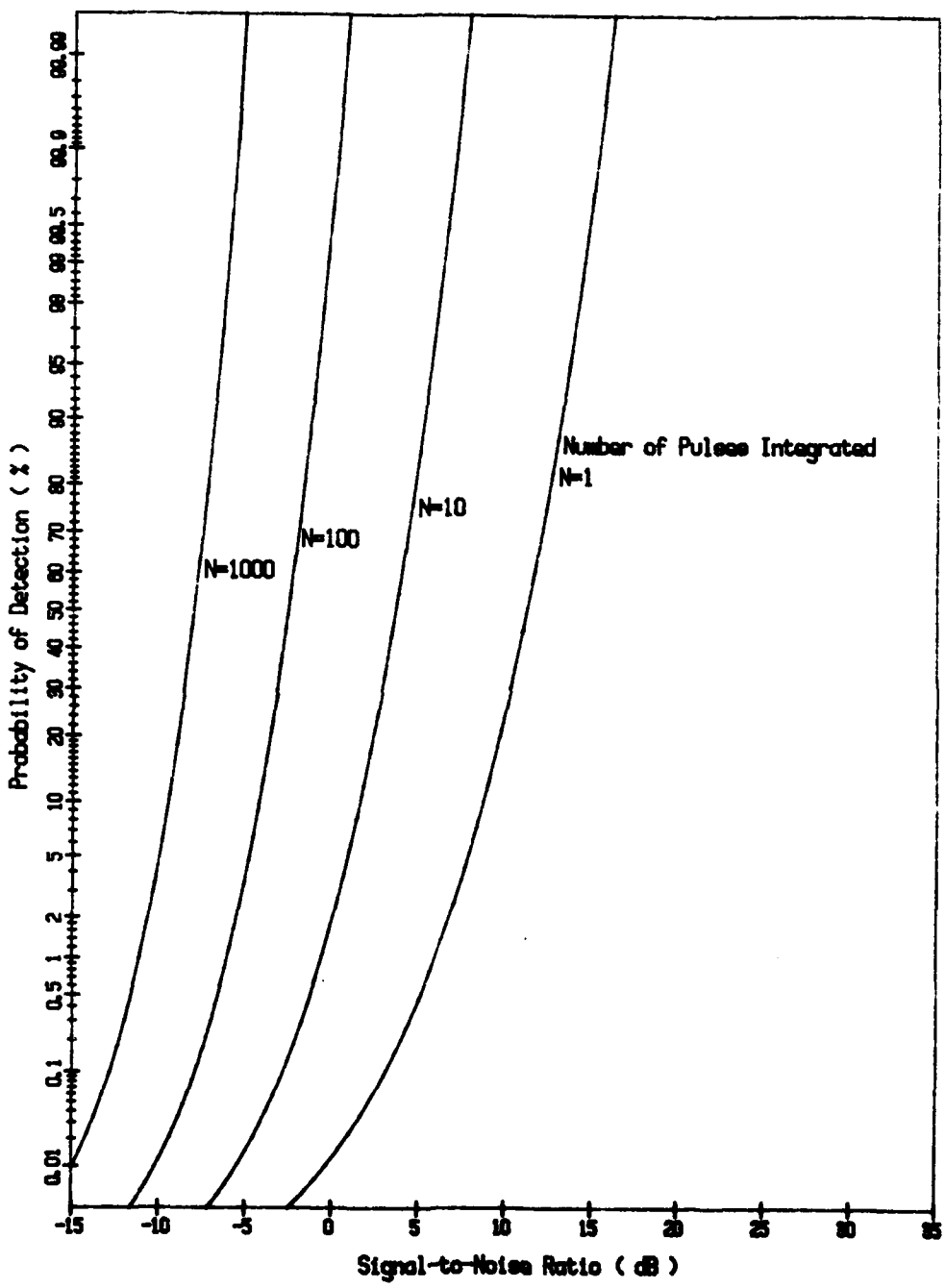

Figure G-5. Probability of Detection (Blip/Scan Ratio)
Threshold - Fixed
Probability of False Alarm is 0.000001
Target Statistics - Non-fluctuating

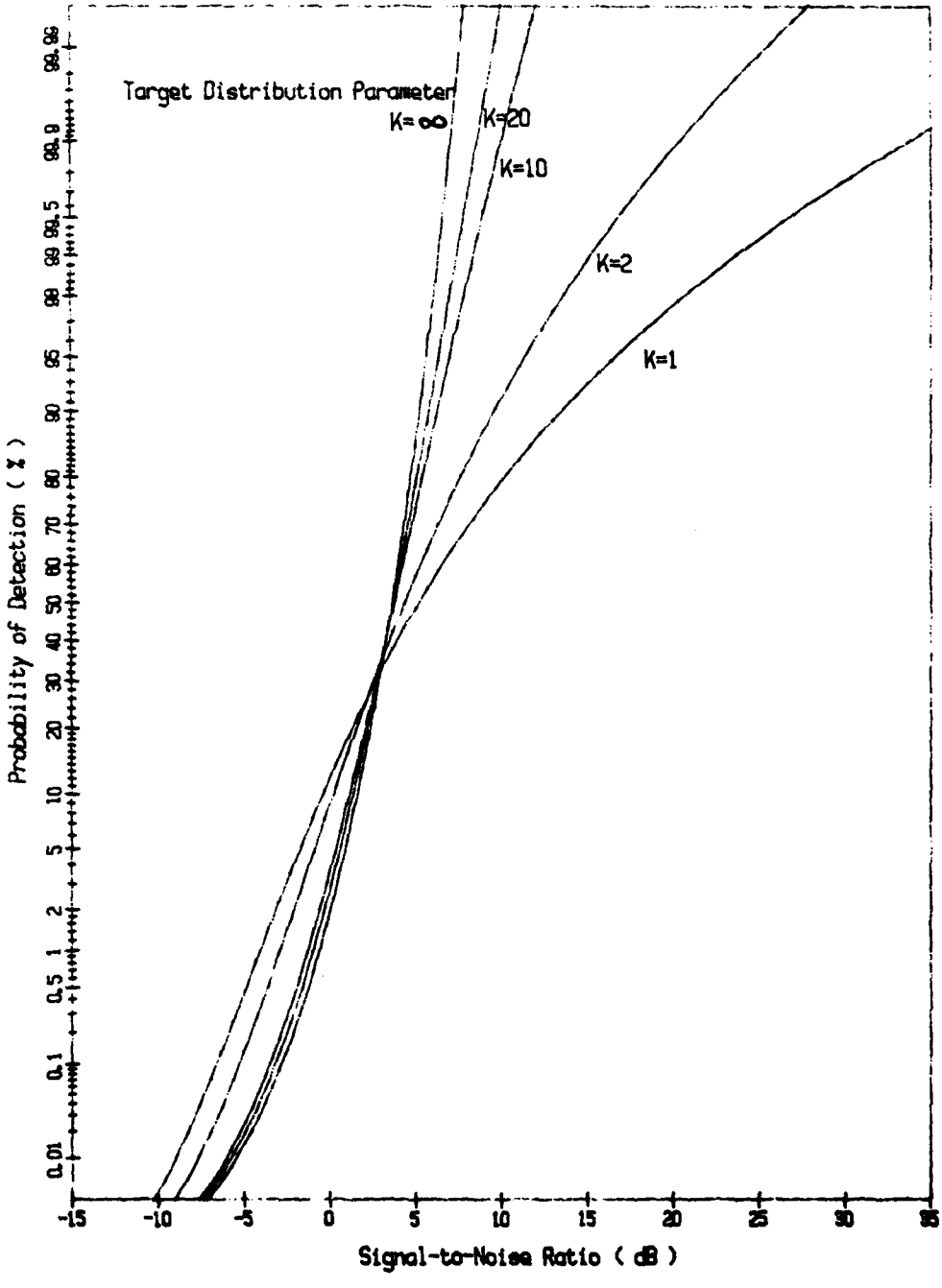

Figure G-8. Probability of Detection (Blip/Scan Ratio)
Threshold - Fixed
Probability of False Alarm is 0.000001
Number of Pulses Integrated is 10

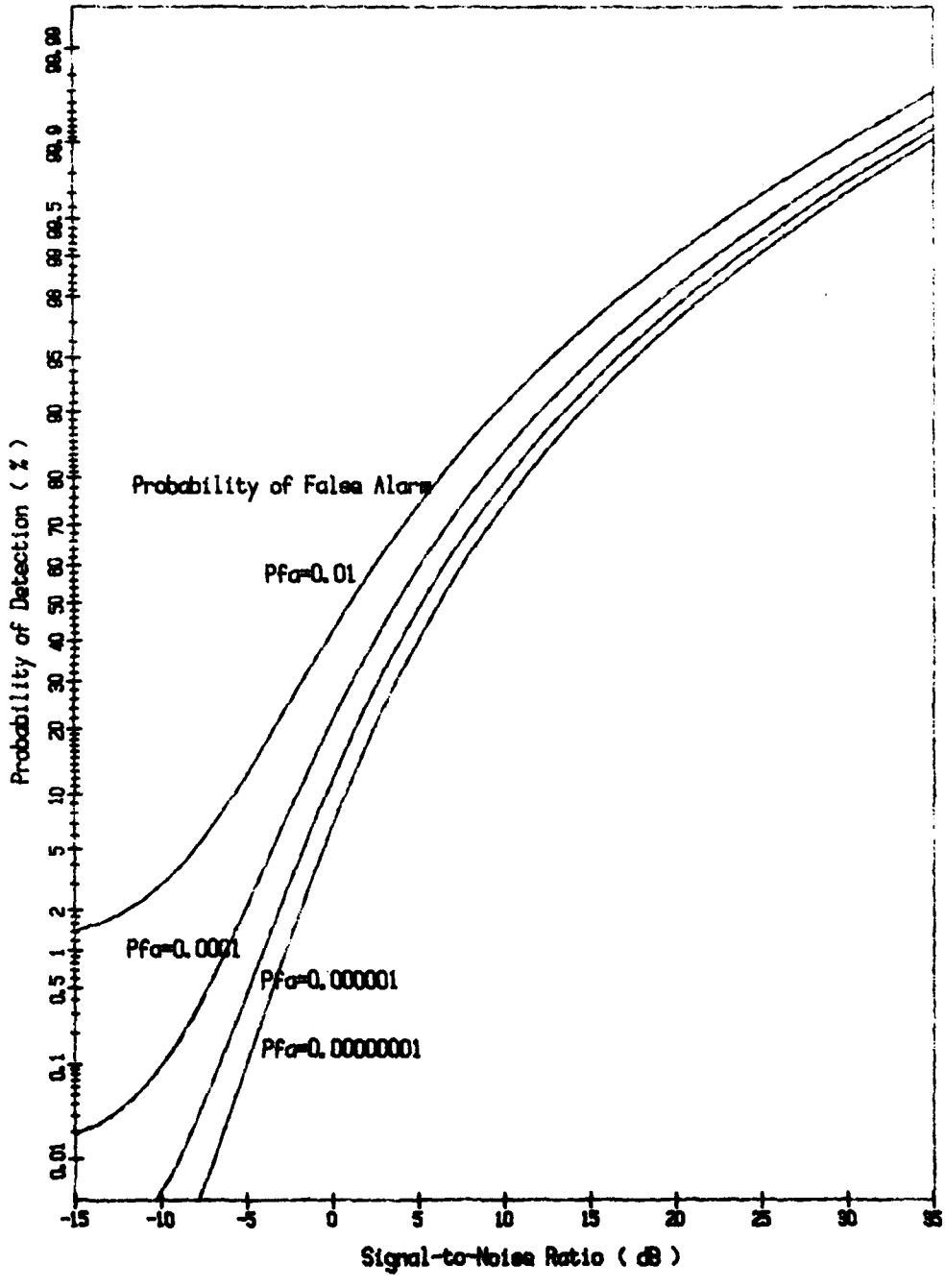

Figure G-7. Probability of Detection (Blip/Scan Ratio)
Threshold - Fixed
Number of Pulses Integrated is 10
Target Statistics - Swerling Case I

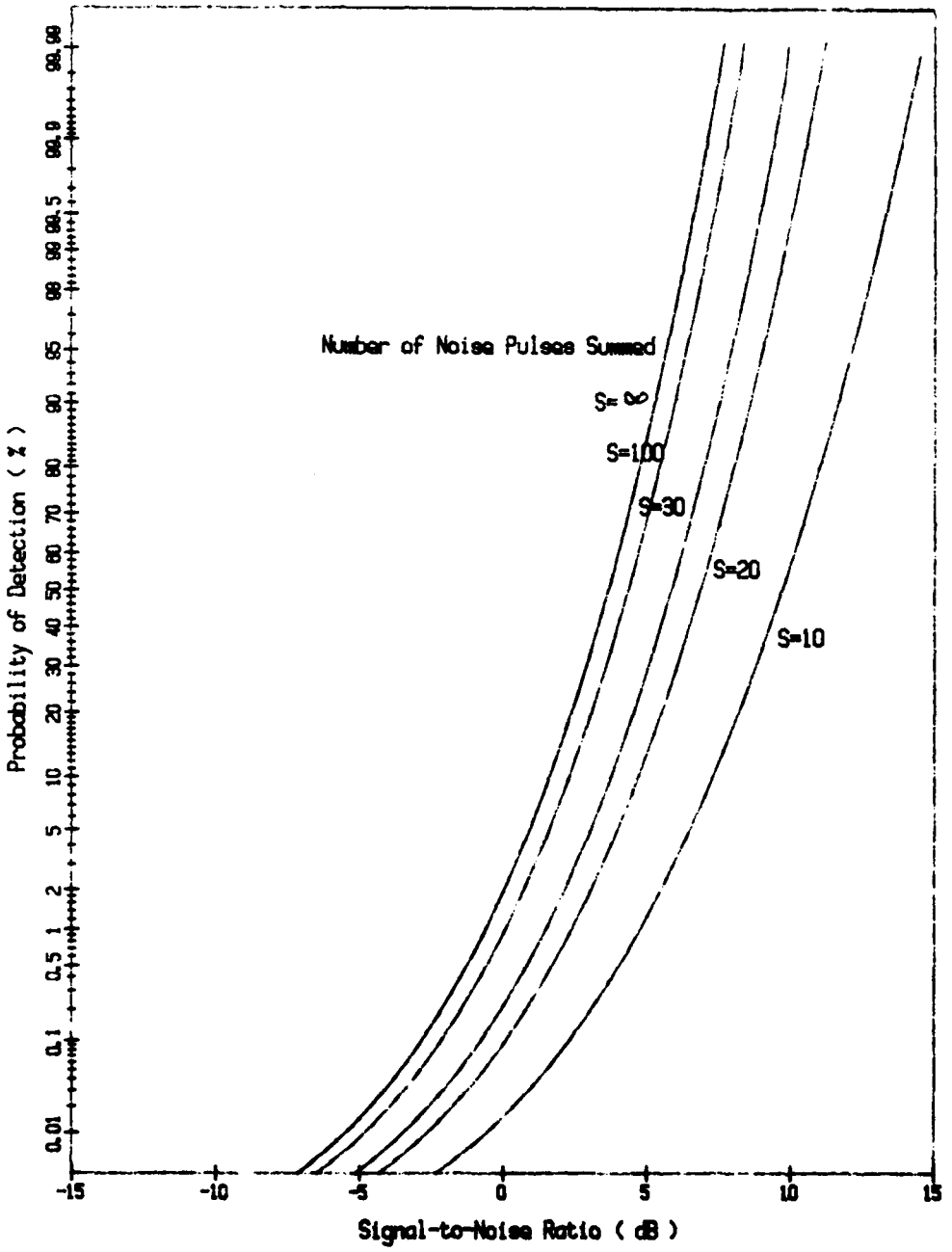

Figure G-8. Probability of Detection (Blip/Scan Ratio)
Threshold - CFAR
Probability of False Alarm is 0.000001
Number of Pulses Integrated is 10
Target Statistics - Non-fluctuating

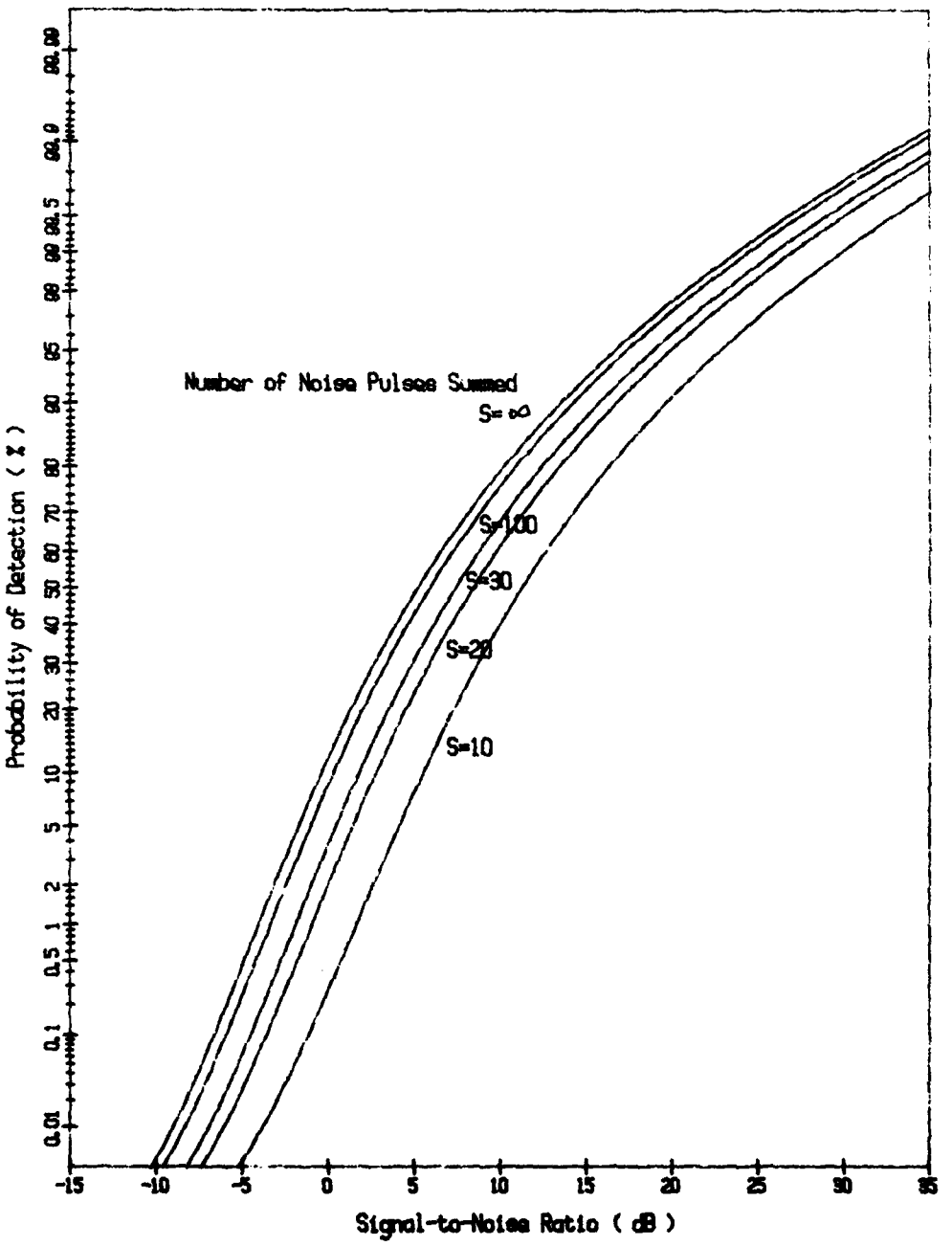

Figure G-9. Probability of Detection (Blip/Scan Ratio)
Threshold - CFAR
Probability of False Alarm is 0.000001
Number of Pulses Integrated is 10
Target Statistics - Swerling Case I

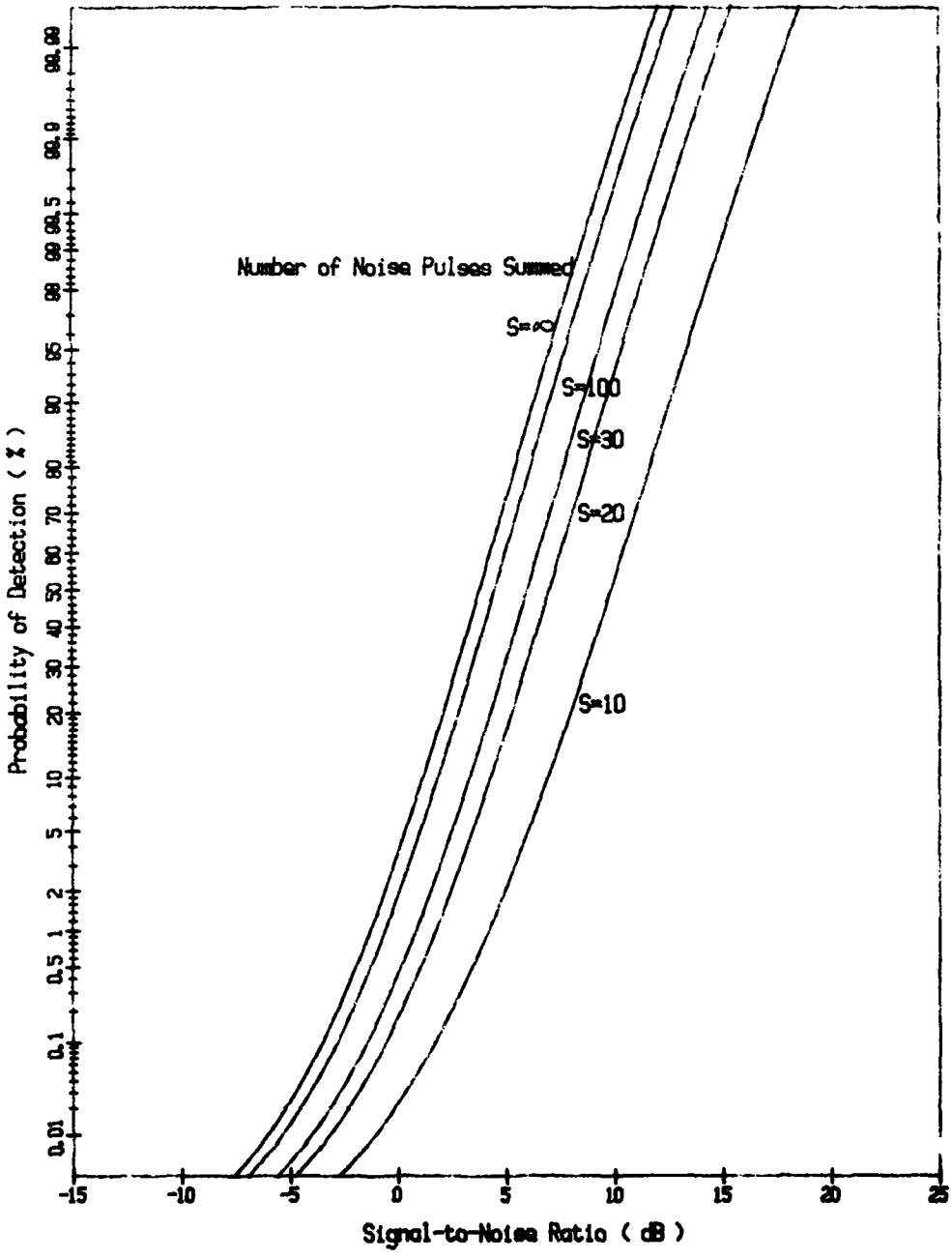

Figure G-10. Probability of Detection (Blip/Scan Ratio)
Threshold - CFAR
Probability of False Alarm is 0.000001
Number of Pulses Integrated is 10
Target Statistics - Swerling Case II

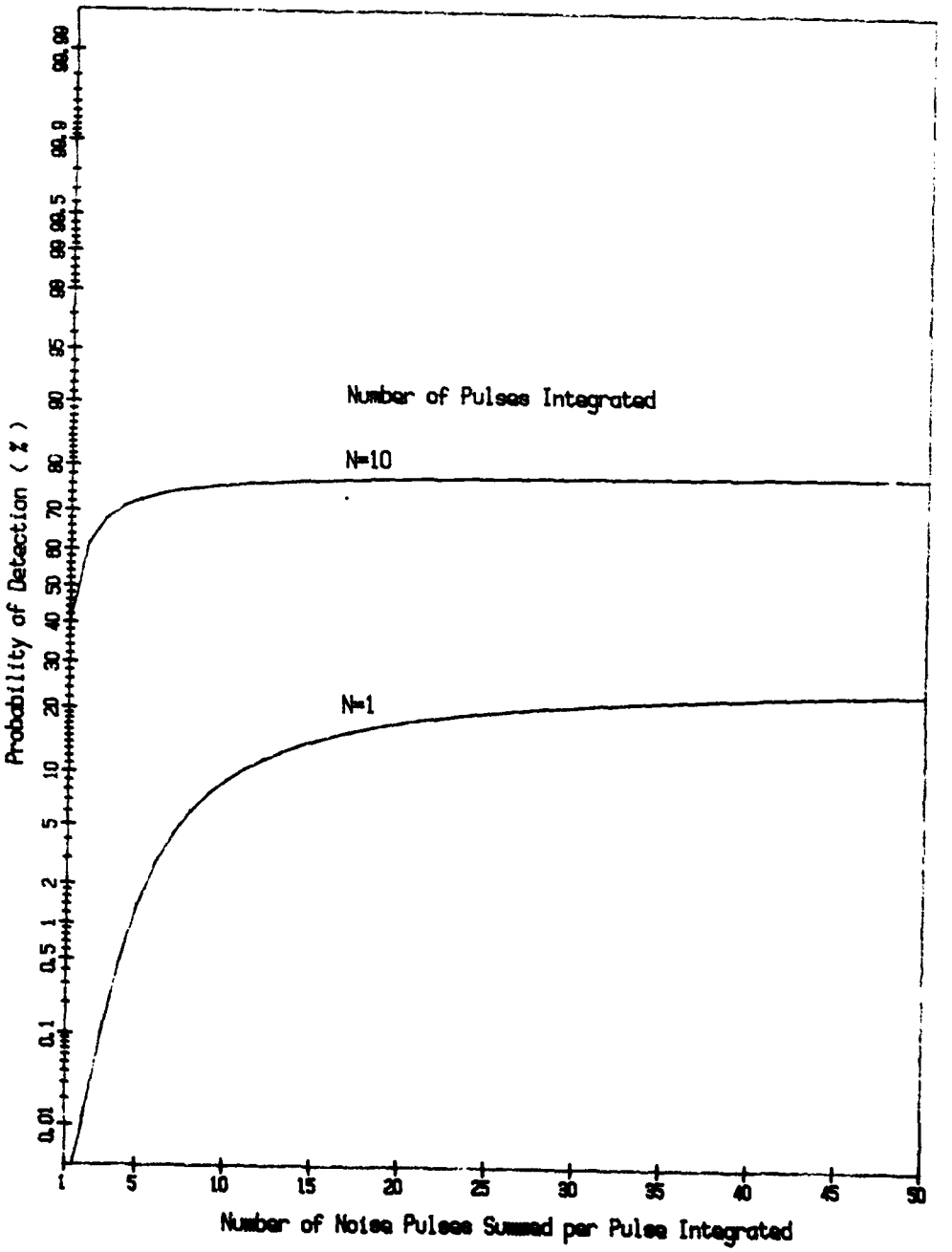

Figure G-11. Probability of Detection (Blip/Scan Ratio)
Threshold - CFAR
Probability of False Alarm is 0.000001
Target Statistics - Swerling Case I
Signal-to-Noise Ratio is 10 dB

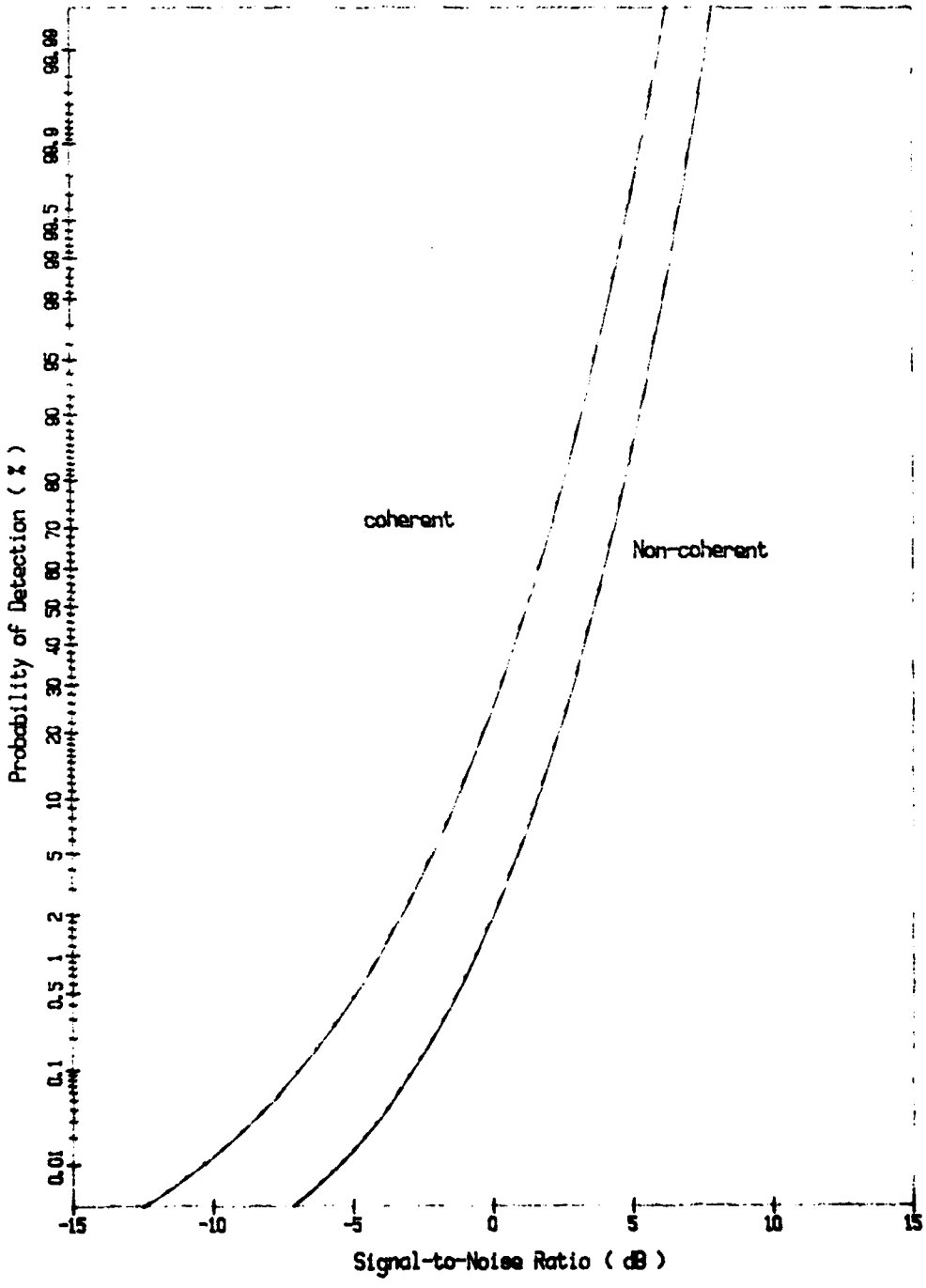

Figure G-12. Probability of Detection (Blip/Scan Ratio)
Non-fluctuating Target, N=10
Comparison of Coherent and Non-coherent Integration.

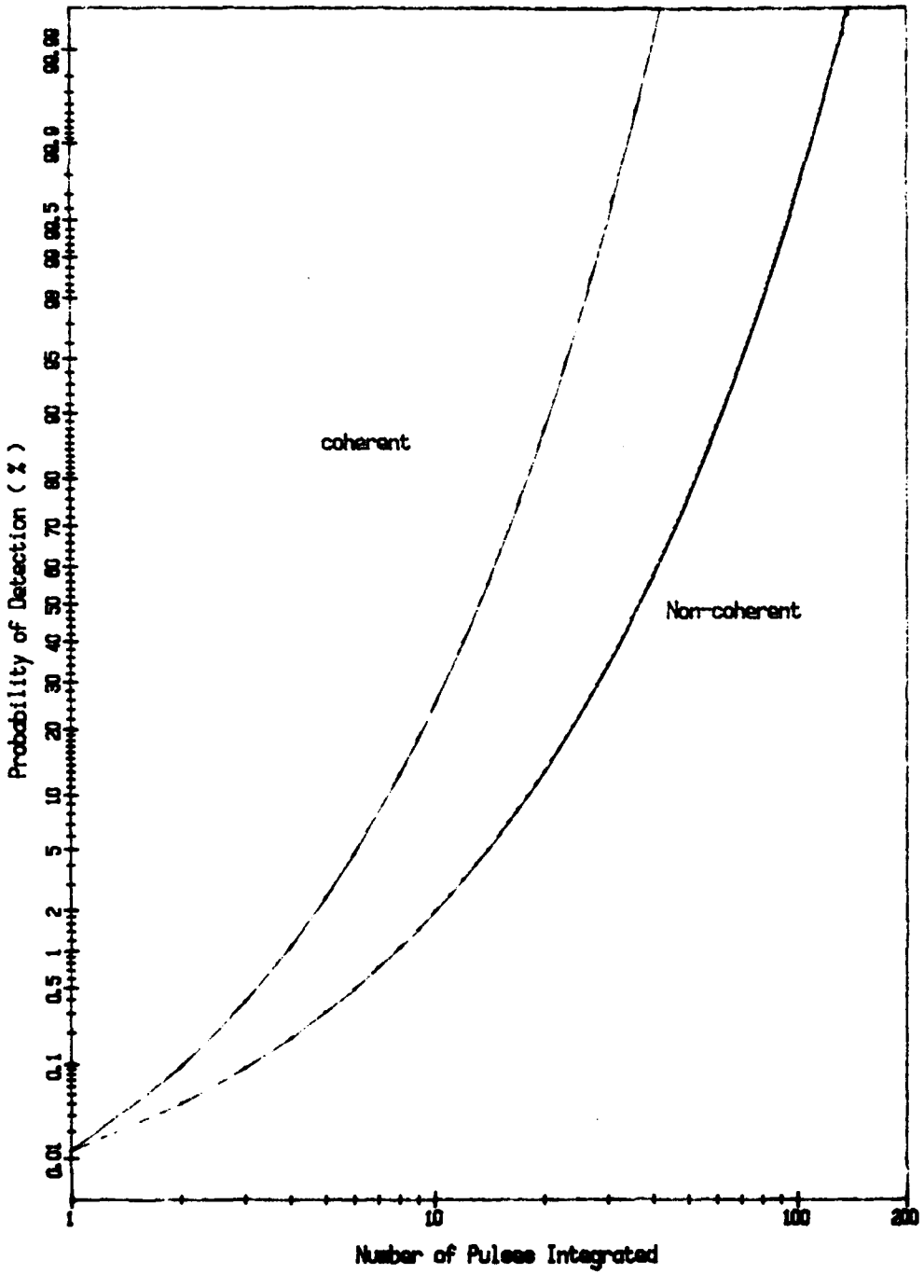

Figure G-13. Probability of Detection for Non-fluctuating Target
Signal-to-Noise Ratio = 0 dB
Comparison of Coherent and Non-coherent Integration

ANNEX H

MOVING TARGET INDICATOR (MTI)

Returns from zero doppler, pulse-to-pulse correlated targets, are reduced in MTI systems by a series of n delay line cancellers. The model assumes that the MTI signal return for an n-delay canceller is modified by a factor

$$\frac{P_{MTI}}{P_r} = 2^{2n} \sin^{2n}\left(\frac{2\pi v}{\lambda prf}\right) \qquad \text{(H-1)}$$

where v is the range rate and λ is the wavelength. Optimum target velocities occur when

$$\frac{v}{prf} = \frac{\lambda}{4}(2m-1) \qquad \text{(H-2)}$$

for integer values of m, and blind speeds occur when

$$\frac{v}{prf} = \frac{m\lambda}{2} \qquad \text{(H-3)}$$

The signal gain when averaged over all target velocities is obtained by integrating equation H-1

$$\bar{G} = \overline{P_{MTI}/P_r} = \frac{(2n)!}{(n!)^2} \qquad \text{(H-4)}$$

When detection is receiver noise limited the increase in noise power is

$$\frac{N_{MTI}}{kT/\tau} = \frac{(2n)!}{(n!)^2} \qquad \text{(H-5)}$$

so that the signal-to-noise ratio remains constant in the absence of clutter, when averaged over all target velocities. The effective number of pulses for post-detection integration is (ref 2)

$$N_{eff} = \frac{N_o^2}{1.5N_o - 0.5} \qquad \text{for n=1} \qquad \text{(H-6)}$$

$$N_{eff} = \frac{N_o^2}{(35/18)N_o - 1} \qquad \text{for n=2} \qquad \text{(H-7)}$$

$$N_{eff} = \frac{N_o^2}{2.31N_o - 1.625} \qquad \text{for n=3} \qquad \text{(H-8)}$$

.../H-2

where $N_o = N-n$ and N is the number of pulses input to the canceller.

Performance in clutter is determined by the pulse repetition frequency and the spectrum of the clutter return W(f). If the gain profile is

$$G(f) = 2^{2n} \sin^{2n}\left(\frac{\pi f}{prf}\right) \tag{H-9}$$

and

$$W(f) = W_o e^{-f^2/2\sigma_c^2} \tag{H-10}$$

the clutter power at the output of the n-stage MTI is

$$P_{oc} = \int_{-prf/2}^{+prf/2} W(f)G(f)\, df \tag{H-11}$$

$$\simeq \int_{-\infty}^{+\infty} W(f)G(f)\, df \tag{H-12}$$

$$= W_o\left(\frac{2\pi}{prf}\right)^{2n}[(1.3.5....(2n-1))\sqrt{2\pi}]\sigma_c^{2n+1} \tag{H-13}$$

while the corresponding clutter power entering the canceller is

$$P_{ic} = \sqrt{2\pi}\, W_o \sigma_c \tag{H-14}$$

A measure of the ability to see an 'average' moving target in clutter is the gain-weighted cancellation ratio or improvement factor (I)

$$I = \left(\frac{prf}{2\pi\sigma_c}\right)^{2n} \cdot \frac{2^{2n}}{n!} \tag{H-15}$$

Most MTI systems use a linear limiting amplifier preceding the canceller, which ensures that the residual clutter resembles receiver noise. An undesirable effect of limiting is to reduce the effective value n to n' where n'=n for no limiting and n'≈0.9 for hard limiting. Whilst this reduces I for single-delay MTI by only a few dB it can degrade the performance of multiple-delay MTI systems by tens of decibels. This uncertainty justifies the use of simple velocity spectra for sea and rain clutter, viz

σ_v = [illegible] m/s for sea clutter

$(\sigma_v)^2 = 1 + (0.4HK\Theta^V)^2$ m/s for rain clutter

.../H-3

where S is the sea state (Douglas), K is the wind shear (up to 5 m/sec/km of altitude), the doppler spectra of surface clutter is given by equation (H-10) and

$$\sigma_c = 2\sigma_v/\lambda \qquad \text{(H-16)}$$

The variability in I for simulation purposes is accommodated by varying σ_v and n' (between 0.9 and n)

In the evaluation of $S/N = P_r/(P_c+P_n)$ for the probability algorithms, the levels at the output of the MTI are assumed to be

$$(P_r)_{out} = P_r.G(f) \qquad \text{(H-17)}$$

$$(P_n)_{out} = P_n.\bar{G} \qquad \text{(H-18)}$$

$$(P_c)_{out} = P_c.\bar{G}/I \qquad \text{(H-19)}$$

If only 'average' MTI performance is considered $G(f) = \bar{G}$ and so S/N in the absence of clutter is independent of the MTI gain. For simulation purposes, where target velocity is known, it is important to determine whether the target is located near a blind doppler region (Equation H-3). Often the MTI pulse repetition frequency is varied, on a scan-to-scan basis, between two frequencies f_1 and f_2. If $f_1/f_2 \approx 1+1/2m$ (where m is a multiplier of the first blind speed) then for typical target speed, average performance will be obtained overall at this target doppler although the target return may be severely degraded on alternate scans. In the worst case a target may remain in a blind zone even with alternating pulse repetition frequencies.

ANNEX I

EXAMPLES OF PROGRAM OUTPUT

Figures I-1 to I-6 illustrate the graphical output of the programs for a variety of target and detection parameters, as described in annex G. All samples are for the same radar and environmental parameters which are summarized in table I-1.

In figure I-1 the single pulse signal-to-noise-plus-clutter ratio is plotted against target ground range for the interference and intermediate regions. Under the non-ducting conditions assumed here, ray theory remains valid from zero range to the peak of the lowest interference maximum (at approx. 20 n.miles). The barely perceptible change in slope near 20 n.miles justifies the use of the exponential interpolation for the intermediate region. For ranges less than the clutter horizon (12.1 n.miles), the S/N envelope begins to be dominated by the clutter return at sea state 3.

The probability of detection computational procedures of annex G are illustrated in the remaining plots. In figure I-2 the S/N data has been used to compute the paint probabilities for a scan-to-scan fluctuating target. The 50% paint probability, or unity signal-to-noise ratios, are often used to produce nominal detection ranges - from these data both criteria would lead to a computed detection range of approximately 23-24 n.m. Even these crude detection criteria illustrate dramatically the importance of including multipath effects since the notional detection range is only about 75% of the radar horizon at 5 GHz. This degradation against low altitude targets is even greater for UHF radars (ref 1).

Performance against very slowly fluctuating targets is illustrated for the Weinstock target (K = 0.4) in figure I-3. Between 20 and 40% paint probabilities there is negligible difference from the scan-to-scan scintillation rate previously discussed. The difference is, however, fairly large in the region of greatest interest (50%-99%).

A more significant detection range estimate is obtained from the cumulative probability of initial detection. This is illustrated in

.../I-2

figure I-4 for the single blip detection criterion and a range of operator efficiencies. These plots illustrate graphically the essential difference between applying an operator loss (typically 3dB) and scaling the probability by an operator effiency or alertness factor. For modest signal-to-noise ratios the former would normally lead to a predicted detection range near the peak of the first multipath maximum. By contrast the use of a realistic alertness factor for a fatigued operator (20%-50%) leads to the much wider distribution shown in figure I-4 for a typical aircraft closing speed. If the detection criterion is changed to two consecutive blips the degradation is even more dramatic. As shown in figures I-5 and I-6 for moderately and slowly fluctuating targets the median detection range could easily be less than 50% of the range calculated using simplistic detection range methods.

Table I-1.

Radar and Environmental Parameters

Transmitted Frequency	5000 MHz
Peak Power	200 kW
Transmitted Pulse Width	1 μs
IF Bandwidth	1 MHz
Pulse Repetition Frequency	500 Hz
Receiver Noise Figure	5 dB
Plumbing and Miscellaneous Losses	10 dB
Horizontal Beamwidth	1 degree
Vertical Beamwidth	20 degrees
Level of First Vertical Sidelobe	17.6 dB
Antenna Tilt Angle	0 degrees
Antenna Rotation Rate	20 rpm
Antenna Height	100 feet
Polarization	Horizontal
Sea Surface Temperature	15 degree C
Salinity	3.4 %
Sea State (Douglas)	3
Air Temperature at Sea Level	15 degree C
Barometric Pressure at Sea Level	1013.25 mbar
Humidity	50 %

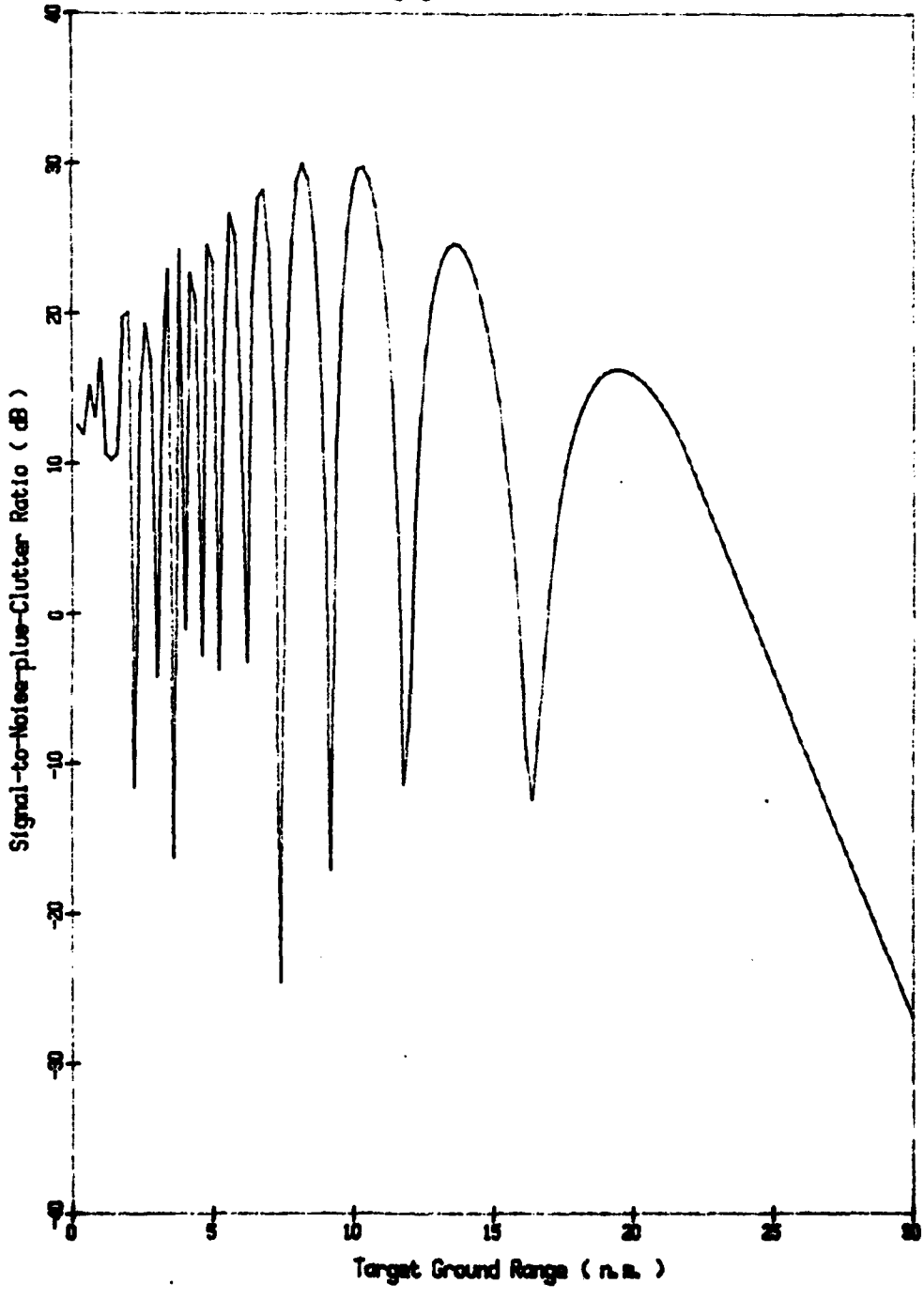

Figure I-1. Signal-to-Noise-plus-Clutter Ratio
Target - 1 sq.m. Radar Cross Section
200 Feet Altitude

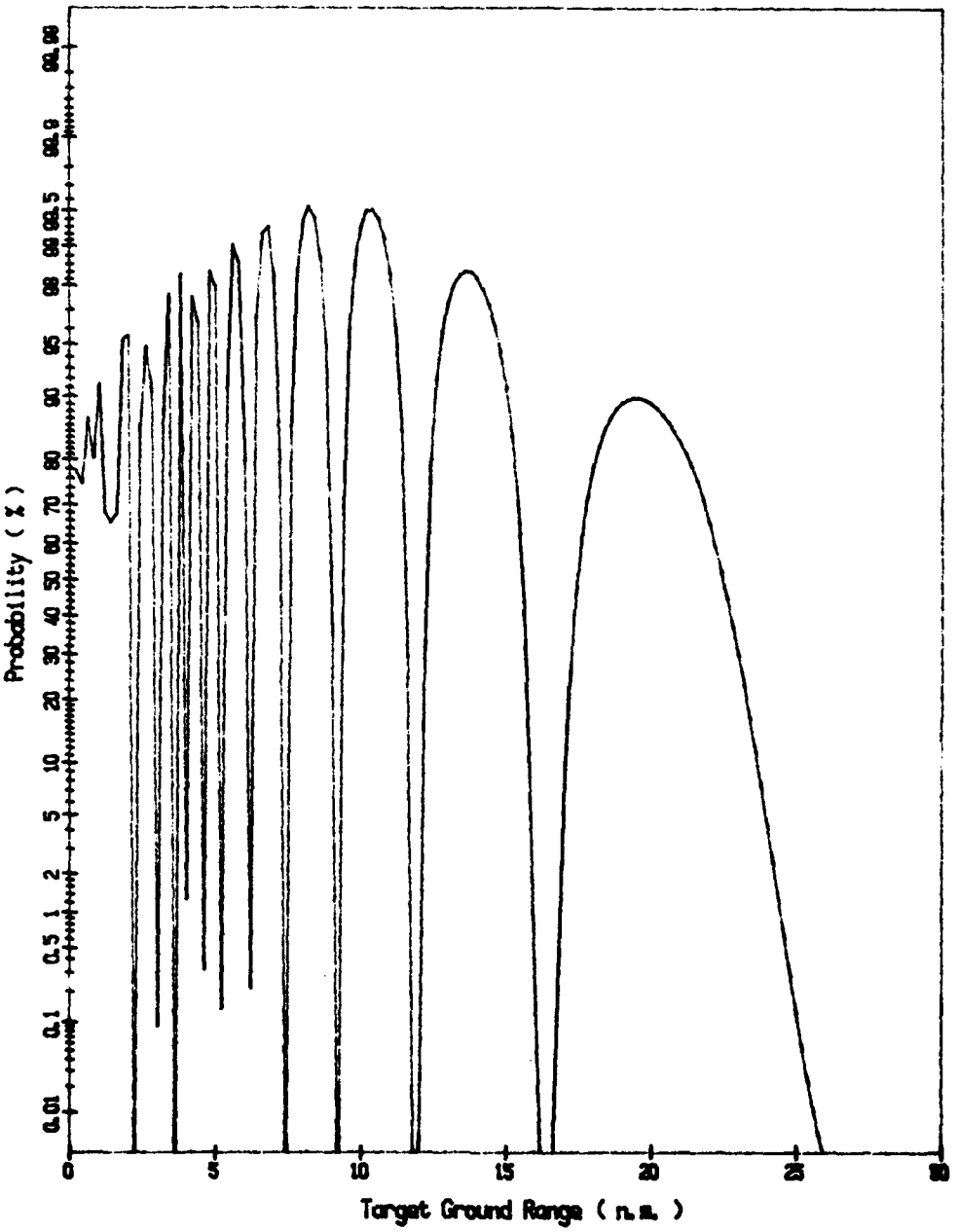

Figure I-2. Probability of Detection (Blip/Scan Ratio)
Target - Swerling Case I
1 sq.m. Radar Cross Section
200 feet Altitude
Threshold is Fixed
Probability of False Alarm is 0.000001

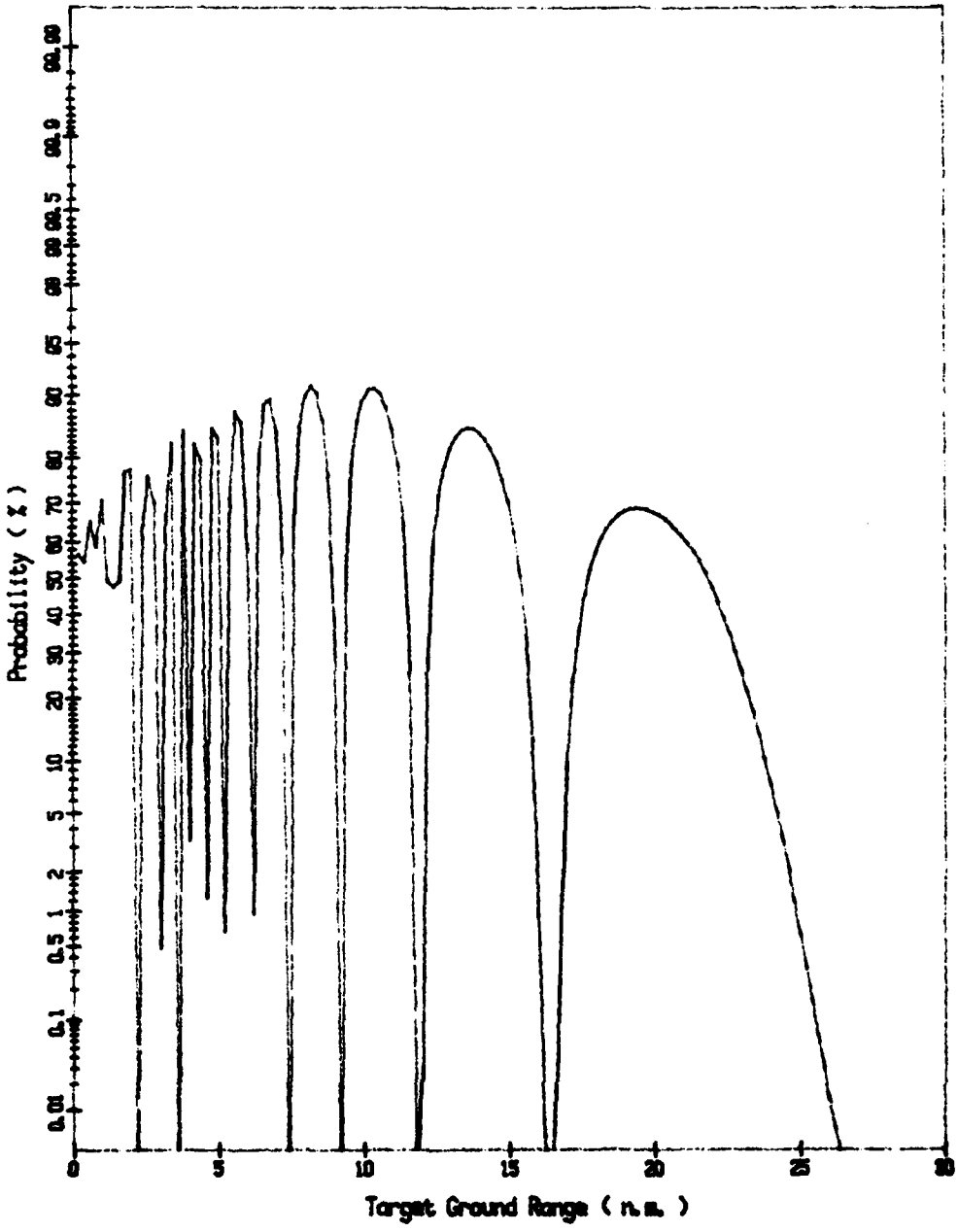

Figure I-3. Probability of Detection (Slip/Scan Ratio)
Target - Generalized Gamma Distribution (K = 0.4)
1 sq.m. Radar Cross Section
200 Foot Altitude
Threshold is Fixed
Probability of False Alarm is 0.000001

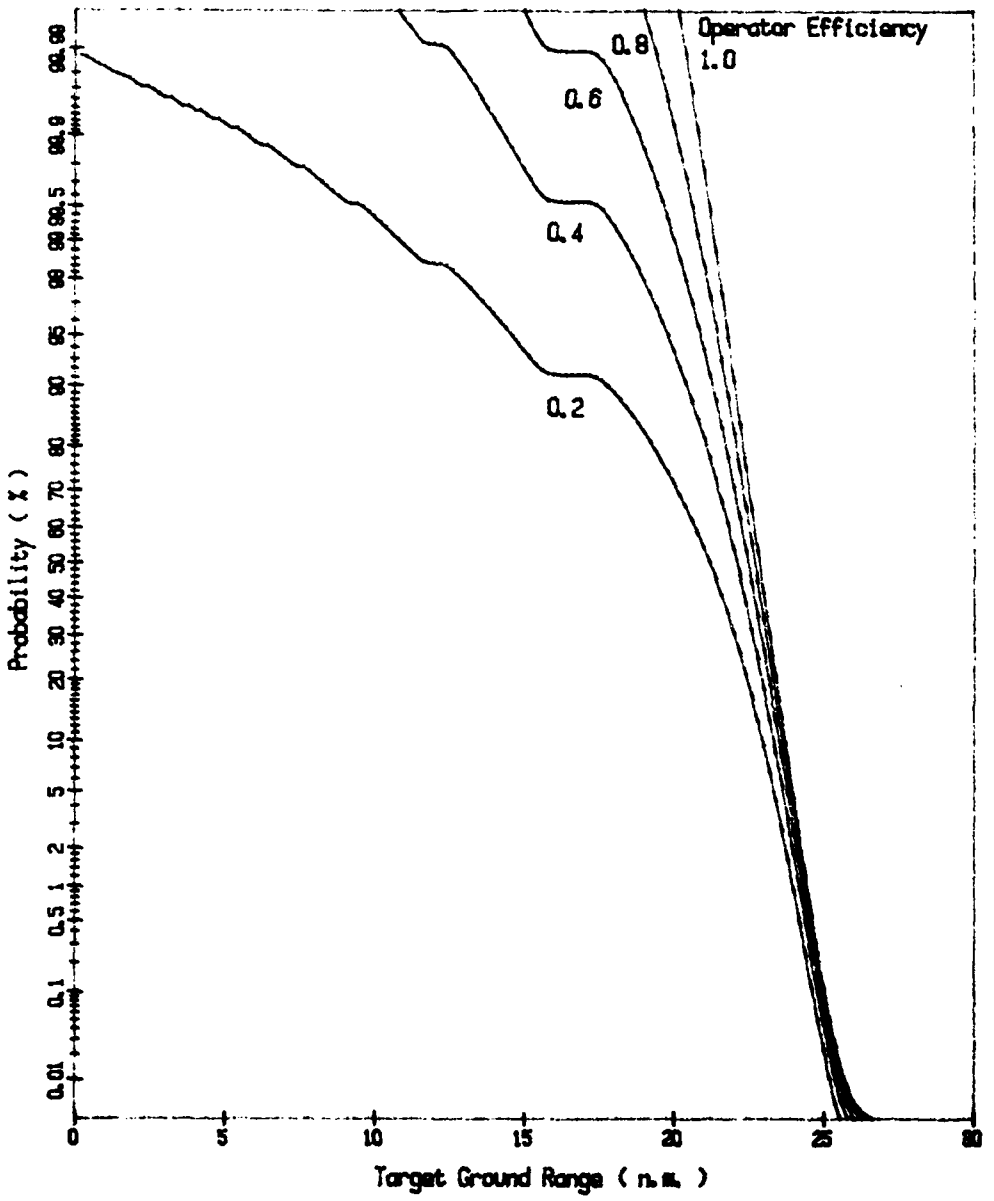

Figure I-4. Cumulative Probability of Initial Detection
Detection Criteria is a Single Blip
Targets - Swerling Case I
1 sq.m. Radar Cross Section
200 feet Altitude
480 knots Closing Rate
Threshold is Fixed
Probability of False Alarm is 0.000001

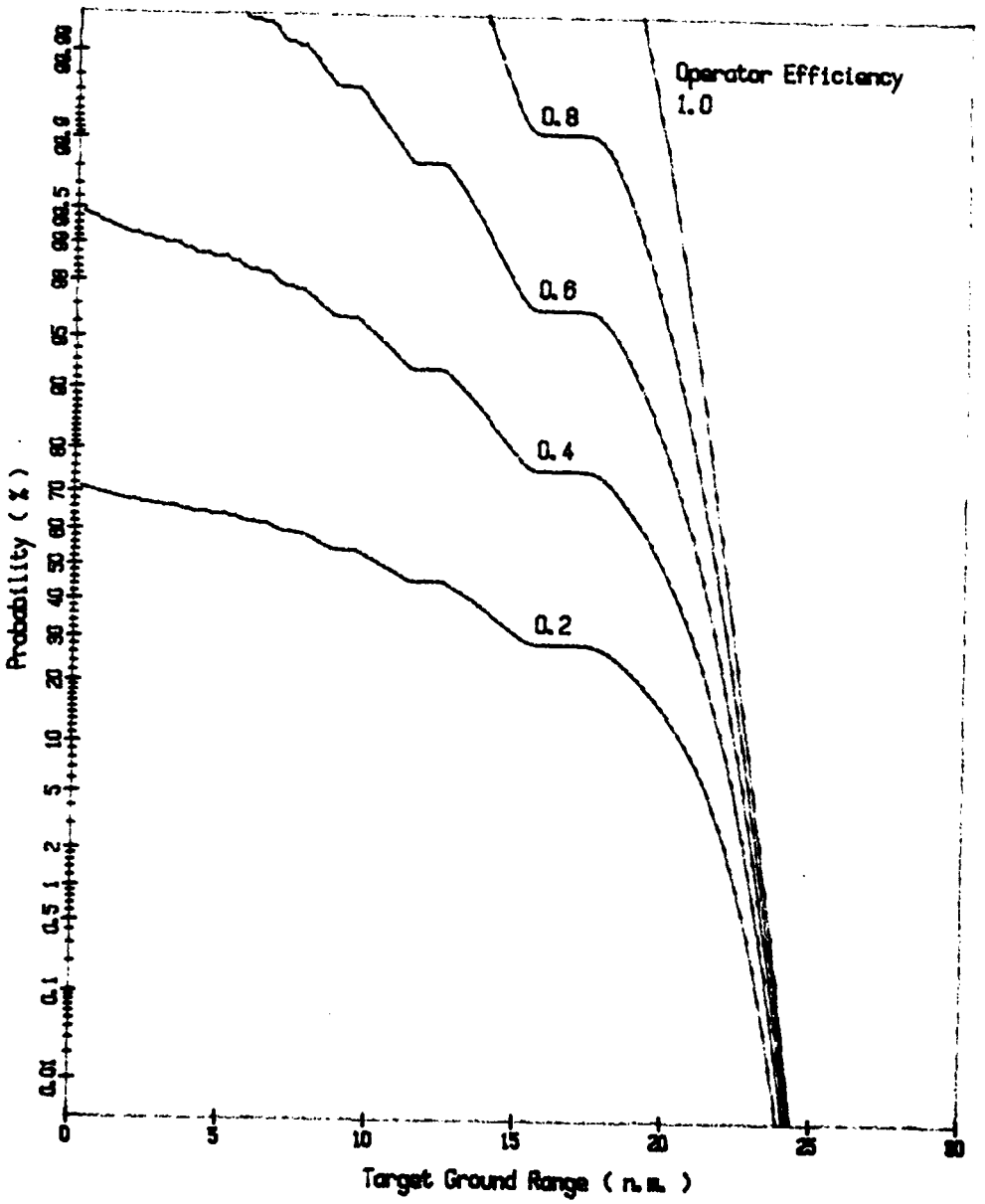

Figure I-5. Cumulative Probability of Initial Detection
Detection Criteria is Two Consecutive Blips
Targets - Swerling Case I
1 sq.m. Radar Cross Section
200 feet Altitude
480 knot Closing Rate
Threshold is Fixed
Probability of False Alarm is 0.000001

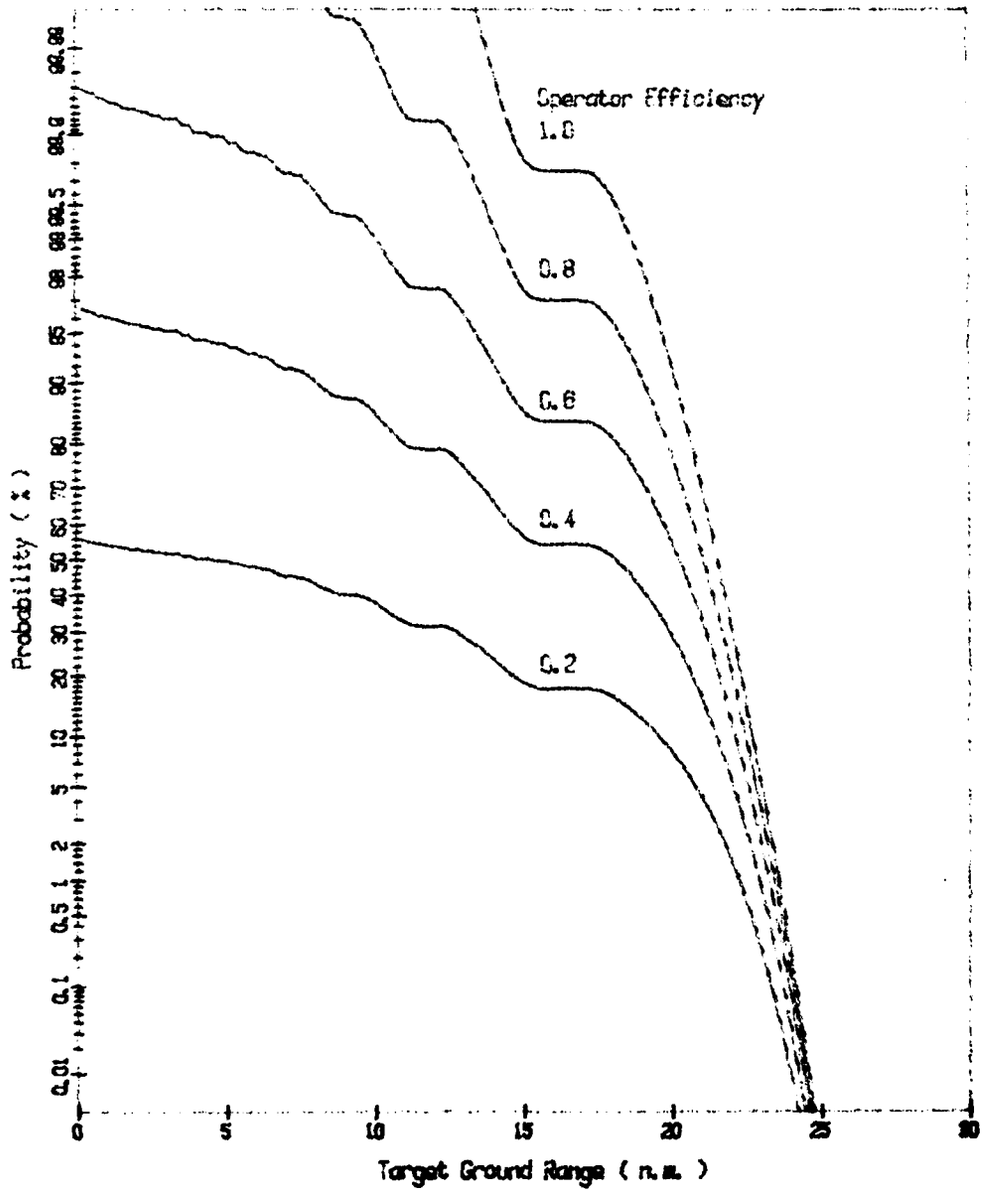

Figure I-8. Cumulative Probability of Initial Detection
Detection Criterion is Two Consecutive Blips
Targets - Generalized Gamma Distribution (K = 0.4)
1 sq. m. Radar Cross Section
200 feet Altitude
480 knots Closing Rate
Threshold is Fixed
Probability of False Alarm is 0.000001

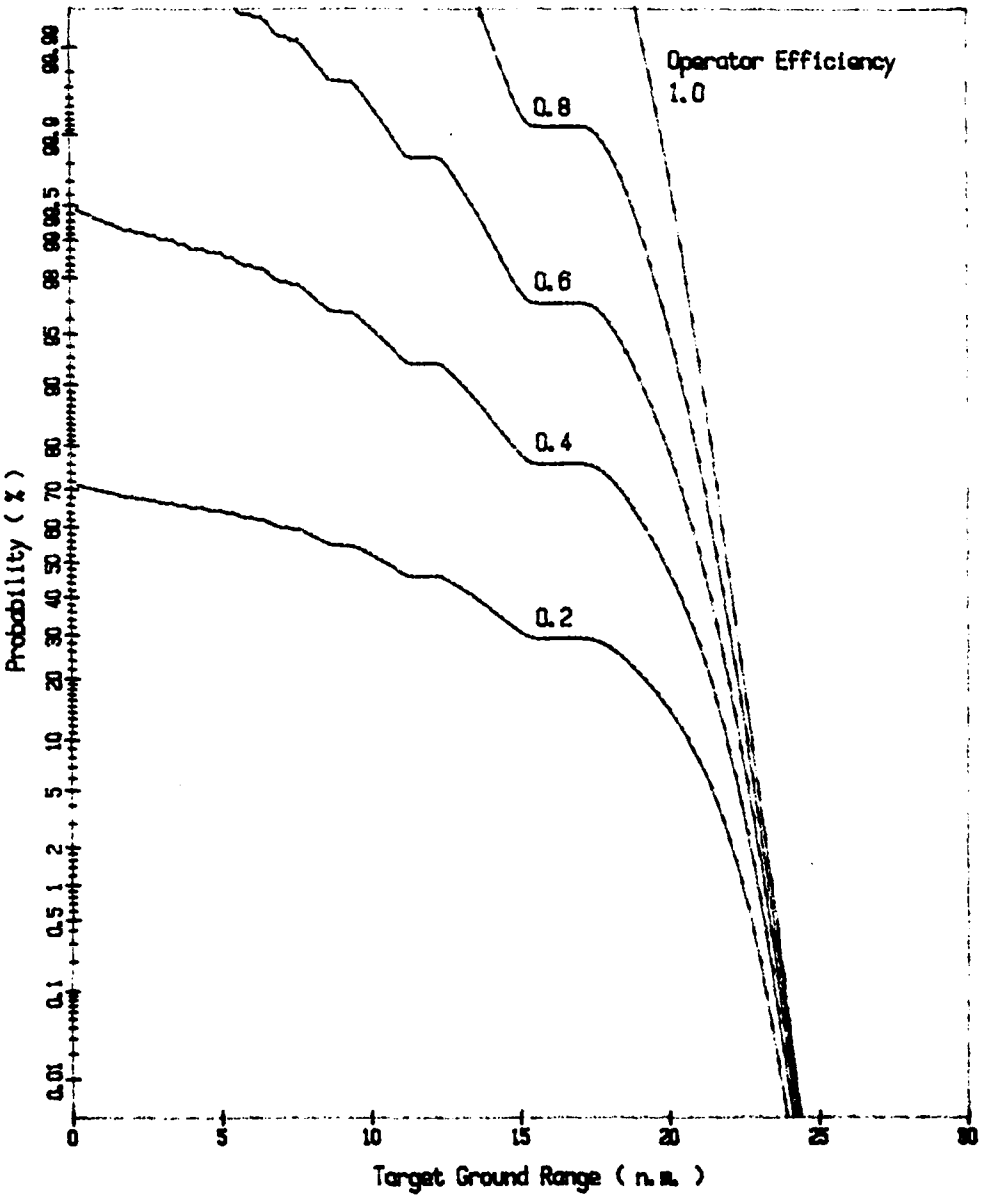

Figure I-5. Cumulative Probability of Initial Detection
Detection Criteria is Two Consecutive Blips
Target - Swerling Case I
1 sq.m. Radar Cross Section
200 feet Altitude
480 knot Closing Rate
Threshold is Fixed
Probability of False Alarm is 0.000001

AD A139 531 A MODEL OF RADAR PROPAGATION AND DETECTION(U) ROYAL AUSTRALIAN NAVY RESEARCH LAB EDGECLIFF M R BATTAGLIA ET AL. DEC 83 RANRL-TN-2/83 2/2

UNCLASSIFIED F/G 17/9 NL

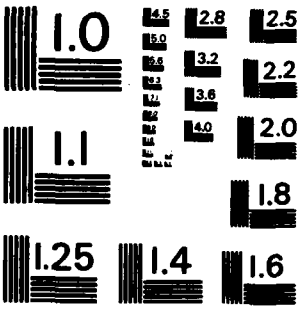

MICROCOPY RESOLUTION TEST CHART
NATIONAL BUREAU OF STANDARDS - 1963 - A

DOCUMENT CONTROL DATA SHEET

1. a. A.R. No.	1.b. Establishment No.	2. Document Date	3. Task No
002-708	RANRL Tech Note (External) 2/83	December 1983	A8/81

4. Title	5. Security	6.No Pages
A Model of Radar Propagation and Detection	a. document UNCLAS b. title UNCLAS c. abstract	108 7.No Refs 28

8. Author(s)	9.Downgrading Instructions
BATTAGLIA, M.R. and WILLIAMS, P.	N/A

10. Corporate Author and Address	11.Authority (as appropriate) a.Sponsor b. Security c.Downgrading d.Approval
RAN Research Laboratory P.O. Box 706, Darlinghurst. N.S.W. 2010	a.Operations Research Div. b.HORD c.N/A (unclass) d.M.D.Frost, Director RANRL M D Frost

12. Secondary Distribution (of this document)

Approved for Public Release

13. a. This document may be ANNOUNCED in catalogues and awareness services available to :

No limitations

13. b. Citation for other purposes (ie casual announcement) may be as for 13a.

14. Descriptors	15. COSATI Group
Radar, model, multipath, clutter, attenuation, backscatter, probability of detection	17090

16. Abstract

A computer model of radar propagation and detection is described. The details of multipath, clutter, attenuation, and probability of detection algorithms are contained in separate annexes.

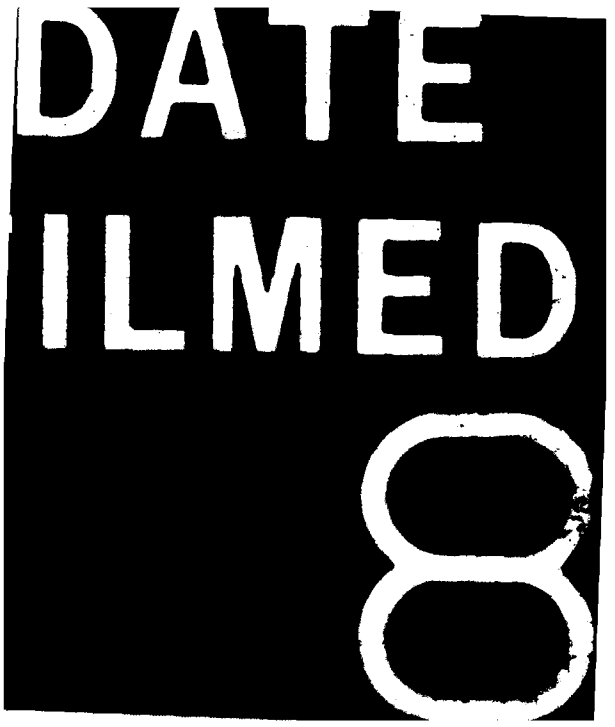
DATE
ILMED
8